COMMERCIAL, INDUSTRIAL AND HOUSEHOLD ELECTRICAL LOAD MODELLING AND SHORT-TERM LOAD FORECASTING

By

Hla U May Marma

A thesis submitted to the

School of Graduate Studies

in partial fulfillment of the requirements for the degree of

Master of Engineering

Faculty of Engineering and Applied Science

Memorial University of Newfoundland

October 2020

St. John's Newfoundland and Labrador Canada

Abstract

In this thesis, a transfer function-based load model is determined for commercial and industrial load. This model is derived from the composite load model which consist of an induction motor and static load. This developed model is compared to composite load model by considering two cases: 1) a small motor composition load or commercial load and 2) higher motor composition load or industrial load. The research is conducted through MATLAB/Simulink simulation. In order to compare the dynamic response of developed model, a comparative study has been done between the two models. In addition, the influence of voltage and frequency dependency terms on the overall model accuracy for developed model has been evaluated through several case studies considering both voltage and frequency dependency disturbances.

A short-term load forecast model is developed for an electrically heated house. This research work is based on experimental data collected by installing current sensors in a house in St. Johns, Newfoundland, Canada. The data was collected for three years and only one-year data is used for this model. The model is based on Recurrent Neural Network (RNN) with wavelet transform. The proposed model is verified by comparing other developed models in the literature through MATLAB deep learning toolbox and wavelet toolbox**.** The proposed model can more accurately forecast the load.

Acknowledgements

Foremost, I convey my earnest gratitude and sincerest appreciation to my supervisor, Dr. M. Tariq Iqbal for his invaluable guidance, support, motivation, and enthusiasm. His constructive discussions helped me in all the time of development of research and writing of this thesis.

I would like to acknowledge Dr. Xiaodong Liang for her guidance, valuable advice, and important contributions to this research.

Besides my advisor, I would like to thank to Dr. Faisal Khan, Associate Dean of the Graduate Studies for all the efforts he put to ensure a smooth administrative operation for graduate programs at the faculty of Engineering and Applied Science.

A very special gratitude goes out to School of Graduate Studies (SGS) and Natural Sciences and Engineering Research Council of Canada (NSERC) for generous financial supports.

Finally, I like to give special thanks to my wonderful mother, U Nue Prue; my fiancé, Thomas Seary; and my Seary's family for their unconditional love, mental supports and encouragement through the entire time of this M.Eng. program.

Table of Contents

List of Tables

List of Figures

List of Abbreviations

IEEE	Institute of Electrical and Electronics Engineers
EIA	Energy Information Administration
CLOD	Complex Load Model
WECC	Western Electricity Coordinating Council
STLF	Short-Term Load Forecast
LTLF	Long Term Load Forecast
MTLF	Medium Term Load Forecast
ZIP	Constant Impedance, Constant Current and Constant Power
IM	Induction Motor
LSTM	Long Short-Term Memory
Bi-LSTM	Bidirectional long short-term memory
SWT	Stationary wavelet transform
ISWT	Inverse Stationary wavelet transform
DWT	Discrete Wavelet Transform
IDWT	Inverse Discrete Wavelet Transform
NN	Neural Network
CNN	Convolutional Neural Network
RNN	Recurrent Neural Network
ANN	Artificial Neural Network
SVM	Support Vector Machine
ARIMA	Autoregressive Integrated Moving Average

CRT	Collaborative Representation
PV	Solar Photovoltaic
RMSE	Root Mean Square Error
MSE	Mean Square Error
SSE	Sum Square Error
MAPE	Mean Absolute Percentage Error

List of Symbols

P	Active Power
Q	Reactive Power
P_{IM}	Real Power of Induction Motor
Q_{IM}	Reactive Power of Induction Motor
P_{IM0}	Real Power of the Induction Motor in Steady State
Q_{IM0}	Reactive Power of the Induction Motor in Steady State
P_{ZIP}	Real Power of ZIP Model
Q_{ZIP}	Reactive Power of ZIP Model
P_{ZIP0}	Real Power of ZIP Model in Steady State
Q_{ZIP0}	Reactive Power of ZIP Model in Steady State
v	Voltage of Load Bus
v_0	Voltage of Load Bus In Steady State
E	Rms Phase-to-Ground Voltage of Load Bus
E_0	Rms Phase-to-Ground Voltage of Load Bus In Steady-State
a_p, a_q	Parameters of Constant Impedance Load
b_p, b_q	Parameters of Constant Current Load
c_p, c_q	Parameters of Constant Power Load
f	Load Bus Frequency
f_g	Rated Frequency
f_0	Load Bus Frequency in Steady State

k_{pf}, k_{qf}	Parameters Frequency Sensitivity
Ψ_{ds}, Ψ_{qs}	Stator $d-$ And $q-$ Axis Flux Linkages
Ψ_{dr}, Ψ_{qr}	Rotor $d-$ And $q-$ Axis Flux Linkages
v_{ds}, v_{qs}	Stator $d-$ And $q-$ Axis Voltages
v_{dr}, v_{qr}	Rotor $d-$ And $q-$ Axis Voltages
v_{dg}, v_{qg}	D- And Q- Axis Power Source Voltages
i_{ds}, i_{qs}	Stator D- And Q- Axis Currents
i_{ds0}, i_{qs0}	D- And Q- Axis Currents In Steady State
i_{dr}, i_{qr}	Rotor D- And Q- Axis Currents
E_0	Power Source Steady-State Rms Voltage Per Phase
ω_{s0}	Stator Steady-State Electric Angular Frequency
ω_{r0}	Rotor Steady-State Electric Angular Frequency
R_s	Stator Resistance
R_r	Rotor Resistance
L_m	Exciting Inductance
l_s	Stator Leakage Inductance
L_s	Total Stator Inductance
l_r	Rotor Leakage Inductance
L_r	Total Rotor Inductance
H	Motor Inertia
J	Inertia

p	Pole Pairs
T_e	Electromagnetic Torque
T_m	Shaft Mechanical Torque
n_r	Target Speed
n_{rated}	Nominal Speed
$P_{composite}$	Total Real Power of Composite Load Model
$P_{proposed}$	Total Real Power of Transfer Function-Based Load Model
P_{error}	Error of Total Real Power Between Two Models
$Q_{composite}$	Total Reactive Power of Composite Load Model
$Q_{proposed}$	Total Reactive Power of Transfer Function-Based Load Model
Q_{error}	Error of Total Reactive Power Between Two Models
i_t	Input Gate at Time Step t
f_t	Forget Gate at Time Step t
g_t	Cell Candidate at Time Step t
o_t	Output Gate at Time Step t
c_t	Cell State at Time Step t
h_t	Hidden State at Time Step t
$W, R\ and\ b$	The Input Weights, The Recurrent Weights, and the Bias Of $i, f, g\ and\ o$
σ_c	State Activation Function
σ_g	Gate Activation Function
$\vec{h}_t$	The Forward Output Layer Sequence

$\overleftarrow{h_t}$	The Backward Output Layer Sequence
x_i	The Ith Sampled Measurement Point, I = 1, 2, …, N for N Observations
μX	Mean
med	Median
N	Number

Note: Other symbols not mentioned are defined in the text.

List of Appendices

Chapter 1

Introduction

1.1 Background

Load model and forecasting has significant impact on power systems and smart grids analysis, planning and control. The advantages of adequate load representation are briefly presented in [1,2]. Different uncertainty factors such as weather-dependent compositions load, diverse load components, the lack of high frequency data and detailed load information cause the most challenging part to develop an adequate load model and improvement of the load forecasting accuracy in power system simulation.

Load modeling means to develop a mathematical representation of the real power (P) and reactive power (Q) in terms of the bus voltage magnitude (V) and the frequency (f) which represents approximate load behaviors [1]. In the industry, it is common practice to use relatively simple load models for power system studies [2]. Load models is used in dynamic power system studies [3]-[9]. The aim of studies dynamic load model is to analysis the transient stability, small-disturbance stability, longer-term dynamics [10]. 35% of Americas and 25% of the overall world industries use different load models for different load classes in dynamic power system studies [10].

Currently, industries use several load models for dynamic load model studies and it is reported in [11] that a composite load model consists of ZIP and induction motor is dominant practice in the USA as shown Fig. 1.1. Another well known dynamic load model form is transfer function-based load model, composed of a static part and a dynamic part and this model

represents the real power and reactive power as a function of both voltage and frequency [12]. In this thesis, the two models have been compared together through the same event.

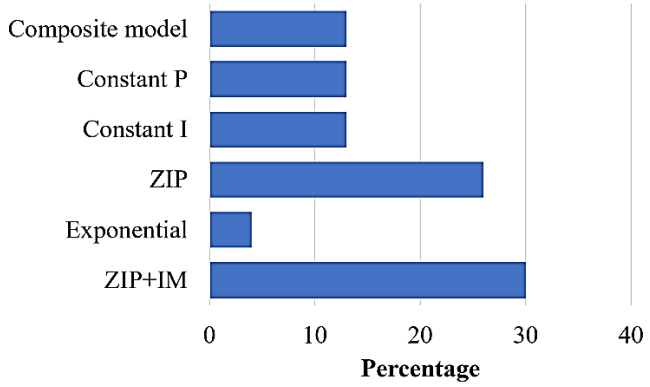

Fig. 1. 1. Adopted load model in USA industries for dynamic power system studies [11].

Load forecasting model are used in power system operation including decision-making in the power system, financial and supply planning, demand-side management and so on, helps to optimize utilities and reduce the electricity cost [15]-[17]. Based on [14] short-term prediction has a direct application for quick electricity demand response among all load forecasting methodologies. Recently, research has designated computational intelligence short-term load forecasting methods and it is shown that hybrid neural networking is more suitable for STLF.

The research of load forecasting based on the house electrical load is limited compared to commercial and industrial electrical load. The U.S. Energy Information Administration (EIA) reported in 2019 that electricity use in the residential and commercial building sectors increases rapidly; and energy consumed in the buildings sector includes residential and commercial building increases by 1.3% per year [13]. Therefore, house electrical load studies are very important as it represents important load class. But individual house power consumption data is highly uncertain compared to commercial and industrial load classes [18]. Although there are

several models used by researchers to improve the load forecast, the characteristic of individual house data causes serious difficulty to improve the accuracy of load forecast [19].

1.2 Objective of the Research

The goal of this thesis is to develop a transfer function-based load model for commercial, industrial load; and model a short-term load forecasting method for electrically heated house load. The goal will be achieved through the following objectives:

1. Derive a transfer function-based load model from the composite load model for commercial and industrial load;
2. Design a transfer function-based load model and composite load model using MATLAB's Simulink and carry out experimental measurements to evaluate the accuracy of the proposed model;
3. Propose a topology for short-term load forecasting of electrically heated house load that is capable of increasing the accuracy of prediction;
4. Construct the proposed short-term load forecasting model using MATLAB's deep learning toolbox and wavelet toolbox; and carry out experimental measurements to validate the performance of the proposed model.

1.3 Contribution of the Research

The specific contributions of the research are presented in four categories based on the chapters of the thesis as follows:

1. Investigation and Study of the dynamic load models and short-term load forecasting methods (Chapter 2)

The unique principles and features of the basic topologies of load model is discussed in this chapter. Different types of load models and topologies that are used to dynamic load models were presented. In this chapter, several recent proposed short-term load forecasting methods based on RNN were discussed and their features are highlighted.

2. A transfer function-based load model is developed and validate the performance for commercial load (Chapter 3)

A transfer function-based load model is developed analytically from a composite load model. The developed model has a 1^{st} order voltage term, a 1^{st} order frequency term, a 2^{nd} order voltage term, a product of a 1^{st} order voltage and a 1^{st} order frequency term, and a product of a 2^{nd} order voltage and a 1^{st} order frequency term. The coefficients of these voltage and frequency terms are 3rd order transfer-functions and this provides the reason of have better performance of the 3rd order transfer-function in the past research. A comparison between the developed transfer function-based load model and the original composite load model is studied and analyzed in this chapter. Three levels of simplification of the transfer function-based load model are subjected to evaluate the performance of the developed load model.

3. A transfer function-based load model is developed and evaluate the accuracy of developed model for industrial load (Chapter 4)

A transfer function-based load model is derived analytically from a composite load model. A comparison between the developed transfer function-based load model and the original composite load model is evaluated for a high motor composition load (industrial load).

4. A short-term load forecasting method for is developed and validate the accuracy of the proposed model using electrically heated house load data (Chapter 5)

A short-term power load forecast model of an electrically heated house in St. John's, Newfoundland, Canada is proposed in this chapter. The detailed procedure to construct the short-term load forecasting method based on RNN and wavelet transform is discussed. The accuracy of the proposed model is studied and analyzed in detail.

1.4 Thesis Outline

This thesis consists of three manuscripts and all manuscripts have been already published. The thesis outline is organized as follows:

In Chapter 1, the importance of the research topic is introduced; the objectives of the research work are described.

In Chapter 2, a literature review for the research work is presented. The main objective of this thesis is modeling and forecasting of commercial, industrial and a house electrical load.

In Chapter 3, a transfer function-based load model is derived analytically from composite load model based on an induction motor and static load (the Detailed transfer function-based load model derivation and initial value calculation can be found in Appendix A and Appendix B). A comparative study of composite load model and transfer function-based load model has been conducted through MATLAB/Simulink simulation by using small motor composition load for various voltage and frequency disturbances. The developed transfer function-based load model is verified by comparing with composite load model for voltage and frequency disturbance. In this chapter, the error of simplification levels of transfer function-based load model are evaluated, three levels of simplifications are made to the full model of transfer function-based load model. Each simplified model is compared against the original composite model. This study is conducted for a combination of a small induction motor, 25 HP and large

static load, 120KW. This comparative study evaluates the errors caused by simplification levels of the full model. A version of this chapter has been published in the IEEE Transactions on Industry Applications in September/October 2019 regular issue.

In Chapter 4, a transfer function-based load model is developed for industrial load A transfer function-based load model and composite load model have been compared through MATLAB/Simulink simulation by using high motor composition load. The high motor composition load (i.e. induction motors are dominant in the load composition) is an important load class and used for industrial facilities. In this chapter, several case studies are conducted using the sample system to evaluate the accuracy of derived model for voltage and frequency disturbance. A version of this chapter has been published in the proceedings of 2019 IEEE Canadian Electrical Power and Energy Conference (EPEC).

In Chapter 5, a robust short-term power load forecast model of an electrically heated house in St. John's, Newfoundland, Canada is proposed. This method is developed by using neural network based on wavelet transform. SWT are used to decompose the original data and a neural network consists of a Bi-LSTM and a LSTM with dropout layer. The accuracy of the proposed model is evaluated by comparing it against other developed short-term load forecasting models which are subjected to two seasonal load classifications. A version of this chapter has been published by European Journal of Electrical and Computer Engineering, ISSN (Online): 2506-9853.

In Chapter 6, the research outcomes are summarized, and the potential future research scope is addressed.

References

[1] IEEE Task Force on Load Representation for Dynamic Performance, "Load Representation for Dynamic Performance Analysis", *IEEE Trans. Power Syst., vol. 8, no.2, pp. 472 - 482, May 1993.*

[2] A. Ellis, D. Kosterev, and A. Meklin, "Dynamic Load Models: Where Are We?", 2005/2006 IEEE PES Transmission and Distribution Conference and Exhibition, pp. 1320-1324, May 2006.

[3] M. Jin, H. Renmu, and D.J. Hill, "Load modeling by finding support vectors of load data from field measurements," IEEE Trans. Power Syst., vol. 21, no.2, pp. 726 - 735 , May 2006.

[4] H. Renmu, M. Jin, and D.J. Hill, "Composite load modeling via measurement approach," IEEE Trans. Power Syst., vol. 21, no.2, pp. 663 - 672, March 2006.

[5] D. Han, J. Ma, R. He, and Z. Dong, "A Real Application of Measurement-Based Load Modeling in Large-Scale Power Grids and its Validation," IEEE Trans. Power Syst., vol. 24, no.4, pp. 1756 - 1764, November 2009.

[6] Y. Ge, A. J. Flueck, D.-K. Kim, J.-B. Ahn, J.-D. Lee, and D.-Y. Kwon, "An Event-Oriented Method for Online Load Modeling Based on Synchrophasor Data," IEEE Transactions on Smart Grid, vol. 6, no. 4, pp. 2060–2068, July 2015.

[7] J. Kim, K. An, J. Ma, J. Shin, K. Song, J. Park, J. Park, and Kyeon Hur, "Fast and Reliable Estimation of Composite Load Model Parameters Using Analytical Similarity of Parameter Sensitivity," IEEE Trans. Power Syst., vol. 31, no.1, pp. 663 - 671, January 2016.

[8] S. Yu, S. Zhang, and X. Zhang, "Two-step method for the online parameter identification of a new simplified composite load model," IET Generation, Transmission & Distribution, vol. 10, no. 16, pp. 4048–4056, 2016.

[9] J. Kim, J. Ma, K. Sun, J. Lee, J. Shin, Y. Kim, and K. Hur, "A Computationally Efficient Method for Bounding Impacts of Multiple Uncertain Parameters in Dynamic Load Models," IEEE Trans. Power Syst., vol. 34, no.2, pp. 897 - 907, March 2019.

[10] IEEE Task Force on Load Representation for Dynamic Performance, System Dynamic Performance Subcommittee, Power System Engineering Committee, "Standard Load Models for Power Flow and Dynamic Performance Simulation", *IEEE Transactions on Power Systems, Vol.10, No. 3, August 1995, Page(s): 1302 – 1313.*

[11] J. V. Milanović, K. Yamashita. S. M. Villanueva, S. Ž Djokić, and L. M. Korunović, "International Industry Practice on Power System Load Modeling", *IEEE Trans. Power Syst., vol. 28, no. 3, pp. 3038 – 3046, August 2013.*

[12] I.A. Hiskens, and J.V. Milanovic, "Load modelling in studies of power system damping," IEEE Trans. Power Syst., vol. 10, no.4, pp. 1781 - 1788, November 1995.

[13] "U.S. Energy Information Administration - EIA - Independent Statistics and Analysis," *International - U.S. Energy Information Administration (EIA).* [Online]. Available: https://www.eia.gov/international/data/world. [Accessed: 13-May-2020].

[14] C. Kuster, Y. Rezgui, and M. Mourshed, "Electrical load forecasting models: A critical systematic review," *Sustainable Cities and Society, vol. 35, pp. 257–270, 2017.*

[15] C. Keerthisinghe, G. Verbic, and A. C. Chapman, "A Fast Technique for Smart Home Management: ADP With Temporal Difference Learning," *IEEE Transactions on Smart Grid, vol. 9, no. 4, pp. 3291–3303, 2018.*

[16] Y. Wang, D. Gan, M. Sun, N. Zhang, Z. Lu, and C. Kang, "Probabilistic individual load forecasting using pinball loss guided LSTM," *Applied Energy, vol. 235, pp. 10–20, 2019.*

[17] B. Yildiz, J. I. Bilbao, J. Dore, and A. B. Sproul, "Short-term forecasting of individual household electricity loads with investigating impact of data resolution and forecast horizon," *Renewable Energy and Environmental Sustainability, vol. 3, p. 3, 2018.*

[18] "Load Forecasting Case Study - NARUC." [Online]. Available: http://pubs.naruc.org/pub/536E10A7-2354-D714- 5191-A8AAFE45D626 .

[19] W. Kong, Z. Y. Dong, D. J. Hill, F. Luo, and Y. Xu, "Short-Term Residential Load Forecasting Based on Resident Behaviour Learning," *IEEE Transactions on Power Systems, vol. 33, no. 1, pp. 1087–1088, 2018.*

Chapter 2

Literature Review

2.1 Load Model

According to [1], in power system engineering, 'Load' can be defined as 1) 1) Load Device: a device, connected to a power system, that consumes power; 2) System Load: the total power (active and/or reactive power) consumed by all devices connected to a power system; 3) Bus load: a portion of the system that is not explicitly represented in a system model, but rather is treated as if it were a single power-consuming device connected to a bus in the system model; 4) Generator or plant load: the power output of a generator or generating plant. Among these, 'bus load' is the main concern for bulk power system studies.

A load model is a mathematical representation of the relationship between a bus voltage magnitude (V) and the frequency (f) and the real power (P) and reactive power (Q) or current flowing into the bus [1]. In order to analysis the load model with effectively, grouping of loads into several classes are important. As per [1], a load is classified in three categories: 1) residential, 2) commercial and 3) industrial.

A static load models that expresses the active and reactive powers at any instant of time as functions of the bus voltage magnitude (v) and the frequency (f) at the same instant. Static load models are used both for essentially static load components, e.g., resistive and lighting load. The commonly known static load models are exponential load model as shown in (2.1) and (2.2); constant impedance (Z) load model, constant current (I) load model, constant power (P) load

model, ZIP load model as shown in (2.3) and (2.4), EPRI LOADSYN static load model as shown in (5) and (6).

$$P = P_0 \left(\frac{v}{v_0}\right)^p \tag{2.1}$$

$$Q = Q_0 \left(\frac{v}{v_0}\right)^q \tag{2.2}$$

Where, p and q the exponents of (2.1) and (2.2). With these exponents equal to 0, 1, or 2, the model represent constant power, constant current, or constant impedance characteristics, respectively.

$$P = P_0 \left(a_p \left(\frac{v}{v_0}\right)^2 + b_p \left(\frac{v}{v_0}\right) + c_p \right) (1 + k_{pf} \Delta f) \tag{2.3}$$

$$Q = Q_0 \left(a_q \left(\frac{v}{v_0}\right)^2 + b_q \left(\frac{v}{v_0}\right) + c_q \right) (1 + k_{qf} \Delta f) \tag{2.4}$$

Where, $a_p, b_p, c_p, a_q, b_q, c_q, P_{a1}, Q_{a1}$ are the coefficients; k_{pf}, k_{qf} parameters frequency sensitivity.

$$P = P_0 \left\{ P_{a1} \left(\frac{v}{v_0}\right)^{K_{pv1}} \left[1 + K_{pf1} \Delta f\right] + (1 - P_{a1}) \left(\frac{v}{v_0}\right)^{K_{pv2}} \right\} \tag{2.5}$$

$$Q = P_0 \left\{ Q_{a1} \left(\frac{v}{v_0}\right)^{K_{qv1}} \left[1 + K_{qf1} \Delta f\right] + \left(\frac{Q_0}{P_0} - Q_{a1}\right) \left(\frac{v}{v_0}\right)^{K_{qv2}} \left[1 + K_{qf2} \Delta f\right] \right\} \tag{2.6}$$

Where, $K_{pv1}, K_{pv2}, K_{qv1}, K_{qv2}$ voltage exponents for frequency dependent and independent real and reactive power, respectively; K_{pf1}, K_{qf1} are the frequency sensitivity coefficients for real and uncompensated reactive power load; K_{qf2} is the frequency sensitivity coefficient for reactive power compensation.

A dynamic load model that expresses the active and reactive powers at any instant of time as functions of the voltage magnitude and frequency at past instants of time and, usually,

including the present instant. The widely used dynamic load models are induction motor (IM), exponential recovery load model (ERL).

Some scientific papers focus on developing a composite load model, consists of static and dynamic load model. A comparative study among composite load model, static load model and dynamic load model has been conducted in [2], [3] and concludes that composite models can capture more accurate dynamic responses of the loads to disturbance. The widely used composite load models are including a composition of induction motor and ZIP load model [8]-[10]; Complex Load Model (CLOD); and Western Electricity Coordinating Council (WECC) composite load model [4]-[6]. A composite load model consists of ZIP and induction motor is one of appropriate form to describe both dynamic and static properties of the load. [7] estimated that 30% of USA industries practice this model due to its simplicity with clear physical meaning. Mathematically, ZIP model and the induction motor can be represented by third order differential equations [13] and polynomial equations [1], respectively.

There are many published techniques to determine the parameters of load model. Measurement-based approach is usually used in the composite load model based on ZIP and induction motor [8]-[12]. For the measurement-based methods, field measurement data or lab testing results are recorded. Therefore, it provides actual field data to capture load characteristics.

During the past decades, another well-known form for dynamic load studies known transfer function-based load model is reported [14]-[25]. This model also contents static and dynamic properties [16], similar characteristic with the composite load model. In the literature, there are two streams of research on this model: 1) Consider voltage only; 2) Consider both voltage and frequency. Although, most of transfer function-based load model [15],[17],[22]-[24]

mathematically represents the real and reactive power as a function of the bus voltage magnitude (v) and the frequency (f); [17]-[20] considered only the voltage magnitude (v) in order to simplify the model complexity of the model. Therefore, it arises the question that only considering voltage variation is enough to represent the load model or both voltage and frequency variation need to be considered.

Considering only the voltage variation (ΔV), the coefficient of transfer function-based load model can be 1st order [18][19], 2nd order [17][20], or 3rd order [17]. Considering both voltage and frequency variation, the coefficient of this model can be 1st order [17], or 2nd order [15]. Therefore, it raises the question of what order of transfer-functions should be chosen.

However, based on the literature review, there has no comparison between composite load model and transfer function-based load model through the same event and no accuracy of model evaluation by reducing the levels of the model. In this section, the literature review for the research work is focused on load modeling.

2.2 Load Forecast

Load forecasting plays a vital role in planning electricity distribution networks due to proper understanding of the future electric load demand. Improving the accuracy of load forecasting is important to generate scheduling of power system including economic dispatch and reliability. In the literature, researcher focused on short-term load forecasting method for different load scenarios among all power system load forecasting methods due to impact of higher accuracy estimation of electricity demand [37]-[40]. Earlier, load demand was predicted through the help of charts and tables considering weather condition. The methods of load

forecasting have moved from traditional techniques to AI techniques [32] due to more accurate prediction ability compared to others [26],[29]-[31]. The **RNN** method has high performance to predict the short-term load forecasting [33] among modern **AI** techniques including **SVM**, **ANN**, **CNN** and so on.

A hybridization of neural network with wavelet transform or other learning techniques, is most prominent technique that receive more attention for short-term load forecasting. A hybrid deep learning forecasting method provide high performance of load forecasting in terms of time requirement and accuracy due to ability of learning non-stationary and complex time series data. Some of the present hybrid deep learning forecasting techniques are reported in the literature. These methods are a hybrid **ARIMA** and **ANN** with **DWT** based daily peak load forecast [34]; a composition of 1-D **CNN** and **LSTM** based power consumption forecast [35]; a composition of **DWT** and **LSTM** based wind power forecast [36]; a hybrid **DWT** and **CRT** based load forecast [27]; **SWT** with **LSTM** neural network based load forecast [28]. Neural network learns the features of the data [27]-[28],[35]-[36] but it overfits the prediction model for large neural networks [41]. Therefore, it reduces the short-term load forecasting accuracy. In this section, the literature review for the research work is focused on load forecasting method.

2.3 Outcomes of the Thesis

In this thesis, the transfer function-based load model is developed from composite load model for commercial and industrial load. The accuracy of developed load model is verified investigated by several case studies through MATLAB/Simulink simulation. A STLF model is proposed for a house electrical load using RNN with wavelet transform techniques; and proposed model is verified through MATLAB deep learning toolbox and wavelet toolbox by using the collected

current sensors data of a house. The proposed approaches and outcomes of the thesis are described as follows:

- In chapter 3, a transfer function-based load model for commercial load is developed analytically using a composite load model. This model is verified by compering the original composite load model by applying various voltage and frequency disturbances. The influence of voltage and frequency dependency terms on the overall model accuracy for developed model is evaluated by three levels of simplifications of full model.

- In chapter 4, a transfer function-based load model for large motor composition is developed. The dynamic responses of the developed model are compared to original composite model and verified the accuracy of developed model by four cases.

- In chapter 5, a STLF model is developed for a house electrical load using current sensors data of the house. A SWT technique is used to decompose the input data and RNN is used to extract the feature and predict the load. The accuracy of the proposed model is verified by several case studies and can forecast the house electrical load more accurately than other developed model.

References:

[1] IEEE Task Force on Load Representation for Dynamic Performance, "Load Representation for Dynamic Performance Analysis", IEEE Trans. Power Syst., vol. 8, no.2, pp. 472 - 482, May 1993.

[2] W.-S. Kao, C.-J. Lin, C.-T. Huang, Y.-T. Chen, and C.-Y. Chiou, "Comparison of simulated power system dynamics applying various load models with actual recorded data," IEEE Trans. Power Syst., vol. 9, no. 1, pp. 248–254, Feb. 1994.

[3] Li, Yinhong, et al. "Load Models for Modeling Dynamic Behaviors of Reactive Loads: Evaluation and Comparison." *International Journal of Electrical Power & Energy Systems, vol. 30, no. 9, 2008, pp. 497–503., doi:10.1016/j.ijepes.2008.04.007.*

[4] (Jun. 2012). WECC MVWG Load Model Report Ver. 1.0. [Online]. Available: https://www.wecc.biz/Reliability/WECC%20MVWG%20Load%20Model%20Report%20ver%201%200.pdf

[5] D. Kosterev et al., "Load modeling in power system studies: WECC progress update," in Proc. IEEE PES Gen. Meeting, Pittsburgh, PA, USA, 2008, pp. 1–8.

[6] L. Pereira, D. Kosterev, P. Mackin, D. Davies, J. Undrill, and W. Zhu, "An interim dynamic induction motor model for stability studies in the WSCC," IEEE Trans. Power Syst., vol. 17, no. 4, pp. 1108–1115, Nov. 2002.

[7] J. V. Milanović, K. Yamashita. S. M. Villanueva, S. Ž Djokić, and L. M. Korunović, "International Industry Practice on Power System Load Modeling", IEEE Trans. Power Syst., vol. 28, no. 3, pp. 3038 – 3046, August 2013.

[8] H. Renmu, M. Jin, and D. J. Hill, "Composite load modeling via measurement approach," IEEE Trans. Power Syst., vol. 21, no. 2, pp. 663–672, May 2006.

[9] M. Jin, H. Renmu, and D.J. Hill, "Load modeling by finding support vectors of load data from field measurements," *IEEE Trans. Power Syst., vol. 21, no.2, pp. 726 - 735 , May 2006.*

[10] J. Ma, D. Han, R.-M. He, Z.-Y. Dong, and D. J. Hill, "Reducing identified parameters of measurement-based composite load model," IEEE Trans. Power Syst., vol. 23, no. 1, pp. 76–83, Feb. 2008.

[11] D. Han, J. Ma, R.-M. He, and Z.-Y. Dong, “A real application of measurement-based load modeling in large-scale power grids and its validation,” IEEE Trans. Power Syst., vol. 24, no. 4, pp. 1756–1764, Nov. 2009.

[12] J.-K. Kim et al., “Fast and reliable estimation of composite load model parameters using analytical similarity of parameter sensitivity,” IEEE Trans. Power Syst., vol. 31, no. 1, pp. 663–671, Jan. 2016.

[13] Graham J. Rogers, John Di Manno, Robert T.H. Alden, “An Aggregate Induction Motor Model for Industrial Plant”, IEEE Transactions on Power Apparatus and Systems, Vol. PAS-103, No. 4, April 1984, Page(s): 683-690.

[14] X. Liang, “Dynamic load models for industrial facilities,” *PhD thesis, Department of Electrical and Computer Engineering, University of Alberta, Edmonton, AB, Canada, Fall 2013.*

[15] S.A.Y. Sabir, and D.C. Lee, “Dynamic Load Models Derived from Data Acquired During System Transients”, *IEEE Transactions on Power Apparatus and Systems, vol. PAS-101, no. 9, pp. 3365-3372, September 1982.*

[16] I.A. Hiskens, and J.V. Milanovic, “Load modelling in studies of power system damping,” *IEEE Trans. Power Syst., vol. 10, no.4, pp. 1781 - 1788, November 1995.*

[17] C.-J. Lin, A.-T. Chen, C.-Y. Chiou, C.-H. Huang, H.-D. Chiang, J.-C. Wang, and L. Fekih-Ahmed, “Dynamic load models in power systems using the measurement approach,” *IEEE Trans. Power Syst., vol. 8, no. 1, pp. 309–315, February 1993.*

[18] T. Omata, and K. Uemura, “Effects of Series Impedance on Power System Load Dynamics”, *IEEE Trans. Power Syst., vol. 14, no. 3, pp. 1070-1077, August 1999.*

[19] F.T. Dai, J.V. Milanovic, N. Jenkins, and V. Roberts, “Development of a Dynamic Power System Load Model”, *IEE Seventh International Conference on AC-DC Power Transmission, pp. 344-349, November 2001.*

[20] I. F. Visconti, D. A. Lima, J. M. C. d. S. Costa, and N. R. d. B. C. Sobrinho, “Measurement-Based Load Modeling Using Transfer-functions for Dynamic Simulations,” *IEEE Trans. Power Syst., vol. 29, no.1, pp. 111 - 120, January 2014.*

[21] E. O. Kontis, T. A. Papadopoulos, A. I. Chrysochos, and G. K. Papagiannis, "Measurement-Based Dynamic Load Modeling Using the Vector Fitting Technique," *IEEE Trans. Power Syst., vol. 33, no.1, pp. 338 - 351, January 2018.*

[22] X. Liang, "Linearization Approach for Modeling Power Electronics Devices in Power Systems", *IEEE Journal of Emerging and Selected Topics in Power Electronics, vol. 2, no. 4, pp. 1003-1012, December 2014.*

[23] X. Liang and W. Xu, "Modeling variable frequency drives and motor systems in power systems dynamic studies," *in Proc. IEEE IAS Annu. Meeting, pp. 1-11, Oct. 2013.*

[24] X. Liang and J. He, "Load Model for Medium Voltage Cascaded H-Bridge Multi-Level Inverter Drive Systems," *IEEE Power and Energy Technology Systems Journal, vol. 3, no. 1, pp. 13–23, March 2016.*

[25] X. Liang, Y. He, M. Mitolo, and W. Li, "Support Vector Machine Based Dynamic Load Model Using Synchrophasor Data", *Proceedings of IEEE 54th Industrial and Commercial Power Systems (I&CPS) Conference, pp. 1-11, May 2018.*

[26] M. Aydinalp-Koksal and V. I. Ugursal, "Comparison of neural network, conditional demand analysis, and engineering approaches for modeling end-use energy consumption in the residential sector," *Applied Energy, vol. 85, no. 4, pp. 271–296, 2008.*

[27] M. Imani and H. Ghassemian, "Residential load forecasting using wavelet and collaborative representation transforms," *Applied Energy, vol. 253, p. 113505, 2019.*

[28] K. Yan, W. Li, Z. Ji, M. Qi, and Y. Du, "A Hybrid LSTM Neural Network for Energy Consumption Forecasting of Individual Households," *IEEE Access, vol. 7, pp. 157633–157642, 2019.*

[29] M. Aydinalp, V. I. Ugursal, and A. S. Fung, "Modeling of the space and domestic hot-water heating energy-consumption in the residential sector using neural networks," *Applied Energy, vol. 79, no. 2, pp. 159–178, 2004.*

[30] Ringwood JV, Bofell D, Murray FT, "Forecasting electricity demand on short, medium and long time scales using neural networks," *Journal of Intelligent and Robotic Syst 2001;31:129–47.*

[31] Z. W. Geem and W. E. Roper, "Energy demand estimation of South Korea using artificial neural network," *Energy Policy, vol. 37, no. 10, pp. 4049–4054, 2009.*

[32] A. Baliyan, K. Gaurav, and S. K. Mishra, "A Review of Short-Term Load Forecasting using Artificial Neural Network Models," *Procedia Computer Science, vol. 48, pp. 121–125, 2015.*

[33] J. Zheng, C. Xu, Z. Zhang, and X. Li, "Electric load forecasting in smart grids using Long-Short-Term-Memory based Recurrent Neural Network," *2017 51st Annual Conference on Information Sciences and Systems (CISS), 2017.*

[34] A. K. Fard and M.-R. Akbari-Zadeh, "A hybrid method based on wavelet, ANN and ARIMA model for short-term load forecasting," *Journal of Experimental & Theoretical Artificial Intelligence, vol. 26, no. 2, pp. 167–182, 2013.*

[35] J. Kim, J. Moon, E. Hwang, and P. Kang, "Recurrent inception convolution neural network for multi short-term load forecasting," *Energy and Buildings, vol. 194, pp. 328–341, 2019.*

[36] Y. Liu, L. Guan, C. Hou, H. Han, Z. Liu, Y. Sun, and M. Zheng, "Wind Power Short-Term Prediction Based on LSTM and Discrete Wavelet Transform," *Applied Sciences, vol. 9, no. 6, p. 1108, 2019.*

[37] C. Keerthisinghe, G. Verbic, and A. C. Chapman, "A Fast Technique for Smart Home Management: ADP With Temporal Difference Learning," *IEEE Transactions on Smart Grid, vol. 9, no. 4, pp. 3291–3303, 2018.*

[38] Y. Wang, D. Gan, M. Sun, N. Zhang, Z. Lu, and C. Kang, "Probabilistic individual load forecasting using pinball loss guided LSTM," *Applied Energy, vol. 235, pp. 10–20, 2019.*

[39] B. Yildiz, J. I. Bilbao, J. Dore, and A. B. Sproul, "Short-term forecasting of individual household electricity loads with investigating impact of data resolution and forecast horizon," *Renewable Energy and Environmental Sustainability, vol. 3, p. 3, 2018.*

[40] P. Guo, J. C. Lam, and V. O. Li, "Drivers of domestic electricity users' price responsiveness: A novel machine learning approach," *Applied Energy, vol. 235, pp. 900–913, 2019.*

[41] Srivastava, N., G. Hinton, A. Krizhevsky, I. Sutskever, R. Salakhutdinov, "Dropout: A Simple Way to Prevent Neural Networks from Overfitting," *Journal of Machine Learning Research. Vol. 15, pp. 1929-1958, 2014.*

Chapter 3

Comparative Study of Transfer Function-Based Load Model and Composite Load Model

Hla U May Marma[1], *Student Member*, IEEE, Xiaodong Liang[1], *Senior Member*, IEEE, Weixing Li[2], and Huaguang Zhang[3]

[1]Department of Electrical and Computer Engineering, Memorial University of Newfoundland, St. John's, Newfoundland, Canada.

[2]Department of Electrical Engineering, Harbin Institute of Technology, Harbin, Hilongjiang China.

[3]Northeastern University College of Information Science and Engineering, Shenyang, Liaoning, China.

A version of this chapter has been published in *2019 IEEE Industrry Applications Society Annual Meeting*. Hla U May Marma co-authored this paper under the supervision of Dr. Xiaodong Liang. Hla's contributions are listed as follows:

- Performed literature searches required for background information of composite load model transfer function-based load model.
- Implemented transfer function-based load model mathematical derivation from composite load model.
- Conducted comparison of two models through MATLAB/Simulink simulation. Examined the results and depicted the conclusion.
- Involved writing of the paper as the first author.

Dr. Xiaodong Liang provided the main ideas, checked the results, and modified the manuscript. Dr. Weixing Li and Dr. Huaguang Zhang reviewed the manuscript.

This research was supported in part by the Natural Science and Engineering Research Council of Canada (NSERC) Discovery Grant RGPIN-2016-04170.

In this chapter, the manuscript is presented with altered figure numbers, table numbers and reference formats in order to match the thesis formatting guidelines set out by Memorial University of Newfoundland.

Abstract- The composite load model consisting of an induction motor and a static load has been adopted by some utility companies in practical power system dynamic studies. Another form of dynamic load model is the transfer function-based load model. Although both types of dynamic load models are well accepted, there is no comparison done regarding their performance, and no evaluation on the influence of voltage and frequency dependency terms on the overall model accuracy for transfer function-based load models. In this paper, a transfer function-based load model is developed analytically using a composite load model. Dynamic responses of the developed transfer function-based load model and the original composite load model are compared subjected to various voltage and frequency disturbances. The transfer function-based load model is a function of both voltage and frequency, three levels of simplifications are made to the full model in order to evaluate the corresponding accuracy. It is found the reduced model with both the 1^{st} order voltage ΔV term and 1^{st} order frequency Δf term has the smallest error among the three reduced models.

Keywords- Composite load model, induction motors, linearization, static load, transfer function.

3.1 Introduction

Power system planning, operation, and control rely heavily on simulation models. In bulk power system studies, a load refers to the collective power demand at a substation. A load model is a mathematical representation of the relationship between the bus voltage magnitude (V) and the frequency (f), and the real power (P) and reactive power (Q) flowing into the bus, i.e., the load model can be represented mathematically by P = f(V,f), and Q = g(V,f) [1].

The composite load model consists of an induction motor and a static load, which is widely investigated as a dynamic load model for power system dynamic studies in the literature [2]-[10]. A common form of a static load in the composite load model is the ZIP (constant impedance, constant current and constant power) model [4]. Mathematically, the induction motor can be represented by differential equations [11], while the ZIP model can be represented by polynomial equations [1].

In the composite load model, however, the induction motor is represented by the conventional equivalent circuit, identification of the equivalent circuit parameters are the fundamental task of the model creation. The parameters of the composite load model are usually determined using the measurement-based approach based on recorded field measurement data or lab testing results. Due to its simple structure, well defined physical meaning, and the ability to describe both dynamic and static properties of the load, the composite load model has been adopted by many utility companies for practical system studies [10].

Another form of dynamic load model reported in the literature is the transfer function-based load model [11]-[22]. The nature of the power system transfer-function has been investigated in [13], it is found that the power system transfer-function is composed of a static part and a

dynamic part. This characteristic matches with that of a composite load model. The load model is defined as a function of both voltage and frequency, and thus, it has voltage dependency and frequency dependency characteristics. Based on the published papers, the transfer function-based load model developed by the researchers can be categorized into two streams: 1) Consider voltage only; 2) Consider both voltage and frequency.

In [14]-[17][22], only the voltage variation (ΔV) is considered in the transfer function-based load model. The transfer-function as the coefficient of the load model is 1st order [15][16], 2nd order [14][17], or 3rd order [14]. [14] conducted a comparison between 2nd and 3rd order transfer-function, together with a 1st order transfer-function with a different load structure (consider both voltage and frequency). It is found in [14] that the developed 2nd order and 3rd order load model structures are better in capturing load behaviors during transients than the first-order load model structure. However, this conclusion is drawn based on a trial and error basis, there is no explanation in the literature to explain why this occurs in power systems. To determine the proper order of the transfer-function, [22] proposes a variable-order transfer function-based load model, where the automatic derivation of the minimum-required order of the transfer-function for the load model can be achieved through the vector fitting technique. The 2nd order and 3rd order transfer-functions have been shown in [22].

In [12][14], a power system load model is created by considering both voltage and frequency variations. [14] uses the 1st order transfer-function for both voltage and frequency terms for real and reactive power; while [12] proposes a more complicated form, where the reactive power is related to the voltage variation only without involving a transfer-function, but the real power is related to both voltage and frequency variation involving a 2nd order transfer-function. [18]-[20] propose a load model for motor drive systems with 7th order transfer-

functions considering both voltage and frequency variations. However, such load model is for power electronic devices with complicated control systems, it does not well represent general load in power systems.

[12] is the only paper that created both transfer function-based load model and composite load model for a 30 MW paper mill. The transfer-function in [12] has been discussed in above paragraph, and the composite load model consists of an induction motor and a static load (a resistor in parallel with a capacitor). Although each load model is validated by comparing with field measurement data with a separate event, but they have not been compared together through the same event.

The questions to be answered for transfer function-based load model for power systems can be summarized as follows: 1) What is the order of transfer-functions? 2) Should both voltage and frequency variation be considered? If yes, in what order should they be considered, i.e., should we consider ΔV and ΔV^2? 3) What would be the performance comparison between the transfer function-based model and the composite load model for a same system?

In the literature, a composite load model and a transfer function-based load model are both acceptable form of dynamic load models, and the composite load model is more preferred by utility companies partly due to its easier implementation in utility's simulation software and more clear physical meaning [3]. However, there is no comparison conducted for the two load models in the literature for their performance. The voltage and frequency dependency are major characteristics of a load model, however, there is no quantity evaluation regarding errors caused by simplification levels of the model, such as without considering the frequency variation term.

To answer these questions and address existing concerns, in this paper, a transfer function-based load model is derived analytically from a composite load model using the linearization

approach [18]. This composite load model has an induction motor and a static load in the ZIP model form. Once the transfer function-based load model is developed, its dynamic responses are compared with that of the original composite load model. Three levels of simplifications are implemented on the developed transfer function-based load model to evaluate the influence on accuracy due to simplifications. Voltage disturbances, frequency disturbances, and a combination of voltage and frequency disturbances are applied to the load models for performance evaluation.

The major contributions of the paper include: 1) a transfer function-based load model is developed analytically from a composite load model (an induction motor and a ZIP model), the developed full model has a first order voltage term (ΔV), a first order frequency term (Δf), a second order voltage term (ΔV^2), a product of a first order voltage and a first order frequency term ($\Delta V \Delta f$), and a product of a second order voltage and a first order frequency term ($\Delta V^2 \Delta f$), and the coefficients of these voltage and frequency terms are 3rd order transfer-functions, this provides insight why the 3rd order transfer-function appears to have better performance in the past research; 2) the comparison is made between the developed transfer function-based load model with the original composite load model, which has not yet been done in the literature; 3) the accuracy of the transfer function-based load model is evaluated subjected to different levels of simplification.

The paper is arranged as follows: in Section II, the proposed transfer function-based load model is derived analytically from the composite load model; in Section III, the accuracy of the developed transfer function-based load model is verified by several case studies considering different disturbances; in Section IV, the accuracy of the transfer function-based load model is evaluated for different levels of simplification; conclusions are drawn in Section V.

3.2 Mathematical Derivation of a Transfer Function-Based Load Model from a Composite Load Model

A combination of dynamic and static load models is known as a composite load model. An induction motor combined with a ZIP model is a widely used composite load model structure. In this model, the induction motor represents dynamic and steady-state characteristics, and the ZIP model only represents steady-state characteristics. The transfer function-based load model is developed from the composite load model using the linearization approach [18]. Fig. 3.1 represents the transformation from a composite load model to a transfer function-based load model.

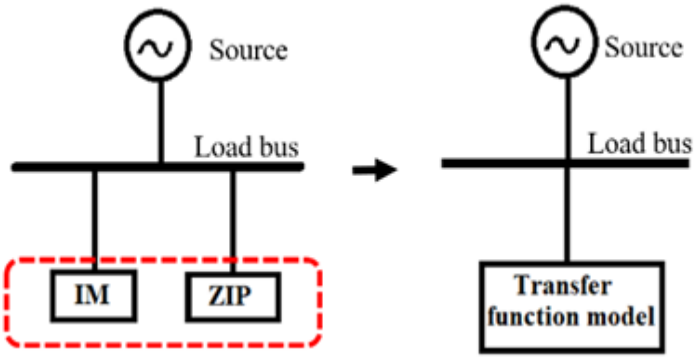

Fig. 3. 1. Transformation from a composite load model to a transfer-function load model.

To derive the transfer function-based load model analytically from the composite load model, the linearization technique is adopted [18] by linearizing the whole system equations including differential equations of the induction motor and polynomial equations of the ZIP model.

The induction motors can be represented by the following differential equations [11]:

$$v_{ds} = R_s i_{ds} - \omega_s \Psi_{qs} + \frac{d\Psi_{ds}}{dt} \quad (3.1)$$

$$v_{qs} = R_s i_{qs} + \omega_s \Psi_{ds} + \frac{d\Psi_{qs}}{dt} \quad (3.2)$$

$$v_{dr} = R_r i_{dr} - (\omega_s - \omega_r)\Psi_{qr} + \frac{d\Psi_{dr}}{dt} \quad (3.3)$$

$$v_{qr} = R_r i_{qr} + (\omega_s - \omega_r)\Psi_{dr} + \frac{d\Psi_{qr}}{dt} \quad (3.4)$$

$$\Psi_{ds} = L_s i_{ds} + L_m i_{dr} \quad (3.5)$$

$$\Psi_{qs} = L_s i_{qs} + L_m i_{qr} \quad (3.6)$$

$$\Psi_{dr} = L_m i_{ds} + L_r i_{dr} \quad (3.7)$$

$$\Psi_{qr} = L_m i_{qs} + L_r i_{qr} \quad (3.8)$$

$$T_e = 1.5P(\Psi_{ds} i_{qs} - \Psi_{qs} i_{ds}) \quad (3.9)$$

$$\frac{d\omega_r}{dt} = \frac{p}{2H}(T_e - T_m) \quad (3.10)$$

$$L_s = l_s + L_m \quad (3.11)$$

$$L_r = l_r + L_m \quad (3.12)$$

$$J = \frac{2H}{p} \quad (3.13)$$

Where,

Ψ_{ds}, Ψ_{qs} stator $d-$ and $q-$ axis flux linkages;

Ψ_{dr}, Ψ_{qr} rotor $d-$ and $q-$ axis flux linkages;

v_{ds}, v_{qs} stator $d-$ and $q-$ axis voltages;

v_{dr}, v_{qr} rotor $d-$ and $q-$ axis voltages;

i_{ds}, i_{qs} stator d- and q- axis currents;

i_{dr}, i_{qr} rotor d- and q- axis currents;

R_s stator resistance;

R_r rotor resistance;

L_m magnetizing inductance;

l_s stator leakage inductance;

L_s total stator inductance;

l_r rotor leakage inductance;

L_r total rotor inductance;

ω_s angular velocity of the stator field in electrical rad/s;

ω_r angular velocity of the rotor field in electrical rad/s;

p number of pole pairs;

J Inertia;

H combined rotor and load inertia constant;

T_e electromagnetic torque;

T_m shaft mechanical torque;

The following two assumptions are considered [13]:

1) the stator transient of induction motor is negligible, i.e.,

$$\frac{d\Psi_{ds}}{dt} = 0 \text{ and } \frac{d\Psi_{qs}}{dt} = 0 \tag{3.14}$$

2) the rotor of induction motor is shorted:

$$v_{dr} = 0 \text{ and } v_{qr} = 0 \tag{3.15}$$

A ZIP model incorporates a constant impedance (Z), a constant current (I), and a constant power (P) term with both voltage and frequency considered as follows [3]:

$$P_{ZIP} = P_{ZIP0}\left(a_p\left(\frac{v}{v_0}\right)^2 + b_p\left(\frac{v}{v_0}\right) + c_p\right)(1 + k_{pf}\Delta f) \tag{3.16}$$

$$Q_{ZIP} = Q_{ZIP0}\left(a_q\left(\frac{v}{v_0}\right)^2 + b_q\left(\frac{v}{v_0}\right) + c_q\right)(1 + k_{qf}\Delta f) \quad (3.17)$$

$$a_p + b_p + c_p = 1 \quad (3.18)$$

$$a_q + b_q + c_q = 1 \quad (3.19)$$

Where, the frequency deviation, $\Delta f = f - f_0$

P_{ZIP}, Q_{ZIP}	real power, reactive power of ZIP model;
P_{ZIP0}, Q_{ZIP0}	real power, reactive power of ZIP model in steady state;
v	voltage of load bus;
v_0	voltage of load bus in steady state;
a_p, a_q	parameters of constant impedance load;
b_p, b_q	parameters of constant current load;
c_p, c_q	parameters of constant power load;
f	load bus frequency;
f_0	load bus frequency in steady state;
k_{pf}, k_{qf}	parameters frequency sensitivity;

Substituting (3.5)-(3.8), (3.14)-(3.17) in (3.1)-(3.4), and (3.9), we have

$$v_{ds} = R_s i_{ds} - \omega_s(L_s i_{qs} + L_m i_{qr}) \quad (3.20)$$

$$v_{qs} = R_s i_{qs} + \omega_s(L_s i_{ds} + L_m i_{dr}) \quad (3.21)$$

$$0 = R_r i_{dr} - (\omega_s - \omega_r)\left(L_m i_{qs} + L_r i_{qr}\right) + L_m \frac{di_{ds}}{dt} + L_r \frac{di_{dr}}{dt} \quad (3.22)$$

$$0 = R_r i_{qr} + (\omega_s - \omega_r)(L_m i_{ds} + L_r i_{dr}) + L_m \frac{di_{qs}}{dt} + L_r \frac{di_{qr}}{dt} \quad (3.23)$$

$$T_e = 1.5P(i_{dr} i_{qs} - i_{qr} i_{ds}) \quad (3.24)$$

Linearize (3.22)-(3.26) and use Laplace transform to convert time-domain variables to frequency-domain variables as expressed as follows:

$$\Delta v_{ds} = R_s \Delta i_{ds} - \omega_{s0} L_s \Delta i_{qs} - \omega_{s0} L_m \Delta i_{qr} - \left(L_s i_{qs0} + L_m i_{qr0}\right)\Delta\omega_s \quad (3.25)$$

$$\Delta v_{qs} = R_s \Delta i_{qs} + \omega_{s0} L_s \Delta i_{ds} + \omega_{s0} L_m \Delta i_{dr} + (L_s i_{ds0} + L_m i_{dr0})\Delta\omega_s \quad (3.26)$$

$$0 = (R_r + L_r S)\Delta i_{dr} + (\omega_{r0} - \omega_{s0}) L_m \Delta i_{qs} + (\omega_{r0} - \omega_{s0}) L_r \Delta i_{qr} + L_m S \Delta i_{ds} + \left(L_m i_{qs0} + L_r i_{qr0}\right)\Delta\omega_r - \left(L_m i_{qs0} + L_r i_{qr0}\right)\Delta\omega_s \quad (3.27)$$

$$0 = (R_r + L_r S)\Delta i_{qr} + L_m S \Delta i_{qs} - (\omega_{r0} - \omega_{s0}) L_m \Delta i_{ds} - (\omega_{r0} - \omega_{s0}) L_r \Delta i_{dr} - (L_m i_{ds0} + L_r i_{dr0})\Delta\omega_r + (L_m i_{ds0} + L_r i_{dr0})\Delta\omega_s \quad (3.28)$$

$$S\Delta\omega_r = \frac{3p^2 L_m}{4H}\left(i_{dr0}\Delta i_{qs} - i_{qr0}\Delta i_{ds} + i_{qs0}\Delta i_{dr} - i_{ds0}\Delta i_{qr}\right) \quad (3.29)$$

The power source voltage in dq reference frame can be expressed by

$$v_{dg} = 0 \quad (3.30)$$

$$v_{qg} = \sqrt{2}E \quad (3.31)$$

Since the source voltage is directly applied to the motor stator in this configuration, therefore, we have

$$v_{ds} = v_{dg} \quad (3.32)$$

$$v_{qs} = v_{qg} \quad (3.33)$$

The real power P and the reactive power Q of the induction motor can be formulated by

$$P_{IM} = \frac{3}{2}\left(v_{ds} i_{ds} + v_{qs} i_{qs}\right) \quad (3.34)$$

$$Q_{IM} = \frac{3}{2}\left(v_{qs} i_{ds} - v_{ds} i_{qs}\right) \quad (3.35)$$

Substitute (3.32)-(3.33) in (3.34) and (3.35), we have

$$P_{IM} = \frac{3}{2}\left(\sqrt{2} E i_{qs}\right) \quad (3.36)$$

$$Q_{IM} = \frac{3}{2}(\sqrt{2}Ei_{ds}) \quad (3.37)$$

For the real power P, the Taylor expansion for (3.36) can be rewritten as follows:

$$P_{IM} = P_{IM0} + a_E\Delta E + a_{iqs}\Delta i_{qs} + a_{Eiqs}\Delta E\Delta i_{qs} \quad (3.38)$$

For the reactive power Q, the Taylor expansion for (3.37) can be rewritten as follows:

$$Q_{IM} = Q_{IM0} + b_E\Delta E + b_{ids}\Delta i_{ds} + a_{Eids}\Delta E\Delta i_{ds} \quad (3.39)$$

Where, the voltage variation $\Delta E = E - E_0$

$$a_E = \frac{3}{2}(\sqrt{2}i_{qs0}) \quad (3.40)$$

$$a_{iqs} = \frac{3}{2}(\sqrt{2}E_0) \quad (3.41)$$

$$a_{Eiqs} = \frac{3}{\sqrt{2}} \quad (3.42)$$

$$b_E = \frac{3}{2}(\sqrt{2}i_{ds0}) \quad (3.43)$$

$$b_{ids} = \frac{3}{2}(\sqrt{2}E_0) \quad (3.44)$$

$$b_{Eids} = \frac{3}{\sqrt{2}} \quad (3.45)$$

Where,

v_{dg}, v_{qg}	d- and q- axis power source voltages;
E	rms phase-to-ground voltage of load bus;
E_0	rms phase-to-ground voltage of load bus in steady-state;
P_{IM}, Q_{IM}	real power, reactive power of induction motor;
P_{IM0}, Q_{IM0}	real power, reactive power of induction motor in steady state;
i_{ds0}, i_{qs0}	d- and q- axis currents in steady state;

The induction motor load model can be obtained by rewriting (3.38) and (3.39) as follows:

$$P_{IM} = P_{IM0} + GP_{EIM}\Delta E + GP_{fIM}\Delta f + GP_{E2IM}\Delta E^2 + GP_{EfIM}\Delta E\Delta f \quad (3.46)$$

$$Q_{IM} = Q_{IM0} + GQ_{EIM}\Delta E + GQ_{fIM}\Delta f + GQ_{E2IM}\Delta E^2 + GQ_{EfIM}\Delta E\Delta f \quad (3.47)$$

Where, the coefficients are expressed by

$$GP_{EIM} = \frac{F_{11}S^3+F_{12}S^2+F_{13}S+F_{14}}{N_1S^3+N_2S^2+N_3S+N_4} \quad (3.48)$$

$$GP_{fIM} = \frac{F_{21}S^3+F_{22}S^2+F_{23}S+F_{24}}{N_1S^3+N_2S^2+N_3S+N_4} \quad (3.49)$$

$$GP_{E2IM} = \frac{F_{31}S^3+F_{32}S^2+F_{33}S+F_{34}}{N_1S^3+N_2S^2+N_3S+N_4} \quad (3.50)$$

$$GP_{EfIM} = \frac{F_{41}S^3+F_{42}S^2+F_{43}S+F_{44}}{N_1S^3+N_2S^2+N_3S+N_4} \quad (3.51)$$

$$GQ_{EIM} = \frac{F_{51}S^3+F_{52}S^2+F_{53}S+F_{54}}{N_1S^3+N_2S^2+N_3S+N_4} \quad (3.52)$$

$$GQ_{fIM} = \frac{F_{61}S^3+F_{62}S^2+F_{63}S+F_{64}}{N_1S^3+N_2S^2+N_3S+N_4} \quad (3.53)$$

$$GQ_{E2IM} = \frac{F_{71}S^3+F_{72}S^2+F_{73}S+F_{74}}{N_1S^3+N_2S^2+N_3S+N_4} \quad (3.54)$$

$$GQ_{EfIM} = \frac{F_{81}S^3+F_{82}S^2+F_{83}S+F_{84}}{N_1S^3+N_2S^2+N_3S+N_4} \quad (3.55)$$

The load model for induction motors are (3.46) and (3.47), their coefficients are 3rd order transfer-functions as specified in (3.48)-(3.55). In (3.48)-(3.55), the coefficients, $F_{11}, F_{12}, \dots, F_{83}, F_{84}, \dots, N_3, N_4$, are characteristic parameters in real constant numbers. In this load model, there are four terms: a first order voltage term (ΔV), a first order frequency term (Δf), and a term with the product of the first order voltage and first order frequency (ΔVΔf).

The ZIP load model can be written in the similar format, and Eqs. (3.16) and (3.17) can be rewritten as follows:

$$P_{ZIP} = P_{ZIP0} + GP_{EZIP}\Delta E + GP_{fZIP}\Delta f + GP_{E2ZIP}\Delta E^2 + GP_{EfZIP}\Delta E\Delta f + GP_{E2fZIP}\Delta E^2\Delta f$$

(3.56)

$$Q_{ZIP} = Q_{ZIP0} + GQ_{EZIP}\Delta E + GQ_{fZIP}\Delta f + GQ_{E2ZIP}\Delta E^2 + GQ_{EfZIP}\Delta E\Delta f + GQ_{E2fZIP}\Delta E^2\Delta f$$

(3.57)

Where, the coefficients are expressed by

$$GP_{EZIP} = \frac{P_{ZIP0}(b_p+2a_p)}{E_0} \quad (3.58)$$

$$GP_{fZIP} = P_{ZIP0}k_{pf} \quad (3.59)$$

$$GP_{E2ZIP} = \frac{P_{ZIP0}a_p}{{E_0}^2} \quad (3.60)$$

$$GP_{EfZIP} = \frac{P_{ZIP0}(b_p+2a_p)k_{pf}}{E_0} \quad (3.61)$$

$$GP_{E2fZIP} = \frac{P_{ZIP0}a_p k_{pf}}{{E_0}^2} \quad (3.62)$$

$$GQ_{EZIP} = \frac{Q_{ZIP0}(b_q+2a_q)}{E_0} \quad (3.63)$$

$$GQ_{fZIP} = Q_{ZIP0}k_{qf} \quad (3.64)$$

$$GQ_{E2ZIP} = \frac{Q_{ZIP0}a_q}{{E_0}^2} \quad (3.65)$$

$$GQ_{EfZIP} = \frac{Q_{ZIP0}(b_q+2a_q)k_{qf}}{E_0} \quad (3.66)$$

$$Gq_{E2fZIP} = \frac{Q_{ZIP0}a_q k_{qf}}{{E_0}^2} \quad (3.67)$$

In the ZIP load model represented by (3.56) and (3.57), the $\Delta E^2\Delta f$ term is ignored as the influence of the high order terms are much smaller.

The transfer function-based load model transformed from the composite load model is derived by

$$P = P_{IM} + P_{ZIP} \quad (3.68)$$

$$Q = Q_{IM} + Q_{ZIP} \tag{3.69}$$

The final form of the load model is

$$P = P_0 + GP_1\Delta E + GP_2\Delta f + GP_3\Delta E^2 + GP_4\Delta E\Delta f \tag{3.70}$$

$$Q = Q_0 + GQ_1\Delta E + GQ_2\Delta f + GQ_3\Delta E^2 + GQ_4\Delta E\Delta f \tag{3.71}$$

Where, the initial real power P0 and reactive power Q0 are

$$P_0 = P_{IM0} + P_{ZIP0}$$

$$Q_0 = Q_{IM0} + Q_{ZIP0}$$

$$GP_1 = \frac{P_{11}S^3+P_{12}S^2+P_{13}S+P_{14}}{N_1S^3+N_2S^2+N_3S+N_4} \tag{3.72}$$

$$GP_2 = \frac{P_{21}S^3+P_{22}S^2+P_{23}S+P_{24}}{N_1S^3+N_2S^2+N_3S+N_4} \tag{3.73}$$

$$GP_3 = \frac{P_{31}S^3+P_{32}S^2+P_{33}S+P_{34}}{N_1S^3+N_2S^2+N_3S+N_4} \tag{3.74}$$

$$GP_4 = \frac{P_{41}S^3+P_{42}S^2+P_{43}S+P_{44}}{N_1S^3+N_2S^2+N_3S+N_4} \tag{3.75}$$

$$GQ_1 = \frac{Q_{11}S^3+Q_{12}S^2+Q_{13}S+Q_{14}}{N_1S^3+N_2S^2+N_3S+N_4} \tag{3.76}$$

$$GQ_2 = \frac{Q_{21}S^3+Q_{22}S^2+Q_{23}S+Q_{24}}{N_1S^3+N_2S^2+N_3S+N_4} \tag{3.77}$$

$$GQ_3 = \frac{Q_{31}S^3+Q_{32}S^2+Q_{33}S+Q_{34}}{N_1S^3+N_2S^2+N_3S+N_4} \tag{3.78}$$

$$GQ_4 = \frac{Q_{41}S^3+Q_{42}S^2+Q_{43}S+Q_{44}}{N_1S^3+N_2S^2+N_3S+N_4} \tag{3.79}$$

This developed transfer function-based load model are represented by (3.70) and (3.71), taking the same format as the induction motor model. Their coefficients are 3rd order transfer-functions as specified in (3.72)-(3.79). In (3.72)-(3.79), the coefficients, $P_{11}, P_{12}, \dots, Q_{43}, Q_{44}$, $\dots, N_3, N_4$, are characteristic parameters in real constant numbers.

In the composite load model, the level of the induction motor load in the total load is defined by, $K_{pm} = \frac{P_{IM0}}{P_0}$.

Because a power system can be essentially represented by an induction motor and a static load, therefore, the 3rd order transfer-functions in the load model developed in this study can represent a general large power system, it provides theoretical explanation why the 3rd order transfer-functions have good performance through previous trial and error practice when building a transfer function-based load model.

3.3 Case Study through a Motor Load Composition

The derived transfer function-based load model is verified by comparing with the original composite load model through MATLAB/Simulink simulation using a case study. In this case study, a composite load model consisting of a 25 HP induction motor and a 120 kW ZIP static load model, they are parallel connected to the load bus. A three phase programmable voltage source is used to determine real and reactive power at the load bus. It is assumed that the source voltage is directly applied to the load bus. As the source voltage is directly connected to the induction motor stator, the relationship between parameters of the source voltage and the induction motor are linked together easily.

The composite load model built in Simulink is shown in Fig. 3.2(a). The derived transfer function-based load model for real and reactive power equations are built in Simulink as shown in Figs. 3.2(b) and 3.2(c), respectively. The transfer function-based load model includes both voltage and frequency terms, which represents voltage and frequency dependency of the load model. To verify their dynamic performance, the same voltage and frequency disturbances are applied to both models in Fig. 3.2(a) and Figs. 3.2(b) & 3.2(c). In this section, four fault cases

are considered. In each case, the voltage disturbance and/or frequency disturbance occur(s) at 2.33 s and clear(s) at 0.53 s.

To evaluate the accuracy of dynamic response characteristic curves between the derived transfer function-based load model and the composite load model, RMSE [23] and the Relative Error are calculated. The RMSE is used to measure how accurately the model fit the response. A lower value of RMSE indicates a better fit. The Relative Error in percentage (%) is scale independent and considered for a good measure.

$$RMSE = \sqrt{\frac{1}{n} \times \sum_{i=1}^{n} (L_a - L_f)^2} \tag{3.80}$$

$$Relative\ error = \frac{\sqrt{\frac{1}{n} \times \sum_{i=1}^{n} (L_a - L_f)^2}}{\sqrt{\frac{1}{n} \times \sum_{i=1}^{n} {L_f}^2}} \times 100 \tag{3.81}$$

3.3.1 Data Preparation

In the Case Study, the static load is playing the dominant role i.e. Kpm is small (Kpm =0.124). The parameters of the induction motor and the ZIP load model inside the composite load model are listed in Table 3.1. The parameters for the induction motor from [18] and the parameters for the ZIP model from [6] are adopted. These parameters are used to calculate coefficients of the 3rd order transfer-functions of the load model, which are given in Table 3.2. These coefficients are used as the transfer-function blocks in Figs. 3.2(b) and 3.2(c).

Table 3. 1: Parameters of the induction motor and the zip static load in the composite load model used in the case study

Components	Parameters
Induction motor [18]	Nominal power =25 HP Nominal voltage $v_b = 460$ V(rms) Nominal frequency $f_{rated} = 60$ Hz $R_s = 0.249\ \Omega$; $l_s = 0.0015$ H; $R_r = 0.536\ \Omega$ $l_r = 0.0015$ H; $L_m = 58.7 \times 10^{-3}$ H Inertia, $J = 0.554$ kgm2 Nominal speed, $n_{rated} = 1695$ rpm Pole pairs, $p = 2$ Load torque, $T_L = 87.5$ Nm Target speed, $n_r = 1695$ rpm
ZIP static load [6]	Real power in steady-state, $P_{ZIP0} = 120$ kW Power factor = 0.88 $a_p = 0.28$; $b_p = 0.75$; $c_p = -0.03$ $a_q = 0.20$; $b_q = 0.82$; $c_q = -0.02$ $k_{pf} = 0.14$; $k_{qf} = 0.29$
Power Source	Rated voltage 480 V (rms) Rated frequency $f_g = 60$ Hz

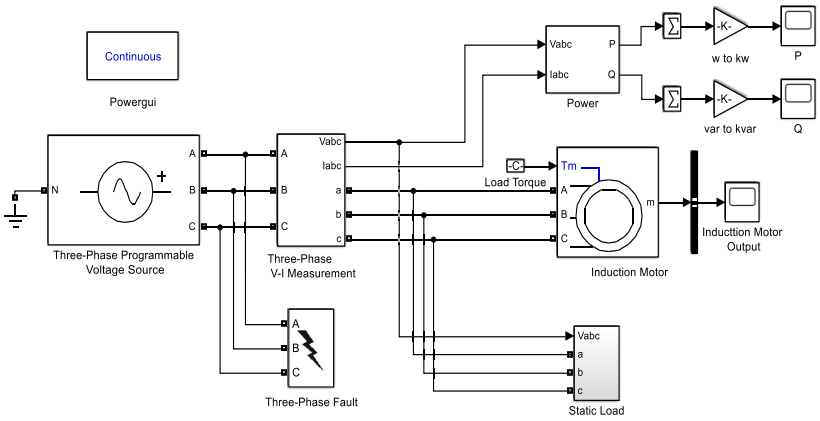

(a)

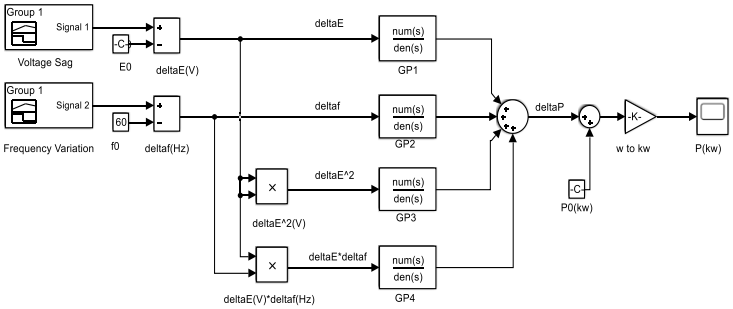

(b)

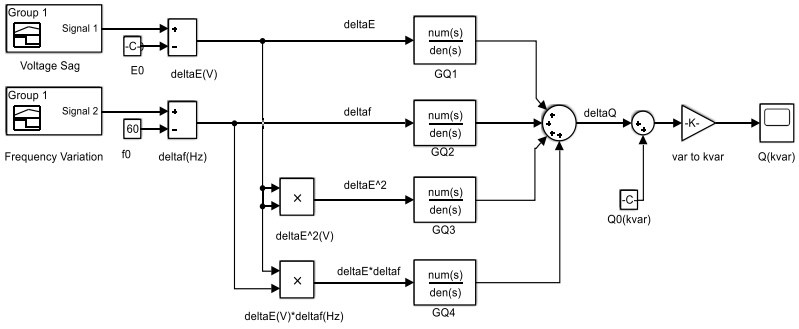

(c)

Fig. 3. 2. The Simulink model structure: (a) the composite load model; (b) the transfer function-based load model for real power; (c) the transfer function-based load model for reactive power.

Table 3. 2: Coefficients of the transfer-function load model in the case study

Coefficients	Detailed transfer-functions
GP_1	$\frac{2.7992\times10^3S^3+7.8789\times10^5S^2+8.7925\times10^7S+5.8218\times10^8}{3.4616S^3+1.1962\times10^3S^2+1.2101\times10^5S+1.0339\times10^6}$
GP_2	$\frac{5.5539\times10^4S^3+2.4028\times10^7S^2+2.7096\times10^9S+1.7774\times10^{10}}{3.4616S^3+1.1962\times10^3S^2+1.2101\times10^5S+1.0339\times10^6}$
GP_3	$\frac{3.4892S^3+558.4885S^2+8.6154\times10^3S+1.2607\times10^5}{3.4616S^3+1.1962\times10^3S^2+1.2101\times10^5S+1.0339\times10^6}$
GP_4	$\frac{265.4623S^3+1.0918\times10^5S^2+1.2051\times10^7S+8.3567\times10^7}{3.4616S^3+1.1962\times10^3S^2+1.2101\times10^5S+1.0339\times10^6}$
GQ_1	$\frac{3.5893\times10^3S^3+8.5802\times10^5S^2+4.9076\times10^7S+3.4656\times10^8}{3.4616S^3+1.1962\times10^3S^2+1.2101\times10^5S+1.0339\times10^6}$
GQ_2	$\frac{5.3539\times10^4S^3+1.9760\times10^7S^2+2.3716\times10^9S+1.9254\times10^{10}}{3.4616S^3+1.1962\times10^3S^2+1.2101\times10^5S+1.0339\times10^6}$
GQ_3	$\frac{9.4376S^3+1.8818\times10^3S^2+5.4239\times10^4S+2.0091\times10^5}{3.4616S^3+1.1962\times10^3S^2+1.2101\times10^5S+1.0339\times10^6}$
GQ_4	$\frac{244.4453S^3+8.9014\times10^4S^2+1.0349\times10^7S+8.4783\times10^7}{3.4616S^3+1.1962\times10^3S^2+1.2101\times10^5S+1.0339\times10^6}$

3.3.2 Case 1: 90% Voltage Sag

In Case 1, a 90% voltage sag is applied to the source of both the composite load model (Fig. 3.2(a)) and the transfer function-based load model (Figs. 3.2(b) and 3.2(c)). The dynamic responses of the real and reactive power for both models during the event are shown in Fig. 3.3. It is noted that due to linearization, the transfer function-based load model doesn't fit the transient response of the composite load model point by point, but rather predicts faster decay of the transient.

Table 3.3 show that the Relative Error and RMSE of real power for Case 1 with respect to the composite load model are 0.1718% and 0.9107, respectively. Table 3.4 show that the Relative Error and RMSE of reactive power for Case 1 are 0.2142% and 1.0828, respectively. Therefore, dynamic responses of the transfer function-based load model match that of the

composite load model quite accurately in Case 1. The errors between the two models are due to the linearization of the nonlinear induction motor.

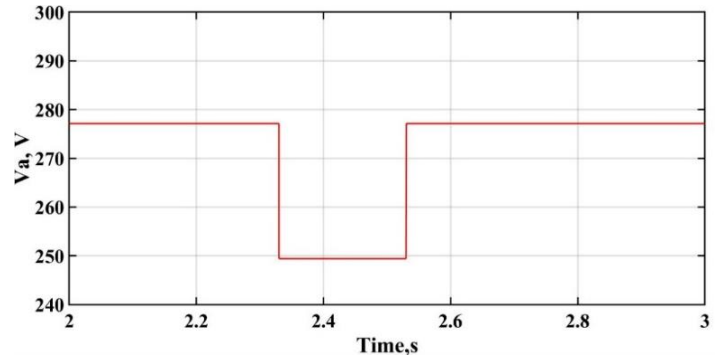

(a)

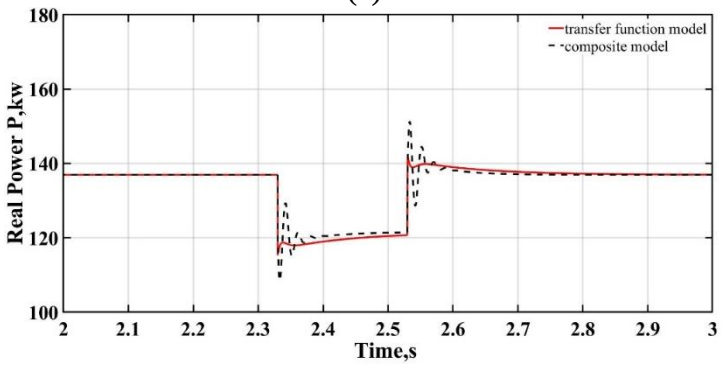

(b)

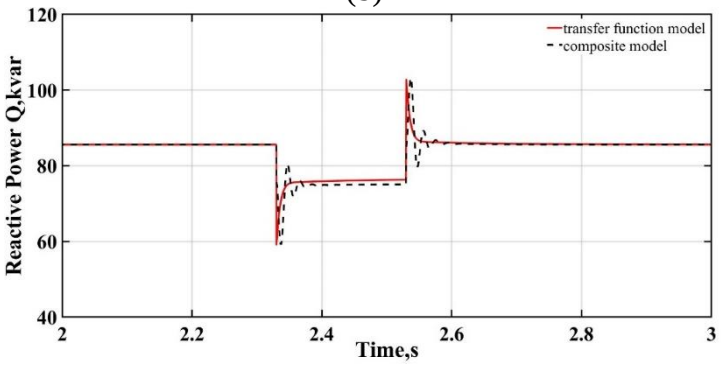

(c)

Fig. 3. 3. Dynamic responses of both load models for a 90% voltage sag (Case 1): (a) voltage sag for both models; (b) real power; (c) reactive power.

3.3.3 Case 2: 50% Voltage Sag

A 50% voltage sag is applied in Case 2 to evaluate the accuracy of the transfer function-based load model on a more severe voltage disturbance. The dynamic responses for a 50% voltage sag fluctuates more than a smaller voltage sag, as shown in Fig. 3.4, but the dynamic characteristics of the transfer function-based load model follows the trend of the composite load model.

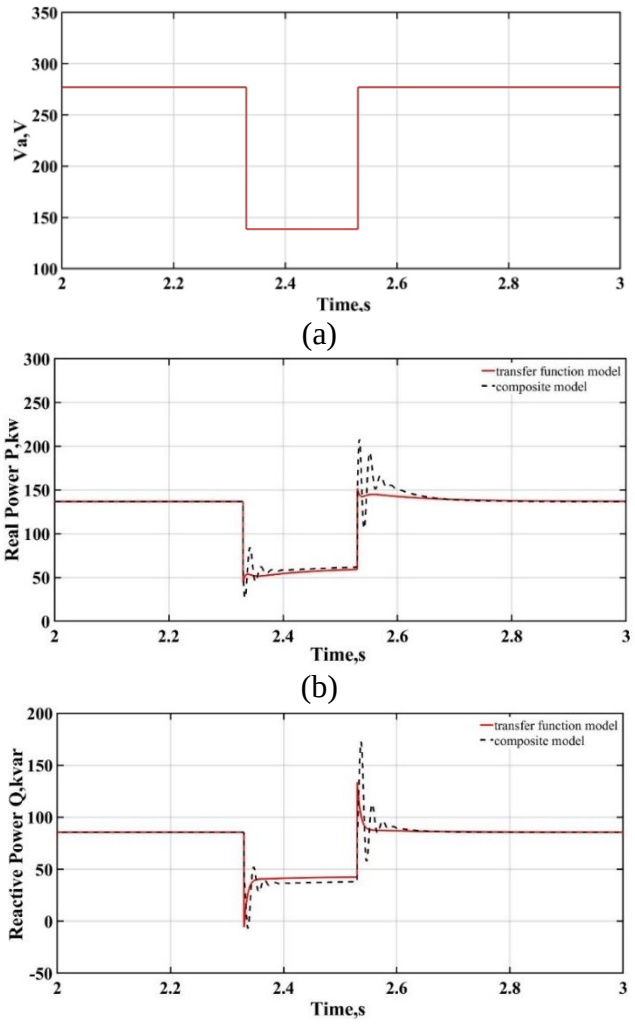

Fig. 3. 4. Dynamic response of the two load models for a 50% voltage sag (Case 2): (a) voltage for both transfer-function load model and composite load model; (b) real power; (c) reactive power

Table 3.3 show that the Relative Error and RMSE of real power for Case 2 with respect to the composite load model are 0.9512% and 4.1852, respectively. Table 3.4 show that the Relative Error and RMSE of reactive power for Case 2 are 3.6642% and 4.5672, respectively. The errors in Case 2 between the two models responses are much larger than the small 90% voltage sag.

3.3.4 Case 3: A Frequency Sag

To verify the accuracy of the derived transfer function-based load model for frequency disturbances, a large frequency drop (1 Hz) is applied to both models. The dynamic responses of the two load models for Case 3 are compared in Fig. 3.5. Both models have minor dynamic variations for this disturbance. They match well in general.

Table 3.3 show that the Relative Error and RMSE of real power for Case 3 with respect to the composite load model are 0.2616% and 1.0070, respectively. Table 3.4 show that the Relative Error and RMSE of reactive power for Case 3 are 0.1467% and 0.2866, respectively.

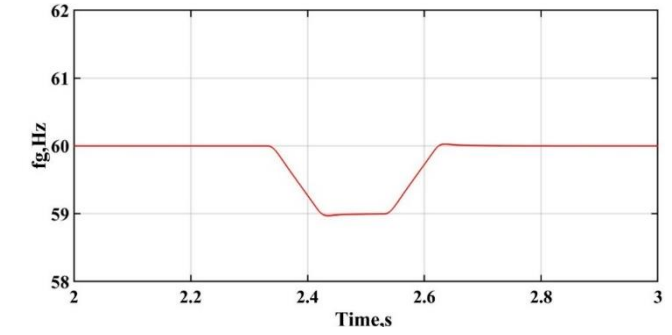

(a)

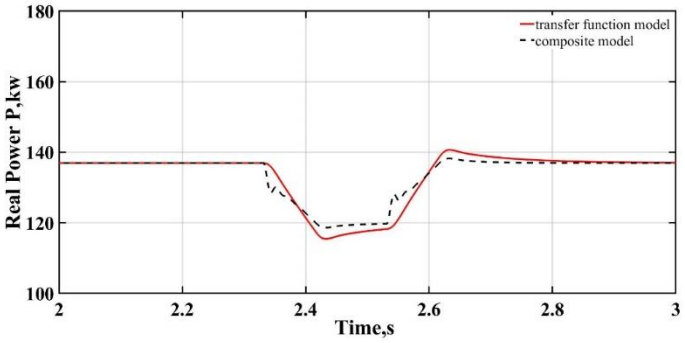

(b)

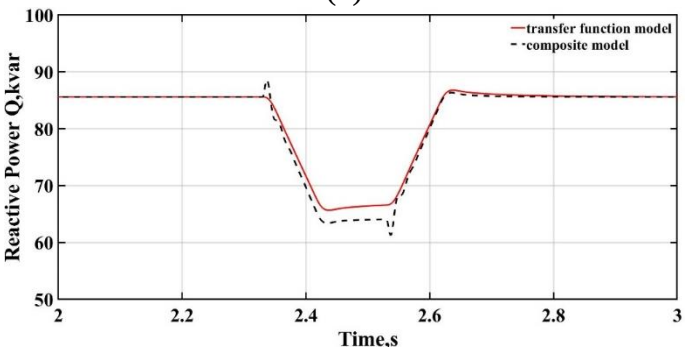

(c)

Fig. 3. 5. Dynamic responses of both models for a 1 Hz frequency sag (Case 3): (a) frequency sag for both models; (b) real power; (c) reactive power.

3.3.5 Case 4: A combination of a 50% Voltage Sag and a Frequency Sag

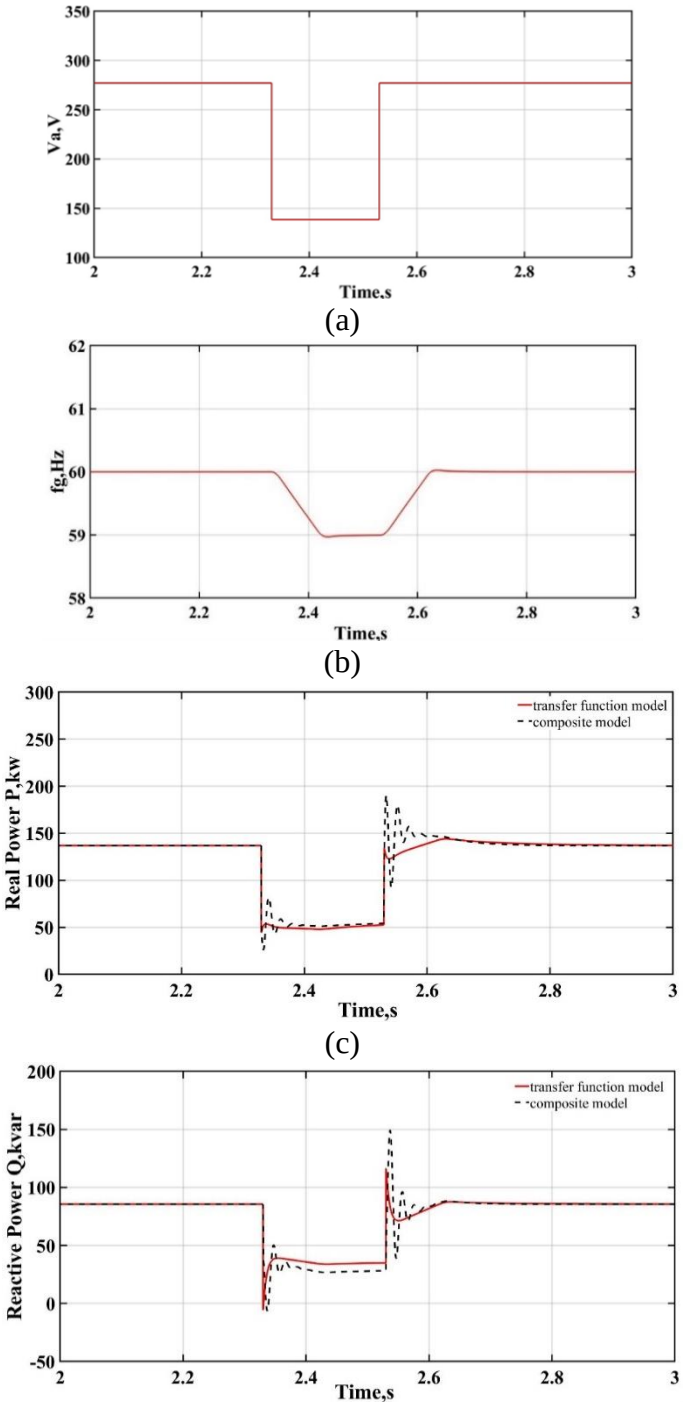

Fig. 3. 6. Dynamic response of both models for a 50% voltage sag and 1 Hz frequency drop (Case 4): (a) voltage sag for both models; (b) frequency drop for both models; (c) real power; (d) reactive power.

Voltage and frequency disturbances are combined in Case 4. A 50% voltage sag along with 1 Hz frequency drop is applied to both models. The dynamic responses of real and reactive power for both models in Case 4 are compared in Fig. 3.6. Under this combined disturbance, it shows larger discrepancies at transient responses, however, the transfer function-based load model still follows the trend of the composite load model well.

Table 3. 3: Errors between transfer function-based load model and composite load model for real power

Cases	Relative Error (%)	RMSE (kw)
Case 1: 90% voltage sag	0.1718	0.9107
Case 2: 50% voltage sag	0.9512	4.1852
Case 3: 1 Hz frequency drop	0.2616	1.0070
Case 4: a combination of a 50% voltage sag and 1 Hz frequency drop	1.0982	4.4209

Table 3. 4: Error between transfer function-based load model and composite load model for reactive power

Cases	Relative Error (%)	RMSE(kvar)
Case 1: 90% voltage sag	0.2142	1.0828
Case 2: 50% voltage sag	3.6642	4.5672
Case 3: 1 Hz frequency drop	0.1467	0.2866
Case 4: a combination of a 50% voltage sag and 1 Hz frequency drop	3.1118	4.7154

Table 3.3 show that the Relative Error and RMSE of real power for Case 4 with respect to the composite load model are 1.0982% and 4.4209, respectively. Table 3.4 show that the

Relative Error and RMSE of reactive power for Case 4 are 3.1118% and 4.7154, respectively. It is found that voltage dependency is more dominant than the frequency dependency even for a large frequency sag at the scale of 1 Hz. The reactive power responses show larger errors than the real power responses between the two models.

Based on Tables 3.3 and 3.4, dynamic responses of real power in most cases are less divergent compared to the corresponding dynamic responses of reactive power. The frequency drop has relatively less effect on the errors than voltage sags, and the errors for 1 Hz frequency drop alone is very small.

In general, dynamic responses of both models match very well on the trend, which verifies that the transfer function-based load model has adequate accuracy for any type of voltage and frequency disturbances compared to the original composite load model.

3.4 Simplification of Transfer Function-Based Load Model

In this section, three levels of the simplification are made toward the derived transfer-function load model in Equation (3.70) and (3.71) to evaluate their accuracy comparing with the original composite load model. The transfer-function load model has a 1st order voltage term (ΔV), a 2nd order voltage term (ΔV^2), a 1st order frequency term (Δf), and the product of the 1st order voltage and 1st order frequency term ($\Delta V \Delta f$). Three simplified load models are considered from the full model: 1) Scenario 1– with the 1st order voltage term alone as shown in (3.82) and (3.83); 2) Scenario 2 – with the 1st and 2nd order voltage terms as shown in (3.84) and (3.85); 3) Scenario 3 –with the 1st order voltage and 1st order frequency terms as shown in (3.86) and (3.87). Scenarios 1 and 2 consider only the voltage dependency of the load model,

and Scenario 3 considers both voltage and frequency dependency.

$$P = P_0 + GP_1\Delta E \tag{3.82}$$

$$Q = Q_0 + GQ_1\Delta E \tag{3.83}$$

$$P = P_0 + GP_1\Delta E + GP_3\Delta E^2 \tag{3.84}$$

$$Q = Q_0 + GQ_1\Delta E + GQ_3\Delta E^2 \tag{3.85}$$

$$P = P_0 + GP_1\Delta E + GP_2\Delta f \tag{3.86}$$

$$Q = Q_0 + GQ_1\Delta E + GQ_2\Delta f \tag{3.87}$$

To evaluate level accuracy is represented by each reduced model, the same voltage and frequency disturbances are applied to the transfer function-based full load model, the composite load model, and the reduced transfer function-based load model. In each case, the voltage and/or frequency disturbances occur at 2.33 s with a duration of 0.2 s. The mean square error (MSE) is added to the error evaluation together with RMSE and Relative Error, which can be calculated by

$$MSE = \frac{1}{n} \times \sum_{i=1}^{n} (L_a - L_f)^2 \tag{3.88}$$

3.4.1 Scenario 1 - 1st Order Voltage Term

In Scenario 1, the reduced transfer function-based load model only consider the 1st order voltage term alone ((3.82) and (3.83)). This is a very commonly used format for transfer function-based load models reported in the literature. Since there is no frequency dependency considered, the error caused by frequency variations must be evaluated.

To provide proper verification, we apply two types of disturbances, one type is the voltage sag alone, another type is the combination of voltage sag and frequency variation. In real life,

both types of disturbances occur, and a voltage sag is often accompanied by a frequency variation.

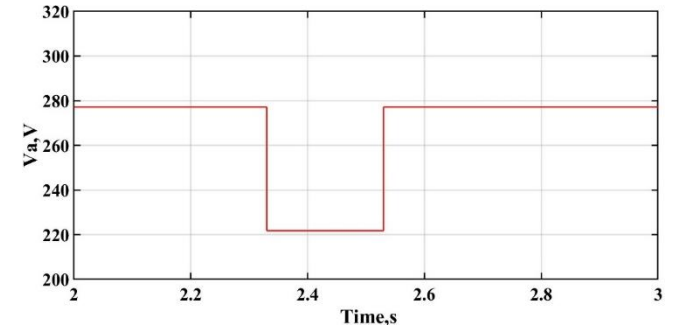

(a)

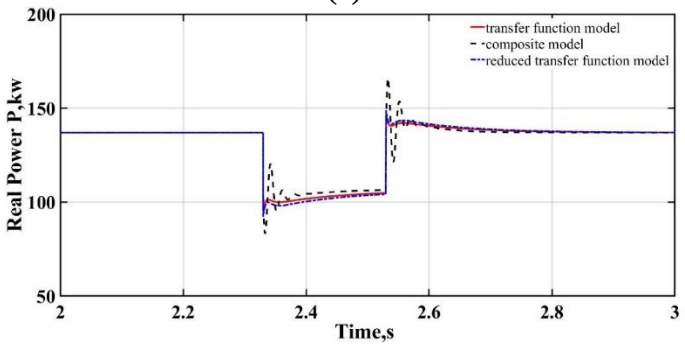

(b)

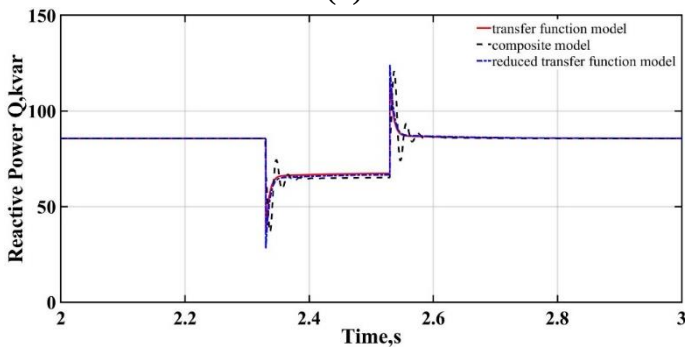

(c)

Fig. 3. 7. Dynamic responses of the composite load model, and transfer function-based full and reduced models (Scenario 1) for an 80% voltage sag; (a) voltage sag for the three models; (b) real power; (c) reactive power.

Firstly, it is assumed that the power source frequency remains constant, an 80% voltage sag is applied at 2.33 s with a duration of 0.2 s to the three models (the composite load model, the transfer function-based full model and reduced model in Scenario 1). Dynamic responses of real

and reactive power for this event are shown in Fig. 3.7. It is found that the three models are matching very well when the fault is a voltage disturbance only.

Secondly, a combination of an 80% voltage sag and a 1Hz frequency drop is applied to the three models at 2.33 s with a duration of 0.2 s. Dynamic responses of real and reactive power for this event are shown in Fig. 3.8. It is found that the reduced model has a large discrepancy compared to the other two models because the reduced model does not have frequency term to include the frequency variation effect.

Tables 3.5 and 3.6 show errors of dynamic responses for both real and reactive power between the transfer function-based full or reduced model and the composite load model. For Scenario 1, when the fault is only a voltage disturbance, the reduced model only shows a slightly higher error than the full model vs. the composite load model. However, when the fault is with both voltage and frequency disturbances, the reduced model in Scenario 1 create significantly large errors compared to the full model. For example, the MSE error of real power responses is 2.9375 for the full model and 3.4197 for the reduced model (Scenario 1) when the fault is the voltage sag only. However, the MSE error of real power responses is 3.5740 for the full model and 8.8828 for the reduced model (Scenario 1) when the fault is a combination of a voltage sag and a frequency variation. The reactive power responses follow the similar trend but with a much higher error for a combination of a voltage sag and a frequency variation.

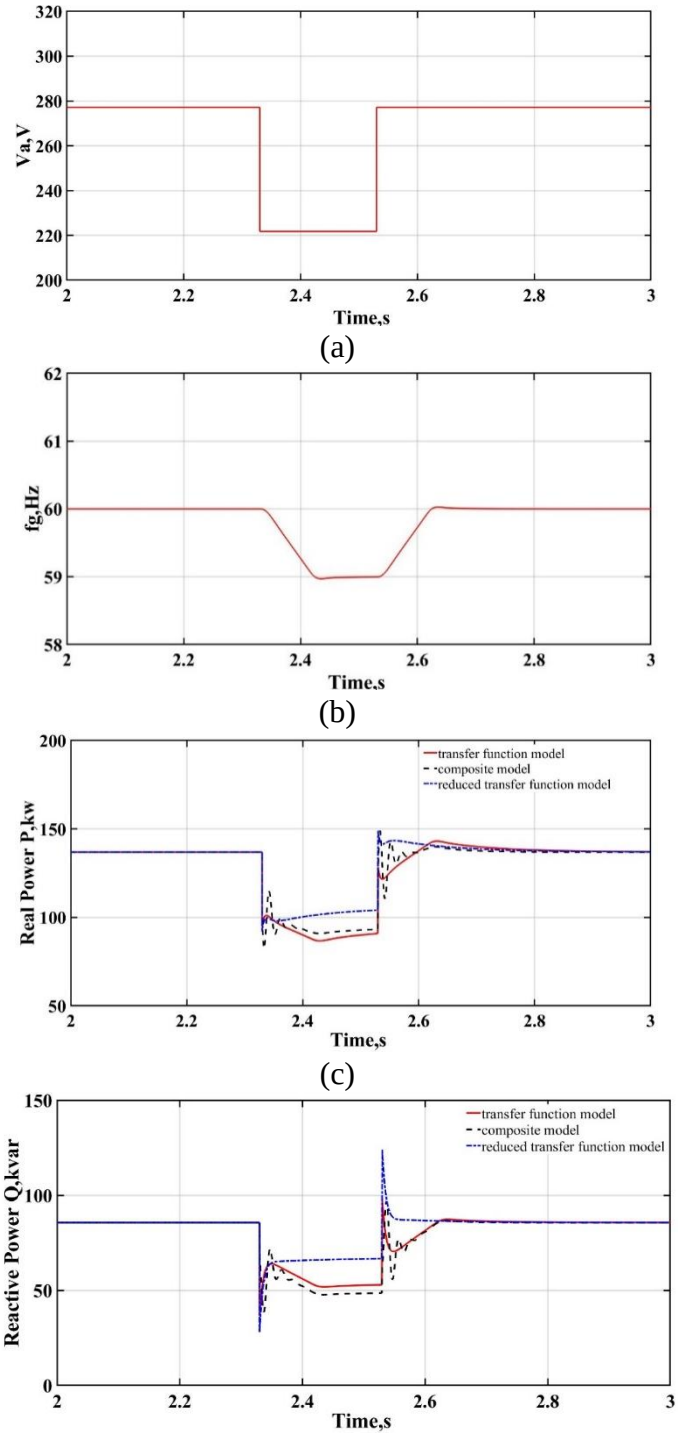

Fig. 3. 8. Dynamic responses of the composite load model, and transfer function-based full and reduced models (Scenario 1) for a combination of an 80% voltage sag and a 1 Hz frequency drop; (a) voltage sag for the three model; (b) frequency drop for the three models; (c) real power; (d) reactive power.

3.4.2 Scenario 2 - 1st Order and 2nd Order Voltage Terms

In Scenario 2, the 1st order and 2nd order voltage terms ((3.84) and (3.85)) are included in the reduced model, the frequency term are not included. Since there is no frequency dependency considered, the error caused by frequency variations must be evaluated. Similar to Scenario 1, we apply two types of disturbances, an 80% voltage sag alone, and a combination of an 80% voltage sag and a 1Hz frequency drop. Both types of faults are applied to the three models, the composite load model, the transfer function-based full and reduced models (Scenario 2).

Firstly, it is assumed that the power source frequency remains constant, an 80% voltage sag is applied at 2.33 s with a duration of 0.2 s to the three models. Dynamic responses of real and reactive power for this event are shown in Fig. 3.9. It is found that the three models are matching very well when the fault is a voltage disturbance only. With the 2nd order voltage term, its accuracy is improved than Scenario 1 without the 2nd order voltage term.

Secondly, a combination of an 80% voltage sag and a 1Hz frequency drop is applied to the three models at 2.33 s with a duration of 0.2 s. Dynamic responses of real and reactive power for this event are shown in Fig. 3.10. It is found that the reduced model has a large discrepancy compared to the other two models because the reduced model does not have frequency term to include the frequency variation effect.

For Scenario 2, when the fault is only a voltage disturbance, the reduced model have the exactly same errors as the full model vs. the composite load model as shown in Tables 3.5 and 3.6. However, when the fault is both voltage and frequency disturbances, the reduced model in Scenario 2 creates significantly large errors compared to the full model. For example, the MSE error of real power responses is 4.8161 for the full model and 9.5088 for the reduced model

(Scenario 2). The reactive power responses follow the similar trend but with a much higher error for a combination of a voltage sag and a frequency variation.

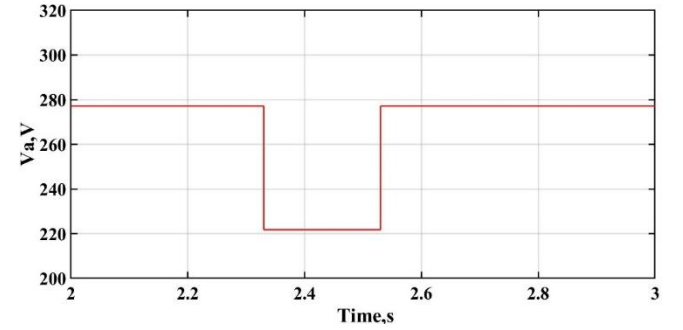

(a)

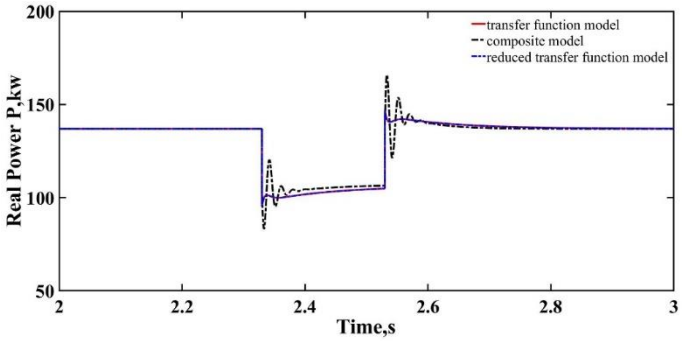

(b)

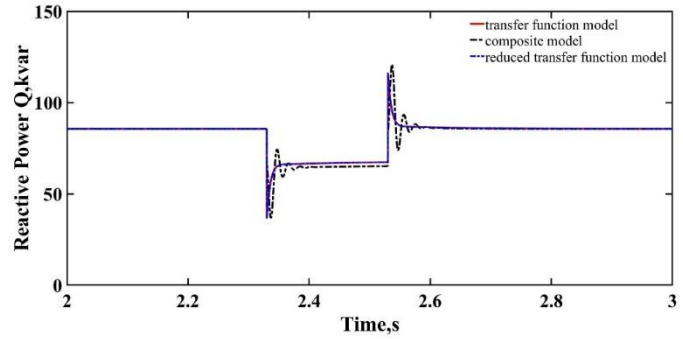

(c)

Fig. 3. 9. Dynamic responses of the composite load model, and transfer function-based full and reduced models (Scenario 2) for an 80% voltage sag; (a) voltage sag for the three models; (b) real power; (c) reactive power.

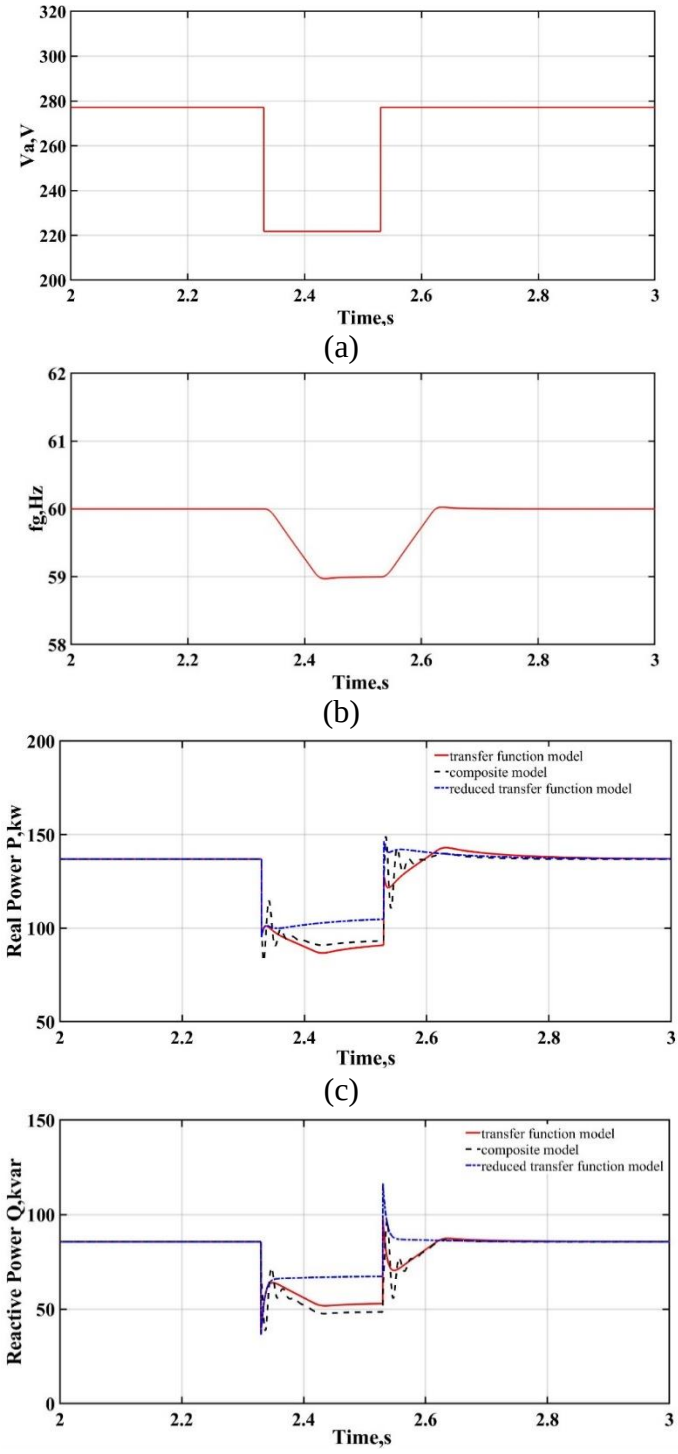

Fig. 3. 10. Dynamic responses of the composite load model, and transfer function-based full and reduced models (Scenario 2) for a combination of an 80% voltage sag and a 1 Hz frequency drop; (a) voltage sag for the three model; (b) frequency drop for the three models; (c) real power; (d) reactive power.

3.4.3 Scenario 3 – 1st Order Voltage and 1st Order Frequency Terms

In Scenario 3, the 1st order voltage and 1st order frequency terms ((3.86) and (3.87)) are included in the reduced model, in this model, both voltage and frequency dependency are considered. A combination of an 80% voltage sag and a 1 Hz frequency drop is applied to the three models at 2.33 s with a duration of 0.2 s. Dynamic responses of real and reactive power for this event are shown in Fig. 3.11. It is found that the reduced model in Scenario 3 still has a large discrepancy compared to the other two models, but its accuracy is much improved than that of Scenarios 1 and 2.

In Scenario 3, the MSE error of real power responses is 3.5740 for the full model and 7.0544 for Scenario 3 (vs. 8.8828 for the reduced model in Scenario 1 and 9.5088 for the reduced model in Scenario 2) when the fault is a combination of a voltage sag and a frequency variation. The reactive power responses follow the similar trend. The error of reactive power for the reduced model in Scenario 3 is much reduced than that of the reduced models in Scenarios 1 and 2.

Fig. 3.12 shows dynamic response errors for real and reactive power for the transfer function-based full model and three reduced models (Scenarios 1-3) compared with the composite load model for a combination of 80% voltage sag and 1 Hz frequency drop at 2.33 s with a duration of 0.2 s. The errors are calculated using (3.89) and (3.90). It shows that among the three reduced models, the reduced order in Scenario 3 considering both 1st order voltage and 1st order frequency terms is the most accurate model.

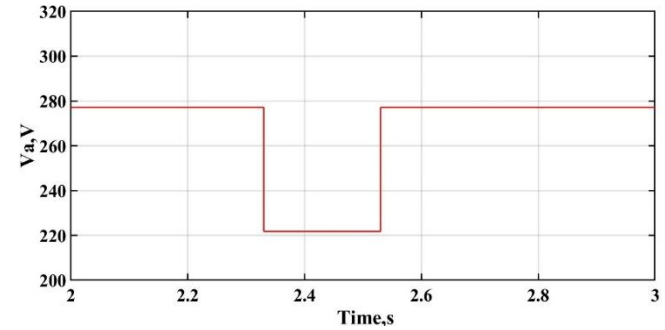

(a)

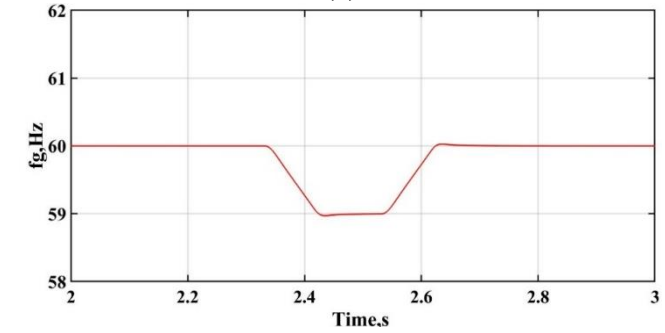

(b)

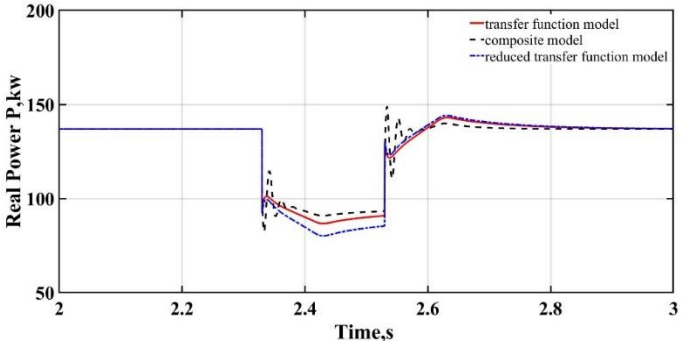

(c)

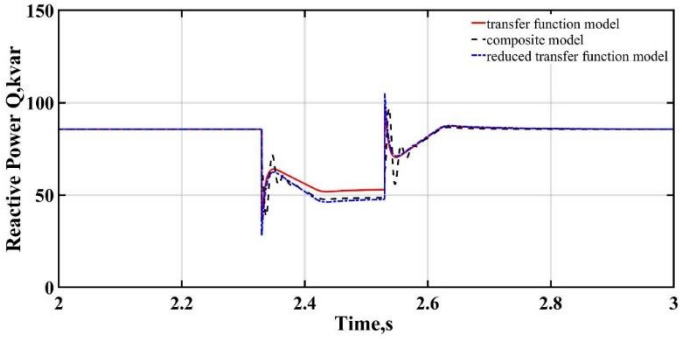

(d)

Fig. 3. 11. Dynamic responses of the composite load model, and transfer function-based full and reduced models (Scenario 3) for a combination of an 80% voltage sag and a 1 Hz frequency drop; (a) voltage sag for the three model; (b) frequency drop for the three models; (c) real power; (d) reactive power.

Table 3. 5: Errors of transfer function-based full and reduced models vs. the composite load model for real power

Simplifications	Events		Relative Error (%)	MSE (kw)	RMSE (kw)
Scenario 1 - 1st order voltage term alone	80% voltage sag	Full model	0.3320	2.9375	1.7139
		Reduced model (Scenario 1)	0.4170	3.4197	1.8492
	80% voltage sag and 1 Hz frequency drop	Full model	0.4925	3.5740	1.8905
		Reduced model (Scenario 1)	0.8378	8.8828	2.9804
Scenario 2 - 1st order and 2nd order voltage terms	80% voltage sag	Full model	0.3320	2.9375	1.7139
		Reduced model (Scenario 2)	0.3320	2.9375	1.7139
	80% voltage sag and 1 Hz frequency drop	Full model	0.4925	3.5740	1.8905
		Reduced model (Scenario 2)	0.8690	9.5088	3.0836
Scenario 3 - 1st order voltage and 1st order frequency terms	80% voltage sag and 1 Hz frequency drop	Full model	0.4925	3.5740	1.8905
		Reduced model (Scenario 3)	0.8282	7.0544	2.6560

Table 3. 6: Errors of transfer function-based full and reduced models vs. the composite load model for reactive power

Simplifications	Events		Relative Error (%)	MSE (kvar)	RMSE (kvar)
Scenario 1 - 1st order voltage term alone	80% voltage sag	Full model	0.4898	4.5528	2.1337
		Reduced model (Scenario 1)	0.5972	5.9853	2.4465
	80% voltage sag and 1 Hz frequency drop	Full model	0.5944	4.8161	2.1946
		Reduced model (Scenario 1)	2.2878	19.2130	4.3833
Scenario 2 - 1st order and 2nd order voltage terms	80% voltage sag	Full model	0.4898	4.5528	2.1337
		Reduced model (Scenario 2)	0.4898	4.5528	2.1337
	80% voltage sag and 1 Hz frequency drop	Full model	0.5944	4.8161	2.1946
		Reduced model (Scenario 2)	2.3172	17.7057	4.2078
Scenario 3 - 1st order voltage and 1st order frequency terms	80% voltage sag and 1 Hz frequency drop	Full model	0.5944	4.8161	2.1946
		Reduced model (Scenario 3)	1.2 156	7.9266	2.8154

$$P_{error} = P_{composite} - P_{proposed} \quad (3.89)$$

$$Q_{error} = Q_{composite} - Q_{proposed} \quad (3.90)$$

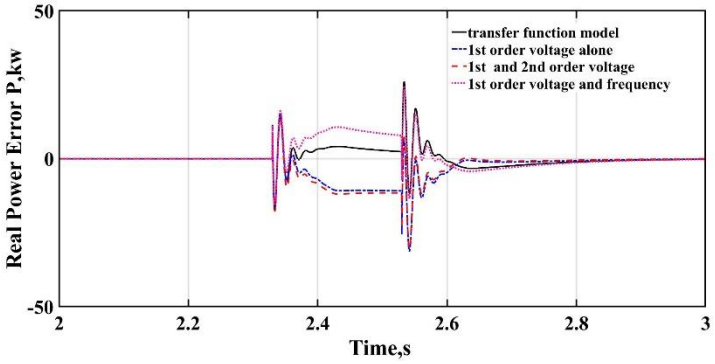

(a)

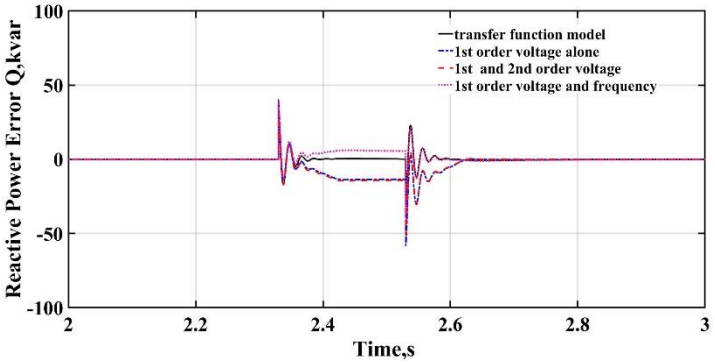

(b)

Fig. 3. 12. Errors of transfer function-based full model and three reduced models (Scenarios 1-3) vs. the composite load model: (a) real power error in kw; (b) reactive power error in kVar.

3.5 Conclusion

In this paper, a transfer function-based load model is derived analytically from a composite load model. The developed model has 3rd order transfer-function, and this provides theoretical explanation why 3rd order transfer-function shows better performance in the past practice for the general power system load modeling.

A comparative study is conducted between the developed transfer function-based load model and its original composite load model by applying various voltage and frequency

disturbances and their combinations. Due to the linearization process, the transfer function-based load model loses some dynamic characteristics, but it follows the trend of the system response very well.

Three simplifications are applied to the developed transfer function-based full model, resulting in three reduced models. It is found that for a combination of a small induction motor and large static load, i.e. small K_{pm}, significant error is introduced by the reduced models. Not considering frequency dependency can cause significant error although this is a common practice for transfer function-based load models in the literature [14]-[17][22]. Of the three reduced models, the reduced model with the 1st order voltage and 1st order frequency terms shows the smallest errors due to its consideration of both voltage and frequency dependency.

References:

[1] IEEE Task Force on Load Representation for Dynamic Performance, “Load Representation for Dynamic Performance Analysis”, IEEE Trans. Power Syst., vol. 8, no.2, pp. 472 - 482, May 1993.

[2] M. Jin, H. Renmu, and D.J. Hill, “Load modeling by finding support vectors of load data from field measurements,” IEEE Trans. Power Syst., vol. 21, no.2, pp. 726 - 735 , May 2006.

[3] H. Renmu, M. Jin, and D.J. Hill, “Composite load modeling via measurement approach,” IEEE Trans. Power Syst., vol. 21, no.2, pp. 663 - 672, March 2006.

[4] J. Ma, D. Han, R.-M. He, Z.-Y. Dong, and D. J. Hill, “Reducing Identified Parameters of Measurement-Based Composite Load Model,” IEEE Trans. Power Syst., vol. 23, no. 1, pp. 76–83, February 2008.

[5] D. Han, J. Ma, R. He, and Z. Dong, “A Real Application of Measurement-Based Load Modeling in Large-Scale Power Grids and its Validation,” IEEE Trans. Power Syst., vol. 24, no.4, pp. 1756 - 1764, November 2009.

[6] Y. Ge, A. J. Flueck, D.-K. Kim, J.-B. Ahn, J.-D. Lee, and D.-Y. Kwon, “An Event-Oriented Method for Online Load Modeling Based on Synchrophasor Data,” IEEE Transactions on Smart Grid, vol. 6, no. 4, pp. 2060–2068, July 2015.

[7] J. Kim, K. An, J. Ma, J. Shin, K. Song, J. Park, J. Park, and Kyeon Hur, “Fast and Reliable Estimation of Composite Load Model Parameters Using Analytical Similarity of Parameter Sensitivity,” IEEE Trans. Power Syst., vol. 31, no.1, pp. 663 - 671, January 2016.

[8] S. Yu, S. Zhang, and X. Zhang, “Two-step method for the online parameter identification of a new simplified composite load model,” IET Generation, Transmission & Distribution, vol. 10, no. 16, pp. 4048–4056, 2016.

[9] J. Kim, J. Ma, K. Sun, J. Lee, J. Shin, Y. Kim, and K. Hur, “A Computationally Efficient Method for Bounding Impacts of Multiple Uncertain Parameters in Dynamic Load Models,” IEEE Trans. Power Syst., vol. 34, no.2, pp. 897 - 907, March 2019.

[10] J. V. Milanović, K. Yamashita. S. M. Villanueva, S. Ž Djokić, and L. M. Korunović, “International Industry Practice on Power System Load Modeling”, IEEE Trans. Power Syst., vol. 28, no. 3, pp. 3038 – 3046, August 2013.

[11] X. Liang, “Dynamic load models for industrial facilities,” PhD thesis, Department of Electrical and Computer Engineering, University of Alberta, Edmonton, AB, Canada, Fall 2013.

[12] S.A.Y. Sabir, and D.C. Lee, “Dynamic Load Models Derived from Data Acquired During System Transients”, IEEE Transactions on Power Apparatus and Systems, vol. PAS-101, no. 9, pp. 3365-3372, September 1982.

[13] I.A. Hiskens, and J.V. Milanovic, “Load modelling in studies of power system damping,” IEEE Trans. Power Syst., vol. 10, no.4, pp. 1781 - 1788, November 1995.

[14] C.-J. Lin, A.-T. Chen, C.-Y. Chiou, C.-H. Huang, H.-D. Chiang, J.-C. Wang, and L. Fekih-Ahmed, “Dynamic load models in power systems using the measurement approach,” IEEE Trans. Power Syst., vol. 8, no. 1, pp. 309–315, February 1993.

[15] T. Omata, and K. Uemura, “Effects of Series Impedance on Power System Load Dynamics”, IEEE Trans. Power Syst., vol. 14, no. 3, pp. 1070-1077, August 1999.

[16] F.T. Dai, J.V. Milanovic, N. Jenkins, and V. Roberts, “Development of a Dynamic Power System Load Model”, IEE Seventh International Conference on AC-DC Power Transmission, pp. 344-349, November 2001.

[17] I. F. Visconti, D. A. Lima, J. M. C. d. S. Costa, and N. R. d. B. C. Sobrinho, “Measurement-Based Load Modeling Using Transfer-functions for Dynamic Simulations,” IEEE Trans. Power Syst., vol. 29, no.1, pp. 111 - 120, January 2014.

[18] X. Liang, "Linearization Approach for Modeling Power Electronics Devices in Power Systems", IEEE Journal of Emerging and Selected Topics in Power Electronics, vol. 2, no. 4, pp. 1003-1012, December 2014.

[19] X. Liang and W. Xu, “Modeling variable frequency drives and motor systems in power systems dynamic studies,” in Proc. IEEE IAS Annu. Meeting, pp. 1-11, Oct. 2013.

[20] X. Liang and J. He, “Load Model for Medium Voltage Cascaded H-Bridge Multi-Level Inverter Drive Systems,” IEEE Power and Energy Technology Systems Journal, vol. 3, no. 1, pp. 13–23, March 2016.

[21] X. Liang, Y. He, M. Mitolo, and W. Li, "Support Vector Machine Based Dynamic Load Model Using Synchrophasor Data", Proceedings of IEEE 54th Industrial and Commercial Power Systems (I&CPS) Conference, pp. 1-11, May 2018.

[22] E. O. Kontis, T. A. Papadopoulos, A. I. Chrysochos, and G. K. Papagiannis, "Measurement-Based Dynamic Load Modeling Using the Vector Fitting Technique," IEEE Trans. Power Syst., vol. 33, no.1, pp. 338 - 351, January 2018.

[23] X. Qu, X. Li, J. Song, and C. He, "An Extended Composite Load Model Taking Account of Distribution Network," IEEE Trans. Power Syst., vol. 33, no. 6, pp. 7317–7320, November 2018.

Chapter 4

Composite Load Model and Transfer Function-Based Load Model for High Motor Composition Load

Hla U May Marma[1], *Student Member*, IEEE, Xiaodong Liang[1], *Senior Member*, IEEE

[1]Department of Electrical and Computer Engineering, Memorial University of Newfoundland, St. John's, Newfoundland, Canada.

A version of this chapter has been published in *2019 IEEE Electrical Power and Energy Conference (EPEC)*. Hla U May Marma co-authored this paper under the supervision of Dr. Xiaodong Liang. Hla's contributions are listed as follows:

- Performed literature searches required for background information of composite load model transfer function-based load model.
- Implemented transfer function-based load model mathematical derivation from composite load model.
- Conducted comparison of two models through MATLAB/Simulink simulation. Examined the results and depicted the conclusion.
- Involved writing of the paper as the first author.

Dr. Xiaodong Liang provided the main ideas, checked the results, and modified the manuscript.

This research was supported in part by the Natural Science and Engineering Research Council of Canada (NSERC) Discovery Grant RGPIN-2016-04170.

In this chapter, the manuscript is presented with altered figure numbers, table numbers and reference formats in order to match the thesis formatting guidelines set out by Memorial University of Newfoundland.

Abstract- There are two common forms of dynamic load models suitable for power system dynamic studies: a composite load model and a transfer function-based load model. The composite load model typically refers to a combination of an induction motor and a static load in the form of ZIP (constant impedance, constant current, and constant power) load. In this paper, the two types of load models are derived for a high motor composition load, and their performance is compared and analyzed through several case studies considering both voltage and frequency dependency of the load models.

Keywords- Composite load model, high motor composition load, transfer function-based load model, ZIP.

4.1 Introduction

In power systems, the load is represented by "load model". A adequate dynamic load model is critical in power system planning and various dynamic studies through computer simulation. The load model is defined to be the active power (P) and reactive power (Q) as the function of the bus voltage magnitude (V) and the frequency (f): $P = f(V, f)$, and $Q = f(V, f)$[1]-[3]. It can be either in a physical component-based model or a mathematical-based model.

For dynamic load modeling, the most commonly used model is the composite load model consisting of an induction motor and a static ZIP (constant impedance, constant current, and constant power) load [4]-[8]. Based on the worldwide survey published in 2013 on load models used for power system stability studies by utility companies, it is found that the dominant

practice in the United States is to use a combination of static (typically ZIP) and dynamic load model (typically induction motor), while use of static load models is prevalent in the rest of the world [9]. Another type of dynamic load model is transfer function-based load model, which has been reported in the literature [3], [8], [10]-[13].

Although the composite load model and transfer function-based load model are well recognized dynamic load models, there is no comparison done between the two types of models for the same load in the literature. In this paper, we have created both types of load models for a same high motor composition load, and a comparison of the two models is demonstrated through case studies. Ref [14] proposes an industrial load model that consists of about 76% small and large motors and 24% static load. A guideline model is built using 70% induction motors and 30% static loads for a 108 MW coking oil refinery facility in [3]. The high motor composition load is very common for industrial facilities, so this study can represent an important load class.

The paper is arranged as follows: the composite load model are provided in Section II, and the transfer function-based load model directly derived from the composite load model is demonstrated in the same section; A sample system with a 1500 HP induction motor and 120 kW static load is used in the paper, and the data preparation and detailed load models of the sample system are determined in Section III; Four case studies are conducted using the sample system for load models' voltage and frequency dependency validation in Section IV; conclusions are drawn in Section V.

4.2 The Formulation of Two Load Models

In this paper, to conduct a comparison between the composite load model and a transfer function-based load model, we choose a same load for load model creation. Fig. 4.1 shows the two load models, and the conversion from a composite load model to a transfer function-based load model. As shown in Fig. 4.1, the composite load model consists of an induction motor (IM) and a static ZIP load. The equivalent circuit of the composite load model can be represented in Fig. 4.2.

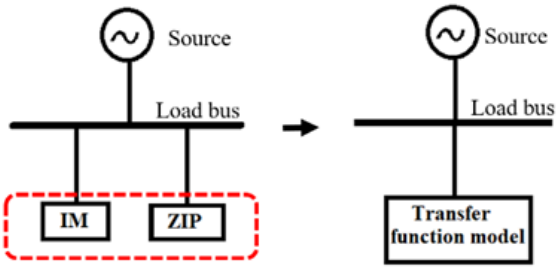

Fig. 4. 1. A composite load model is converted to a transfer function-based load model.

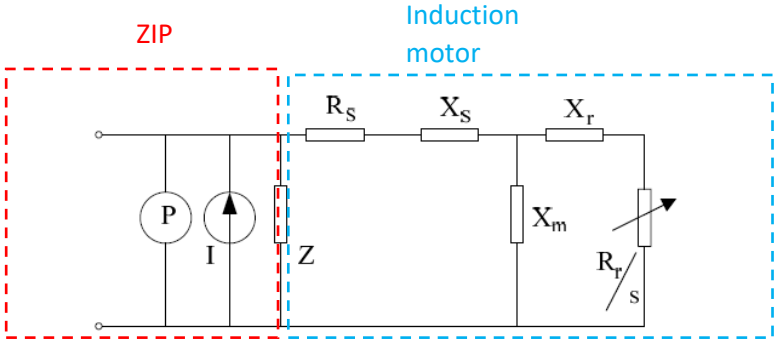

Fig. 4. 2. Equivalent circuit for a composite load model.

Using transfer-functions representing active and reactive power in dynamic load models for power systems was presented in [10] as follows:

$$\frac{\Delta L(S)}{L_0} = \frac{b_n S^n + \Lambda + b_1 S + b_0}{a_n S^n + \Lambda + a_1 S + a_0} \frac{\Delta V(S)}{V_0} \tag{4.1}$$

In (4.1), only the voltage dependency is considered, the frequency dependency is not included. Ref [3] proposed a transfer function-based load model for motor drive systems considering both voltage and frequency dependency.

In this study, to derive the transfer function-based load model from a composite load model for the same load, the two components in the composite load model, an induction motor and a static ZIP load, must be represented mathematically. The induction motor can be represented by a set of differential equations [3]. The static load is a ZIP load, which can also be represented by a set of equations [14]. Through the linearization process of the two sets of equations, a transfer function-based load model is determined.

The general formulation for the transfer function-based model is derived in this research and provided as follows:

$$P = P_0 + GP_1\Delta E + GP_2\Delta f + GP_3\Delta E^2 + GP_4\Delta E\Delta f \tag{4.2}$$

$$Q = Q_0 + GQ_1\Delta E + GQ_2\Delta f + GQ_3\Delta E^2 + GQ_4\Delta E\Delta f \tag{4.3}$$

Where, P and Q are real and reactive power at the load bus in Fig. 4.1. P0 and Q0 are initial real and reactive power, respectively. GP1 – GP4, and GQ1 – GQ4 are two sets of co-efficients for real and reactive power, respectively. ΔE and Δf are the voltage and frequency variation, respectively. This derived transfer function-based load model is in 3rd order.

$$GP_1 = \frac{P_{11}S^3+P_{12}S^2+P_{13}S+P_{14}}{N_1S^3+N_2S^2+N_3S+N_4} \tag{4.4}$$

$$GP_2 = \frac{P_{21}S^3+P_{22}S^2+P_{23}S+P_{24}}{N_1S^3+N_2S^2+N_3S+N_4} \tag{4.5}$$

$$GP_3 = \frac{P_{31}S^3+P_{32}S^2+P_{33}S+P_{34}}{N_1S^3+N_2S^2+N_3S+N_4} \tag{4.6}$$

$$GP_4 = \frac{P_{41}S^3+P_{42}S^2+P_{43}S+P_{44}}{N_1S^3+N_2S^2+N_3S+N_4} \tag{4.7}$$

$$GQ_1 = \frac{Q_{11}S^3+Q_{12}S^2+Q_{13}S+Q_{14}}{N_1S^3+N_2S^2+N_3S+N_4} \quad (4.8)$$

$$GQ_2 = \frac{Q_{21}S^3+Q_{22}S^2+Q_{23}S+Q_{24}}{N_1S^3+N_2S^2+N_3S+N_4} \quad (4.9)$$

$$GQ_3 = \frac{Q_{31}S^3+Q_{32}S^2+Q_{33}S+Q_{34}}{N_1S^3+N_2S^2+N_3S+N_4} \quad (4.10)$$

$$GQ_4 = \frac{Q_{41}S^3+Q_{42}S^2+Q_{43}S+Q_{44}}{N_1S^3+N_2S^2+N_3S+N_4} \quad (4.11)$$

4.3 The Sample System and Data Preparation

Table 4. 1: Parameters of the induction motor and the zip load in the composite load model representing the sample system

Components	Parameters
Induction motor [13]	Nominal power = 1500 HP Nominal voltage $v_b = 2300$ V(rms) Nominal frequency $f_{rated} = 60$ Hz $R_s = 0.056\ \Omega$; $l_s = 0.001$ H; $R_r = 0.037\ \Omega$ $l_r = 0.001$ H; $L_m = 0.0527$ H Inertia, $J = 44.548$ kgm^2 Nominal speed, $n_{rated} = 1783$ rpm Pole pairs, $p = 2$ Load torque, $T_L = 6000$ Nm Target speed, $n_r = 1771$ rpm
ZIP load [15]	Real power in steady-state, $P_{ZIP0} = 120$ kW Power factor = 0.88 $a_p = 0.28$; $b_p = 0.75$; $c_p = -0.03$ $a_q = 0.20$; $b_q = 0.82$; $c_q = -0.02$ $k_{pf} = 0.14$; $k_{qf} = 0.29$
Power source	Rated voltage 2300 V (rms) Rated frequency $f_g = 60$ Hz

In the sample system, a large motor composition load is considered. The parameters of the induction motor and the ZIP load of the composite load model are listed in Table 4.1. The

induction motor is rated at 2300 V and 1500 HP. The detailed dynamic load model for the sample system is calculated using (4.2)-(4.11) and provided in Table 4.2.

To evaluate the accuracy of dynamic responses between the two load models, the RMSE [16] and the relative error are calculated. The RMSE is used to evaluate how accurately the model fits the response. A lower value of RMSE indicates a better fit. The relative error is scale independent and considered as a good measure.

$$RMSE = \sqrt{\frac{1}{n} \times \sum_{i=1}^{n} (L_a - L_f)^2} \tag{4.12}$$

$$Relative\ error = \frac{\sqrt{\frac{1}{n} \times \sum_{i=1}^{n} (L_a - L_f)^2}}{\sqrt{\frac{1}{n} \times \sum_{i=1}^{n} {L_f}^2}} \times 100 \tag{4.13}$$

Table 4. 2: The calculated coefficients of the transfer function-based load model for the sample system

Coefficients	Detailed transfer-functions
GP_1	$\frac{6.3157\times10^5S^3+1.8973\times10^7S^2+4.2258\times10^8S+9.1939\times10^7}{315.5287S^3+1.1721\times10^4S^2+3.4721\times10^5S+3.6875\times10^6}$
GP_2	$\frac{2.2389\times10^6S^3+1.2411\times10^{10}S^2+2.1452\times10^{11}S+1.8763\times10^{11}}{315.5287S^3+1.1721\times10^4S^2+3.4721\times10^5S+3.6875\times10^6}$
GP_3	$\frac{100.4874S^3+353.5277S^2-9.4563\times10^4S-4.3147\times10^6}{315.5287S^3+1.1721\times10^4S^2+3.4721\times10^5S+3.6875\times10^6}$
GP_4	$\frac{2.9235\times10^3S^3+9.3925\times10^6S^2+1.6291\times10^8S+1.5576\times10^8}{315.5287S^3+1.1721\times10^4S^2+3.4721\times10^5S+3.6875\times10^6}$
GQ_1	$\frac{1.9002\times10^6S^3+4.0827\times10^7S^2+1.4090\times10^9S-2.8144\times10^9}{315.5287S^3+1.1721\times10^4S^2+3.4721\times10^5S+3.6875\times10^6}$
GQ_2	$\frac{-3.0351\times10^7S^3+2.3809\times10^9S^2+1.2530\times10^{11}S+1.8833\times10^{11}}{315.5287S^3+1.1721\times10^4S^2+3.4721\times10^5S+3.6875\times10^6}$
GQ_3	$\frac{1.2625\times10^3S^3+2.4486\times10^4S^2+8.7565\times10^5S-4.0888\times10^6}{315.5287S^3+1.1721\times10^4S^2+3.4721\times10^5S+3.6875\times10^6}$
GQ_4	$\frac{-2.1881\times10^4S^3+1.8292\times10^6S^2+9.5432\times10^7S+1.5322\times10^8}{315.5287S^3+1.1721\times10^4S^2+3.4721\times10^5S+3.6875\times10^6}$

4.4 Case Studies using the Sample System

In case studies, the two models are simulated using MATLAB/Simulink for the same load shown in Table 4.1, their dynamic responses are compared under several disturbances. The disturbances include two voltage sags (one small at 90%, one large at 50%), one large frequency drop (1 Hz drop), and a combination of a 50% voltage sag and 1 Hz frequency drop. These disturbances are intended to evaluate two important characteristics of the load model: voltage dependency and frequency dependency.

4.4.1 Case 1: 90% Voltage Sag

In Case 1, a 90% voltage sag is applied to the power source of both the composite load model and the transfer function-based load model in Simulink. The 90% voltage sag means that during the voltage sag, the remaining voltage at the load bus is 90% of the nominal bus voltage. The dynamic responses of the real and reactive power for the 90% voltage sag for both models are shown in Fig. 4.3.

Table 4.3 shows that the relative error and RMSE of real power for Case 1 are 4.1651% and 52.7633, respectively. Table 4.4 shows that the relative error and RMSE of reactive power for Case 1 are 11.6865% and 62.0846, respectively. Therefore, dynamic responses of the transfer function-based load model match that of the composite load model quite accurately in Case 1. In Case 1, only a voltage sag is applied to the system, so the voltage dependency appears to be good for the derived transfer function-based load model. The frequency dependency, however, cannot be evaluated through this case study.

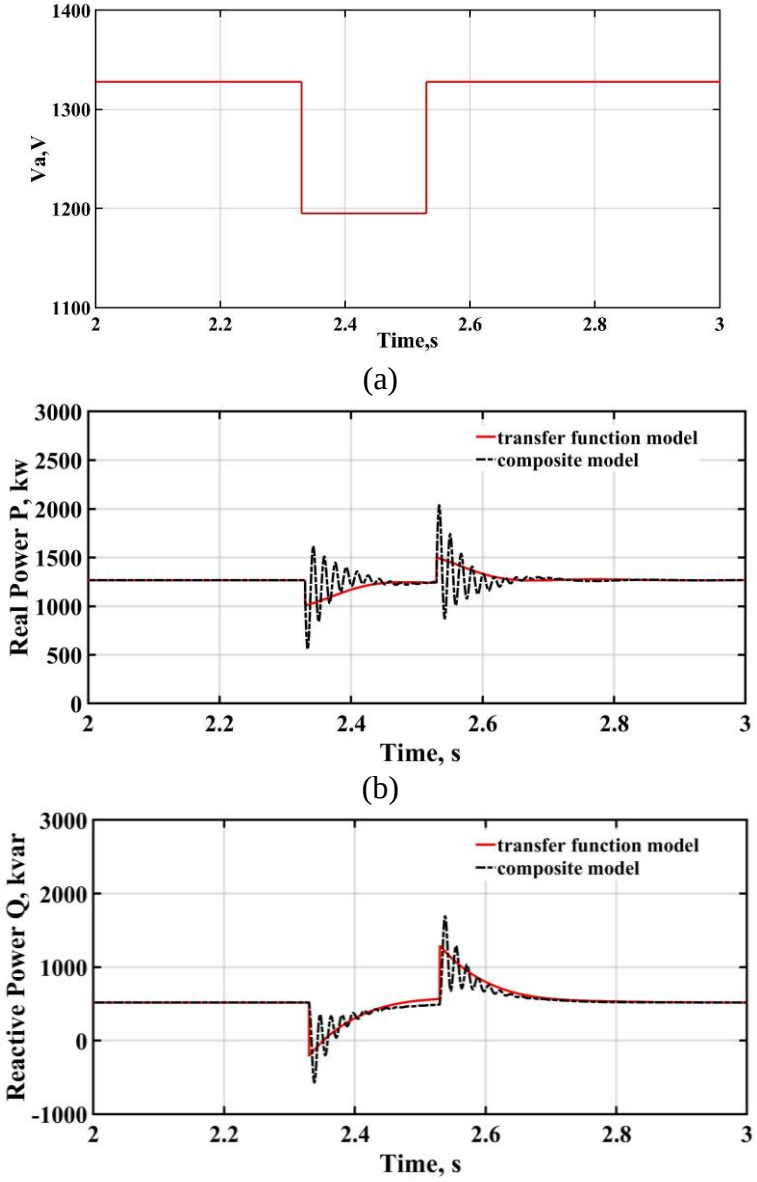

Fig. 4. 3. Dynamic responses of both load models for a 90% voltage sag (Case 1): (a) voltage sag for both models; (b) real power; (c) reactive power.

4.4.2 Case 2: 50% Voltage Sag

In Case 2, a 50% voltage sag is applied to the power source of both load models. The dynamic responses of the real and reactive power for the 50% voltage sag for both models are shown in Fig. 4.4.

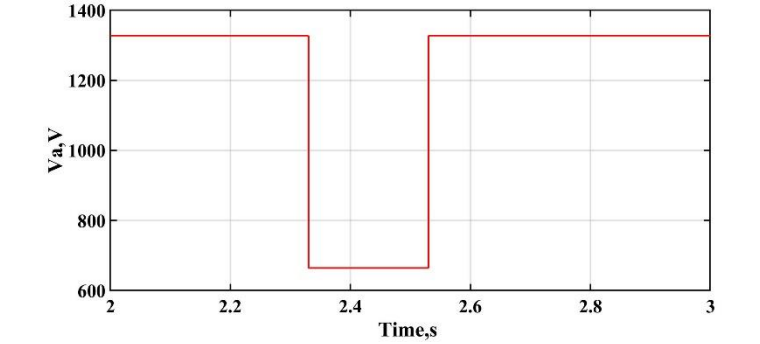

(a)

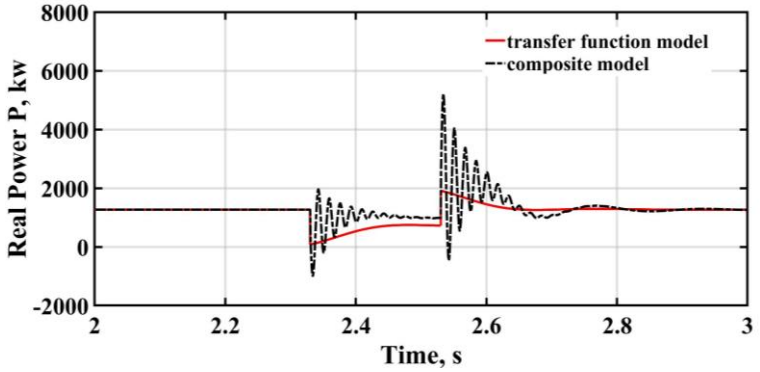

(b)

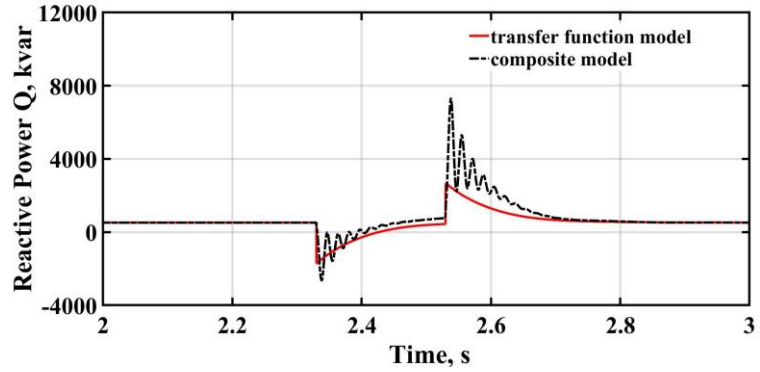

(c)

Fig. 4. 4. Dynamic response of the two load models for a 50% voltage sag (Case 2): (a) voltage for both transfer-function load model and composite load model; (b) real power; (c) reactive power.

Table 4.3 shows that the relative error and RMSE of real power for Case 2 are 18.4402% and 239.1454, respectively. Table 4.4 shows that the relative error and RMSE of reactive power for Case 2 are 45.0440% and 362.9690, respectively. It is found that when the voltage sag become more severe, the dynamic response fluctuations for a 50% voltage sag are much larger than that for a 90% voltage sag, i.e., the errors between the two models in Case 2 are much larger than that in Case 1. The linearization process during the model derivation for transfer function-based load model leads to more linear and less dynamics compared to the original composite load model. However, the tendency of dynamic characteristics for both models still remain quite similar.

4.4.3 Case 3: 1 Hz Frequency Drop

In Case 3, a 1 Hz frequency drop is applied to power sources of both load models to analyze the accuracy of the derived model under frequency disturbances. Fig. 4.5 represents the dynamic responses of the two load models for Case 3. Figs. 4.5(b) and 4.5(c) indicate that the dynamic response of the composite load model for frequency disturbance is smaller than for the voltage disturbance of Cases 1 and 2.

Table 4.3 show that the relative error and RMSE of real power for Case 3 are 16.9217% and 16.9217, respectively. Table 4.4 show that the relative error and RMSE of reactive power for Case 3 are 15.8270% and 82.2352, respectively. It is interesting to note that the derived transfer function-based load model varies quite differently from the original composite load model. The tendency of dynamic characteristics between the two models is not matching very well for frequency disturbances.

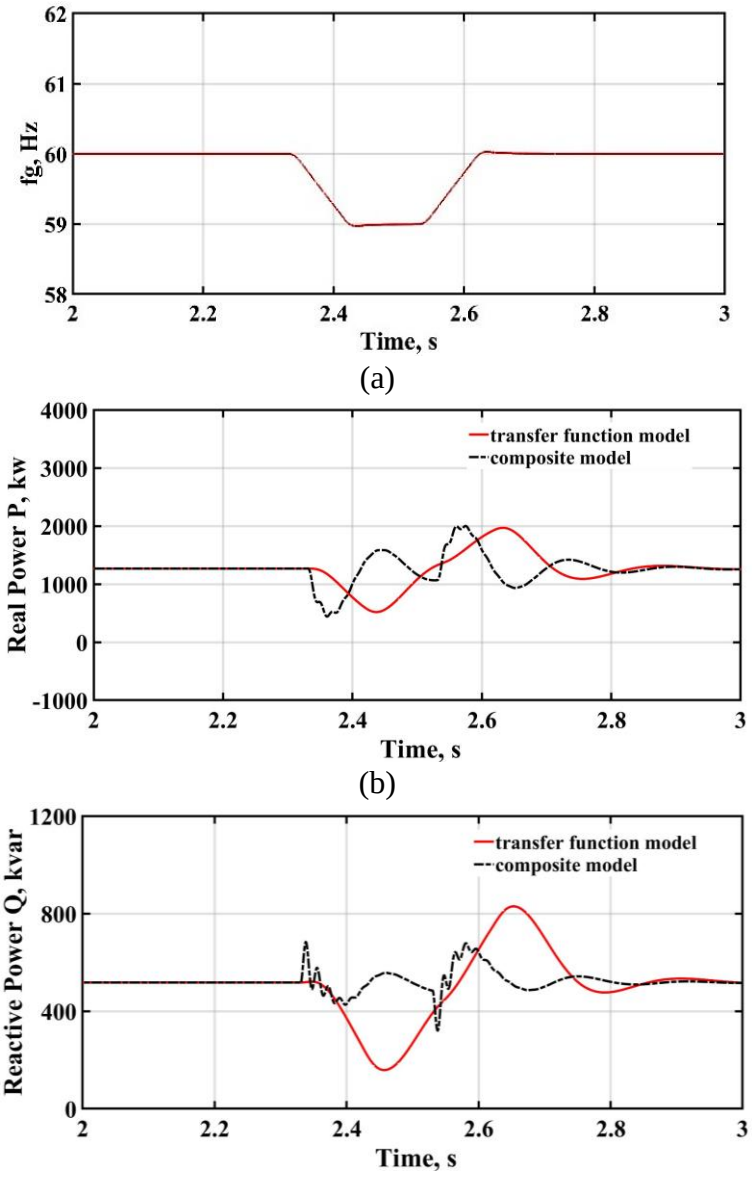

Fig. 4. 5. Dynamic responses of both models for a 1 Hz frequency sag (Case 3): (a) frequency sag for both models; (b) real power; (c) reactive power.

4.4.4 Case 4: A Combination of a 50% Voltage Sag and a 1 Hz Frequency Drop

In Case 4, the combination of a 50% voltage sag and 1 Hz frequency drop is applied simultaneously to the power source of the composite load model and the transfer function-based load model. The dynamic response of real and reactive power for both models in this case are represented in Fig. 4.6.

Table 4.3 shows that the relative error and RMSE of real power for Case 4 are 21.5008% and 280.5499, respectively. Table 4.4 show that the relative error and RMSE of reactive power for Case 4 are 47.5834% and 396.2208, respectively. The error in Case 4 is greater than that of the separate 50% voltage sag and 1 Hz frequency drop of Cases 2 and 3. However, the tendency of dynamic responses of the system in Case 4 is very similar to Case 2 with only a 50% voltage sag. This indicates that although the frequency does have certain influences on the dynamic response, the voltage remains to be a dominant factor in the overall dynamic characteristic of the system.

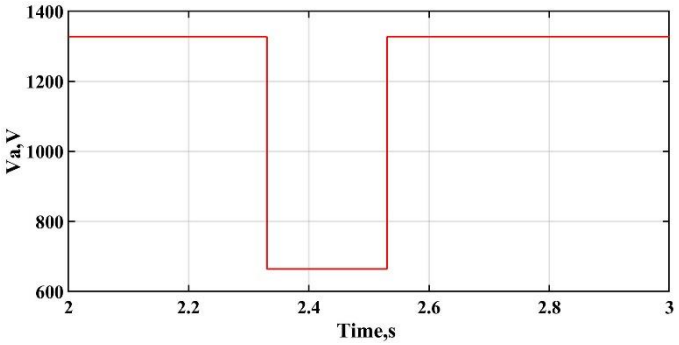

(a)

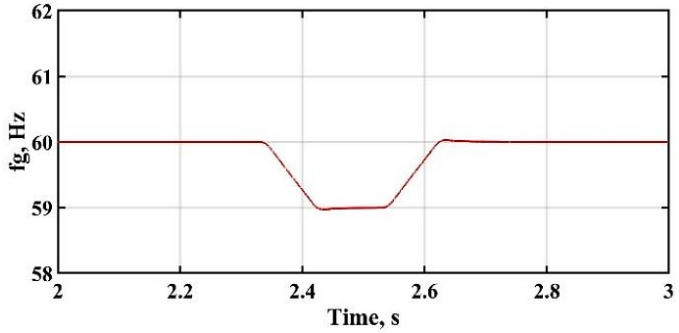

(b)

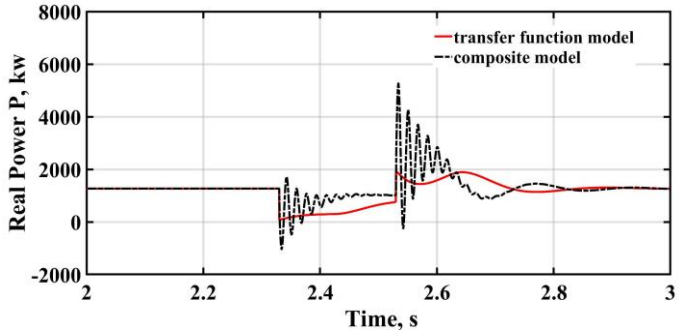

(c)

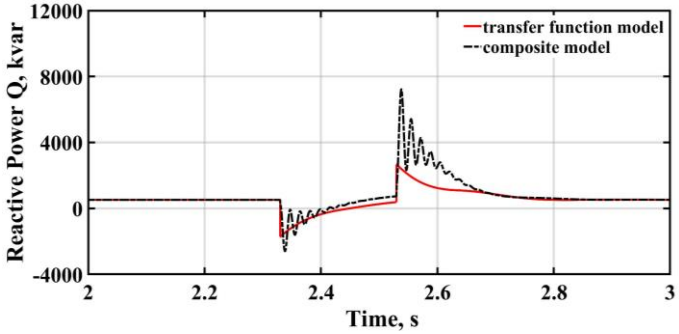

(d)

Fig. 4. 6. Dynamic response of both models for a 50% voltage sag and 1 Hz frequency drop (Case 4): (a) voltage sag for both models; (b) frequency drop for both models; (c) real power; (d) reactive power.

Table 4. 3: Errors for real power between transfer function-based load model and composite load model

CASES	RELATIVE ERROR (%)	RMSE (KW)
Case 1: 90% voltage sag	4.1651	52.7633
Case 2: 50% voltage sag	18.4402	239.1454
Case 3: 1 Hz frequency drop	16.9217	215.5687
Case 4: a combination of a 50% voltage sag and 1 Hz frequency drop	21.5008	280.5499

Table 4. 4: Errors for reactive power between transfer function-based load model and composite load model

CASES	RELATIVE ERROR (%)	RMSE (KVAR)
Case 1: 90% voltage sag	11.6865	62.0846
Case 2: 50% voltage sag	45.0440	362.9690
Case 3: 1 Hz frequency drop	15.8270	82.2352
Case 4: a combination of a 50% voltage sag and 1 Hz frequency drop	47.5834	396.2208

4.5 Conclusion

In this paper, dynamic responses of two dynamic load models, a composite load model consisting of an induction motor and a ZIP load, and a transfer function-based load model for the same load are compared under several disturbances. The transfer function-based load model is derived from the composite load mode directly. The sample system for validation of the derived load models is a high motor composition load. Such load can well represent the load at industrial facilities, where induction motors are dominant in the load composition. The derived transfer function-based load model include both voltage and frequency variation terms, and in a 3rd order transfer-functions format. The accuracy of this derived model is evaluated considering both voltage and frequency dependency of the models.

It is found that tendency of dynamic responses of both models under various disturbances are matching well except the frequency disturbances. However, the voltage is dominant when both voltage and frequency disturbances occur, so the frequency's effect is very small. In the case that only a frequency disturbance occurs, its influence on the system is much less than a voltage disturbance. The linearization process during deriving the transfer function-based load model leads to more linear and less dynamic in its dynamic responses, but the overall tendency remains matching with the original composite load model.

References:

[1] IEEE Task Force on Load Representation for Dynamic Performance, "Load Representation for Dynamic Performance Analysis", IEEE Transactions on Power Systems, vol. 8, no.2, pp. 472 – 482, May 1993.

[2] IEEE Task Force on Load Representation for Dynamic Performance, System Dynamic Performance Subcommittee, Power System Engineering Committee, "Standard Load Models for Power Flow and Dynamic Performance Simulation", IEEE Transactions on Power Systems, vol.10, no. 3, pp. 1302 – 1313, August 1995.

[3] X. Liang, PhD Thesis, "Dynamic Load Models for Industrial Facilities", University of Alberta, Fall 2013.

[4] H. Renmu, M. Jin, and D. J. Hill, "Composite Load Modeling Via Measurement Approach", IEEE Transactions on Power Systems, vol. 21, no.2, pp. 663 – 672, May 2006.

[5] J.-C. Wang, H.-D. Chiang, C.-L. Chang, A.-H. Liu, C.-H. Huang, and C.-Y. Huang, "Development of a Frequency-Dependent Composite Load Model Using the Measurement Approach", IEEE Transactions on Power Systems, vol. 9, no. 3, pp.1546 – 1556, August 1994,

[6] A. Ellis, D. Kosterev, and A. Meklin, "Dynamic Load Models: Where Are We?", 2005/2006 IEEE PES Transmission and Distribution Conference and Exhibition, pp. 1320-1324, May 2006.

[7] J. Ma, H. Renmu, and D.J. Hill, "Load modeling by finding support vectors of load data from field measurements", IEEE Transactions on Power Systems, vol.21, no. 2, pp. 726 - 735, May 2006.

[8] S.A.Y. Sabir, and D.C. Lee, "Dynamic Load Models Derived from Data Acquired During System Transients", IEEE Transactions on Power Apparatus and Systems, vol. PAS-101, no. 9, pp. 3365-3372, September 1982.

[9] J. V. Milanović, K. Yamashita. S. M. Villanueva, S. Ž Djokić, and L. M. Korunović, "International Industry Practice on Power System Load Modeling", IEEE Transactions on Power Systems, vol. 28, no. 3, pp. 3038 – 3046, August 2013.

[10] T. Omata, and K. Uemura, “Effects of Series Impedance on Power System Load Dynamics”, IEEE Transactions on Power Systems, vol. 14, no. 3, pp. 1070-1077, August 1999.

[11] F.T. Dai, J.V. Milanovic, N. Jenkins, and V. Roberts, “Development of a Dynamic Power System Load Model”, IEE Seventh International Conference on AC-DC Power Transmission, pp. 344-349, November 2001.

[12] X. Liang, "Linearization Approach for Modeling Power Electronics Devices in Power Systems", IEEE Journal of Emerging and Selected Topics in Power Electronics, vol. 2, no. 4, pp. 1003-1012, December 2014.

[13] X. Liang, and J. He, "Load Model for Medium Voltage Cascaded H-Bridge Multi-Level Inverter Drive Systems", IEEE Power and Energy Technology Systems Journal, vol. 3, no. 1, pp. 13-23, March 2016.

[14] K. Morison, H. Hamadani, and L. Wang, “Practical Issues in Load Modeling for Voltage Stability Study”, IEEE Power Engineering Society General Meeting, vol. 3, pp. 1392-1397, July 2003.

[15] Y. Ge, A. J. Flueck, D.-K. Kim, J.-B. Ahn, J.-D. Lee, and D.-Y. Kwon, "An Event-Oriented Method for Online Load Modeling Based on Synchrophasor Data," IEEE Transactions on Smart Grid, vol. 6, no. 4, pp. 2060-2068, 2015.

Chapter 5

Short-term Power Load Forecast of an Electrically Heated House in St. John's, Newfoundland, Canada

Hla U May Marma[1], M. Tariq Iqbal [1], Christopher Thomas Seary [1]

[1]Department of Electrical and Computer Engineering, Memorial University of Newfoundland, St. John's, Newfoundland, Canada.

A version of this chapter has been published in European Journal of Electrical and Computer Engineering, ISSN (Online): 2506-9853. Hla U May Marma co-authored this paper under the supervision of Dr. M. Tariq Iqbal. Hla's contributions are listed as follows:

- Performed literature searches required for background information of NN based STLF.
- Implemented transfer function-based load model mathematical derivation from composite load model.
- Conducted comparison of two models through MATLAB/Simulink simulation. Examined the results and depicted the conclusion.
- Involved writing of the paper as the first author.

Dr. M. Tariq Iqbal provided the load data and main ideas of the paper, provided continuous technical guidance, checked the results, reviewed the manuscript, provided important suggestions to accomplish the work, and modified the final version of the manuscript. Christopher Thomas Seary reviewed the developing code in MATLAB deep learning toolbox.

This research was supported in part by the Natural Science and Engineering Research Council of Canada (NSERC) Discovery Grant RGPIN-2016-04170.

In this chapter, the manuscript is presented with altered figure numbers, table numbers and reference formats to match the thesis formatting guidelines set out by Memorial University of Newfoundland.

Abstract- A highly efficient deep learning method for short-term power load forecasting has been developed recently. It is a challenge to improve forecasting accuracy, as power consumption data at the individual household level is erratic for variable weather conditions and random human behaviour. In this paper, a robust short-term power load forecasting method is developed based on a Bidirectional long short-term memory (Bi-LSTM) and long short-term memory (LSTM) neural network with stationary wavelet transform (SWT). The actual power load data is classified according to seasonal power usage behaviour. For each load classification, short-term power load forecasting is performed using the developed method. A set of lagged power load data vectors is generated from the historical power load data, and SWT decomposes the vectors into sub-components. A Bi-LSTM neural network layer extracts features from the sub-components, and an LSTM layer is used to forecast the power load from each extracted feature. A dropout layer with fixed probability is added after the Bi-LSTM and LSTM layers to bolster the forecasting accuracy. In order to evaluate the accuracy of the proposed model, it is compared against other developed short-term load forecasting models which are subjected to two seasonal load classifications.

Keywords- Load forecast, Stationary wavelet transform, Long short-term memory, Neural Network.

5.1 Introduction

Load forecasting with high accuracy is very important for practical power system and smart grids analysis. There are three categories of load forecasting methodologies: LTLF (long term load forecast: more than 1 year), MTLF (medium term load forecast: within 1 month to 1 year) and STLF (short-term load forecast:1 hour to 1 day or 1 week ahead) [1], [9]. Among those, short-term load forecast is more reliable and efficient. STLF improves the efficiency and reliability of smart grid including home energy management, demand response implementation, electricity price market design [18]-[20], [23]. Two techniques are commonly used for STLF: statistical techniques such as the linear regression model, exponential model etc.; and artificial intelligence techniques [9].

It is studied that among all STLF techniques, artificial neural networks (ANNs) is most popular for short-term electric load forecasting. ANNs has distinct advantages and more accurate prediction compared to others [3],[6]-[8]; which influence more research on neural network based STLF. It is found that STLF is implemented by neural fuzzy network, recurrent neural network (RNN), wavelet based neural network or hybrid neural network [5],[10]-[13].

Nowadays, hybrid neural networking has become more popular and suitable for learning non-stationary and complex time series data. A hybrid forecasting method consisting of discrete wavelet transform (DWT), autoregressive integrated moving average (ARIMA) and artificial neural network (ANN) is proposed in [14] to forecast daily peak load. Such hybrid model used load data of Fars Electrical Power Company, Iran in 2009 and predicted daily peak load of the system. Recently, it is invested that the performance of STLF is improved by using LSTM model [24] but using a single LSTM model has less accuracy than the hybrid model combined with

LSTM [5]. The author of [15] designed a hybrid forecasting method called a recurrent inception convolution neural network, a composition of 1-D convolution neural network and LSTM. This model is verified by using power consumption data from three large distribution complexes in South Korea. A combination of short-term wind power forecasting approach based on DWT and LSTM is proposed in [16]; and 12 months data from three wind farms in Mongolia, the Netherlands, and Yunnan, China were used to verify this model. The author of [4] developed a hybrid DWT and collaborative representation (CRT) method. In this method, DWT including CRT is used for feature extraction from the input vector composed by the lagged power load and forecasting is predicted by LSTM. The lagged load variables consist of the load values in last 3 hours of the same day, the last 3 hours and same hour of the day before, and the last 3 hours and same hour of the previous week. It is found that the load features extracted from the lagged power load variable vector provide superior forecasting performance. t the individual household level, a hybrid deep learning methodology combined with LSTM neural network and with SWT is proposed [5], in which SWT decompose the input data into signal components and each signal component is fed to LSTM separately for forecasting. This developed model accuracy is verified by using remote sensor data of five different family houses in London, United Kingdom.

They suggested that SWT alleviates the volatility and increases the data dimensions, improves the accuracy of LSTM forecasting. Although the developed neural network [4]-[5], [15]-[16] can learn the features, overfitting is a threatening problem for large neural networks and reduces the accuracy of forecasting. To avoid the overfitting problem of neural network, [17] developed an hourly natural gas demand forecasting method by adding a dropout layer in the neural network which prevents units from co-adapting too much [27]. This model consists

of multi-layer Bi-LSTM model and LSTM combined with DWT; DWT and multi-layer Bi-LSTM model is used to decompose the actual data into sub-components and capture the features in the sub-components, respectively; and LSTM predict the hourly natural gas demand. A dropout layer is added after each Bi-LSTM and LSTM layer in this model.

Although neural network based STLF is becoming more popular, [2] indicates that neural network was commonly used for an aggregate level load forecasting and limited research has been undertaken based on individual household [3]-[7] before. Recently, the availability of high frequency data collected by new smart metering system in individual households opens the opportunities to research on individual household load forecasting. In addition, having a large amount of data increases the prediction accuracy of load consumption at the individual household level; adding value to improve efficiency of smart grid technologies, such as home energy management and demand response implementation [18]-[20]. Individual household load forecasting will help to project future load consumption and better manage electricity use.

Although smart meter based individual household load consumption data is highly volatile [21], and univariate time series load forecasting is a challenging problem for deep learning; a hybrid model [5] resolves this problem by using SWT combined with LSTM. The developed model of [5] feeds the original energy consumption values to SWT for decomposition of original signal; but [4] mentions that the load value at any time is correlated to the loads in the previous time steps.

It is reported by Natural Resources Canada's Office of Energy Efficiency in 2019 that in the Canada residential sector, the energy was distributed 63% for space heating, 19% for water heating, 16% for appliance and lighting; and 1% for cooling [25]. In winter, the space heating load is dominant which is not included in summer. This creates complexity and difficulty of

intro-class data fitting as space heater is completely unused at summer. In order to overcome the difficulty of data fitting in input and improve the accuracy of forecasting, [26] developed Solar photovoltaic (PV) power forecasting hybrid method based on DWT-CNN-LSTM models; independently established for four weather types : sunny, cloudy, rainy, and heavy rainy days.

In this paper, we propose a robust short-term electric load forecasting model for the individual household level by using the power data from smart meter, installed in house. The deep learning model is based on SWT with a Bi-LSTM and LSTM neural network. A set of lagged power load data vectors is assigned to SWT, it decomposes the vectors and creates sub-components. In order to determine the most appropriate wavelet packet function, a comparison is made among the wavelet functions. The sub-components are individually fed to Bi-LSTM to capture the features by considering the data information bidirectionally. The abstracted features from Bi-LSTM are fed to LSTM for forecast learning. The power forecast is constructed from the predicted sub-components by using ISWT. This process is independently constructed for two seasonal load classifications. The evaluation of the developed model is verified for all seasonal classified load by using the dataset of an individual household in St. John's, Newfoundland and Labrador, Canada. The power consumption profile of individual household is a very common scenario and reflects the power consumption profile in Canada residences, so this study can represent an important load profile forecasting study.

The paper is arranged as follows: in Section II the data description and observation are analyzed, in Section III a curve fitting method for STLF is described; in Section IV the methodology included with five main parts SWT, Bi-LSTM, LSTM, Dropout layer, ISWT of the proposed short-term power load forecasting model are explained; in Section V the accuracy

of the proposed load forecasting model is evaluated by case study using experimental data; and in Section VI conclusions are drawn.

5.2 Data Description and Observations

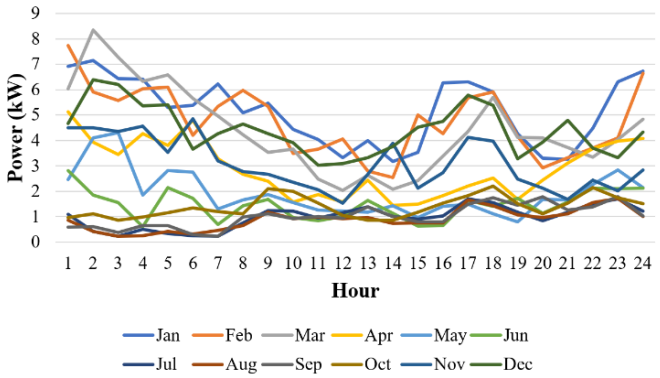

Fig. 5. 1. 24 hourly Weekdays load profile for each month.

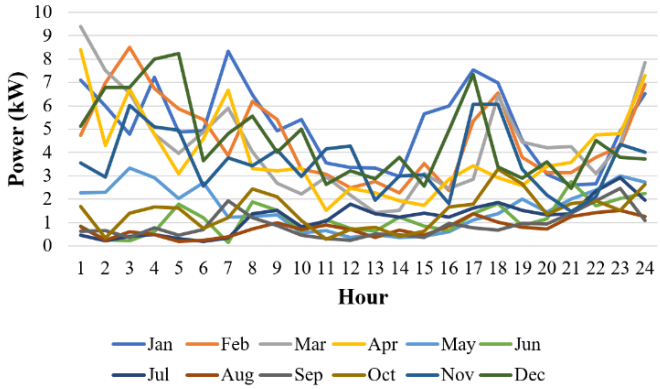

Fig. 5. 2. 24 hourly Weekends load profile for each month.

The power load data of a house in St. Johns was collected by installing current sensors. Five current sensors are installed to measure consumption of the garage, house space heater, domestic water heater, lights and appliances. The total power consumption is calculated by combining the five current sensors dataset. The data was collected every 3 minutes for three years, however only one-year data is used for this study.

The 24-hourly weekdays and weekends load profile for all months are presented in Fig. 5.1 and Fig. 5.2 respectively. It is shown that 24 hourly load consumption profile varies from each month. A box and whisker plot of the seasonal profile is shown in Fig. 5.3. For each month, the top and bottom line corresponds to that month's overall maximum and minimum, respectively. The middle line of the blue box is the overall average for the whole month. The top and bottom of the blue box present the average of the daily maxima and minima of all of the days in the month, respectively. It shows that the overall average is higher from November to May than from June to October.

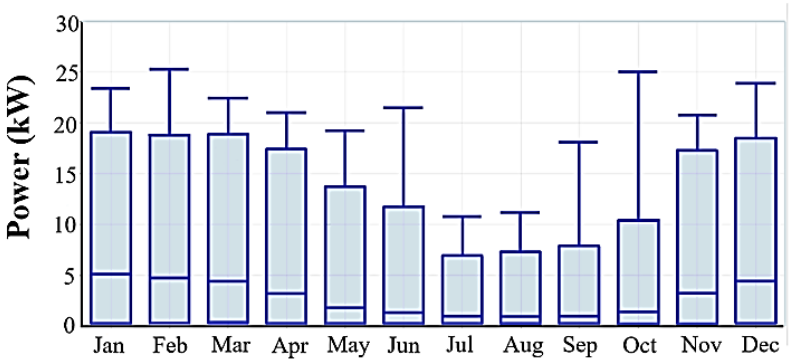

Fig. 5. 3. One-year seasonal load profile of the house

5.3 Curve Fitting Method

Firstly, a curve fitting method is used to develop a prediction model for load forecasting. Two variable regression models have been considered here. Here x stands for hours and y stands for power consumption. MATLAB Surface fitting toolbox has been used to develop the models and to analyze the developed models' accuracy. Five regression models, known as Sum of Sine (5.1), Polynomial (5.2), Power (5.3), Rational (5.4), and Weibull (5.5) models are tested to fit

the load forecasting model shown in Fig. 5.4. it is shown that the actual power load data at the individual household is non-stationary time series data and the developed five regression models are significantly far from the fitting with the actual power load data.

$$y = a_1 \sin(b_1 x + c_1) \tag{5.1}$$

$$y = p_1 x^8 + p_2 x^7 + p_3 x^6 + p_4 x^5 + p_5 x^4 + p_6 x^3 + p_7 x^2 + p_8 x + p_9 \tag{5.2}$$

$$y = ax^b + \mathrm{c} \tag{5.3}$$

$$y = \frac{p_1 x^5 + p_2 x^4 + p_3 x^3 + p_4 x^2 + p_5 x + p_6}{x^5 + q_1 x^4 + q_2 x^3 + q_3 x^2 + q_4 x + q_5} \tag{5.4}$$

$$y = abx^{b-1} e^{-ax^b} \tag{5.5}$$

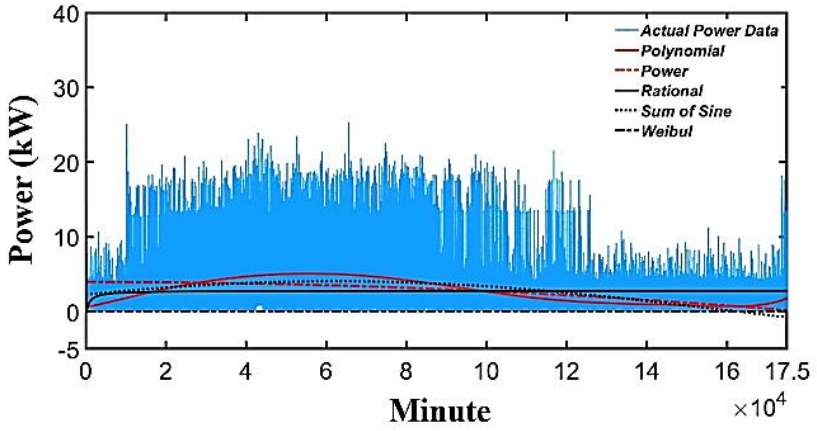

Fig. 5. 4. Curve fitting method for short-term power load forecasting

The accuracy of the developed regression models is evaluated by sum square error (SSE), R-square values and root mean square error (RMSE) between experimental and calculated data using these equations. The R-square value represents how closely the fitted model can follow the variance of the actual data set. It ranges from 0 to 1 where a value closer to 1 and RMSE value closer to 0 represents a better fit. Regression models along with sum square error, R-square values and RMSE are shown in Table 5.1.

From the Table 5.1, it can be seen that for all regression models the R-square value is close to 0; and the SSE and RMSE values are very high, indicating that the curve fitting models are unable to predict load consumption for an individual household load.

Table 5. 1: Regression models along with sum square error, R-square values and RMSE

Model	SSE	R-square	RMSE
Sum of Sine	2.648×10^6	0.1052	3.882
Polynomial	2.517×10^6	0.1495	3.785
Power	2.733×10^6	0.0766	3.944
Rational	2.951×10^6	0.0028	4.099
Weibull	4.252×10^6	0.4369	4.92

5.4 Methodology

This research presents short-term power load consumption forecasting for a house. The residential power is consumed by space heating, water heating, appliances and lighting. Water heater, lighting and other appliance are used daily, on the other hand space heater usage is influenced by variable weather conditions and human behavior. Space heater is used according for certain weather condition specifically November to May in a year as shown Fig. 5.5; and remaining months of the year, it is excluded from the load. Based on Fig. 5.1 and Fig. 5.2, although 24 hourly load profile for June, July, August, September and October vary slowly for both Weekdays and Weekends, the load profile changes abruptly for November, December, January, February, March, April and June. The yearly seasonal load profile Fig. 5.3 shows that the load with space heater consumed higher average power than the load without space heater. Therefore, the actual power load data is classified as two different types: 1) power loads without space heater, and 2) power loads with space heater. Classified data are processed individually

by the proposed short-term power load forecast model as shown in the overall flowchart of proposed model in Fig. 5.6.

The structure of the proposed forecasting model is illustrated in Fig. 5.7. There are five main steps for the proposed model: (1) data preprocessing; (2) a lagged power load variable vector is decomposed by SWT; (3) Bi-LSTM feature extraction from each sub-components; (4) LSTM based prediction with dropout layer are applied for each sub components; and (5) finally, ISWT based re-constructor is used to generates actual power load forecast signal by combining predicted sub-components.

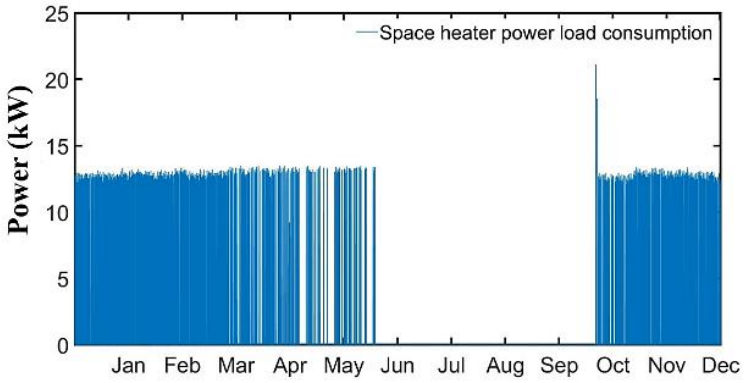

Fig. 5. 5. Yearly space heater load profile for the house.

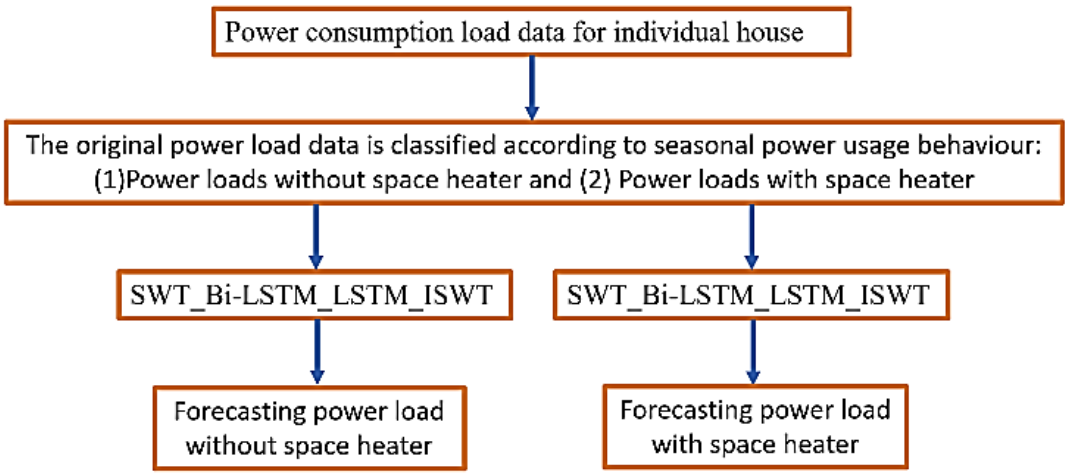

Fig. 5. 6. Overall Flowchart of the short-term power load forecasting model.

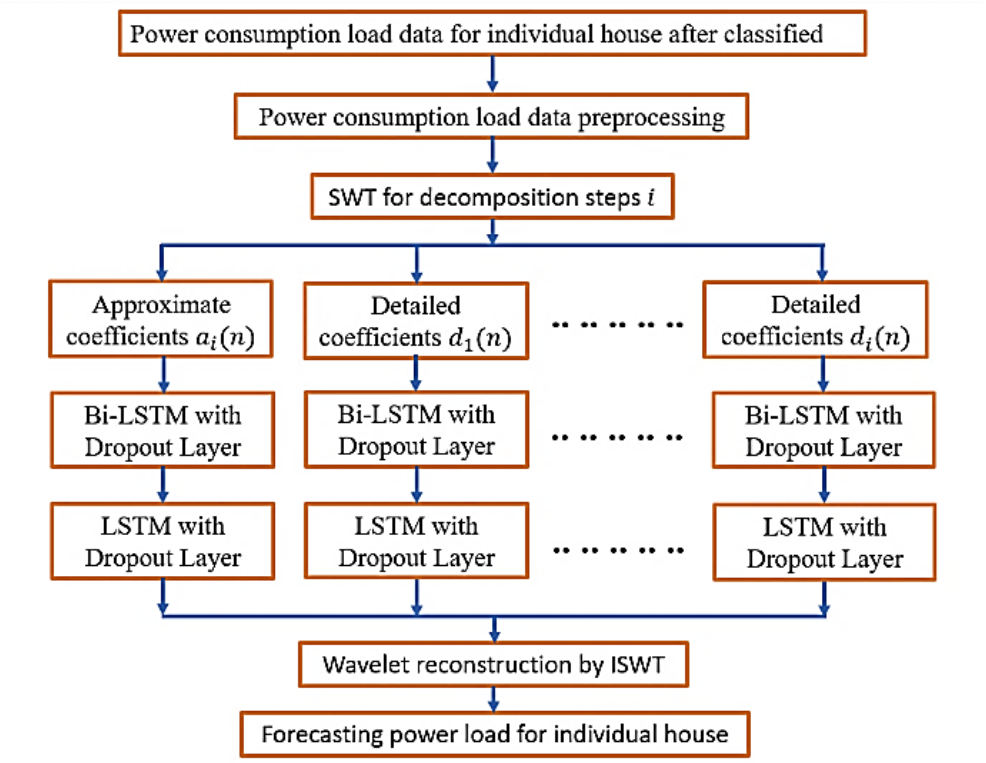

Fig. 5. 7. The structure of the short-term power load forecasting model.

5.4.1 Data Preprocessing

There are 175200 data samples collected per year by 3 minutes interval steps; 116160 and 47040 samples are used for power loads with space heater and without space heater deep learning framework.

The power load value for a certain time is corelated to the previous time steps load value. Hence, in order to increase the data dimension, a set of lagged power load variable vector is created from actual data similar to [4]. The vector is generated by considering only the load values in the last three hours of the same day, the last three hours and same hour of the day before, and the last three hours and same hour of the previous week, in 30 minute time steps as shown in (5.6). The developed variable vector is assigned to each point of the load curve.

$$X = [\, x(t-3431), .. x(t-3361), x(t-551), \ldots\ x(t-481), .. x(t-61), .., x(t-1)]^T$$

(5.6)

X is a set of lagged variable vectors for a certain point with dimension $l \times 1$, l=20. For the m power load samples data, the training data $n = m - 3232$, is considered for the RNN.

5.4.2 SWT Decomposition and Reconstruction

The SWT algorithm is adopted to decompose a signal into wavelets as shown in Fig. 5.8. SWT is known as non-sampling wavelet transform and a time invariance extension of DWT. At the 1st level of SWT, the original signal x(n) splits into approximation coefficients $a_1(n)$ and the detail coefficients $d_1(n)$. Then the next level, $a_1(n)$ splits into two: $a_2(n)$ and $d_2(n)$; and this step is continued for until the number of decomposition steps i. The original signal x(n) can be reconstructed through ISWT whereas x(n) is the last level approximation coefficients $a_i(n)$ and summation of all levels detail coefficients (i.e. $d_1(n)$, $d_2(n)$..... $d_i(n)$).

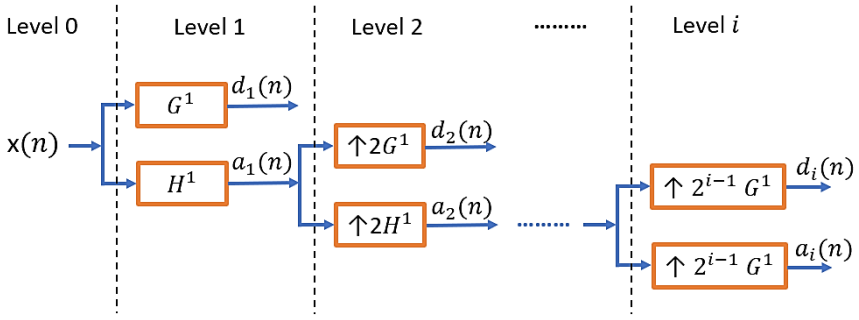

Fig. 5. 8. SWT decomposition for i level

5.4.3 LSTM and Bi-LSTM

LSTM is a special type of RNN and it is effective for processing time series data. LSTM consists of 'self-connected' memory cells, multiplicative gate units in the hidden state as shown in Fig. 5.9. Where, i, f, g and o represent input gate, forget gate, cell candidate and output gate, respectively. LSTM neural network can be explained by following (5.7) to (5.12):

$$i_t = \sigma_g(W_i x_t + R_i h_{t-1} + b_i) \tag{5.7}$$

$$f_t = \sigma_g\left(W_f x_t + R_f h_{t-1} + b_f\right) \tag{5.8}$$

$$g_t = \sigma_c\left(W_g x_t + R_g h_{t-1} + b_g\right) \tag{5.9}$$

$$o_t = \sigma_g(W_o x_t + R_o h_{t-1} + b_o) \tag{5.10}$$

$$c_t = f_t \odot c_{t-1} + i_t \odot g_t \tag{5.11}$$

$$h_t = o_t \odot \sigma_c(c_t) \tag{5.12}$$

$i_t, f_t, g_t, o_t, c_t \; and \; h_t$ denote input gate, forget gate, cell candidate, output gate, cell state and hidden state at time step t, respectively. $W, R \; and \; b$ represent the input weights, the recurrent weights, and the bias of $i, f, g \; and \; o$; respectively. State and gate activation function are denoted by $\sigma_c$and σ_g; respectively.

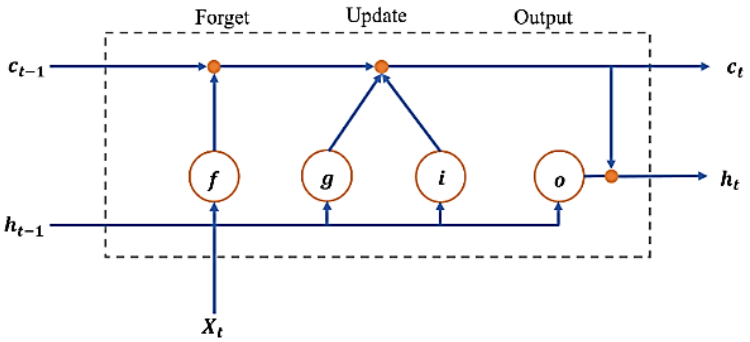

Fig. 5. 9. The architecture of LSTM

In Bi-LSTM model, the same output layer connects the two separate hidden layers known as forward LSTM layer and backward LSTM layer [31]-[33]; as shown in Fig. 5.10. The previous and future data information is used in this model. The forward output layer sequence, $\vec{h}_t$ and the backward output layer sequence, $\overleftarrow{h}_t$ are computed by using input in a positive time sequence and reversed time sequence, respectively. The output layer y_t can be expressed as follows:

$$y_t = G\left(\vec{h}_t, \overleftarrow{h}_t\right) \tag{5.13}$$

Where, G is a function, used to generate output based on $\vec{h}_t$ and $\overleftarrow{h}_t$.

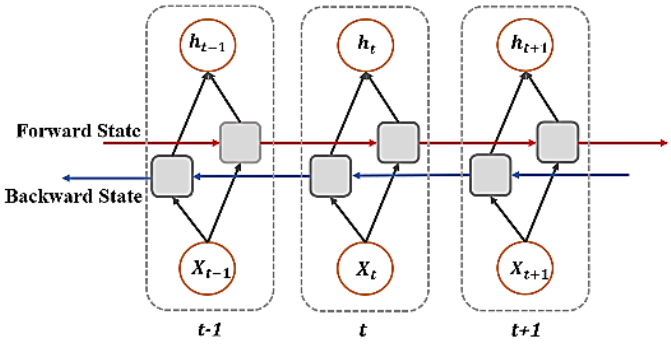

Fig. 5. 10. The architecture of Bi-LSTM

5.4.4 Dropout Layer

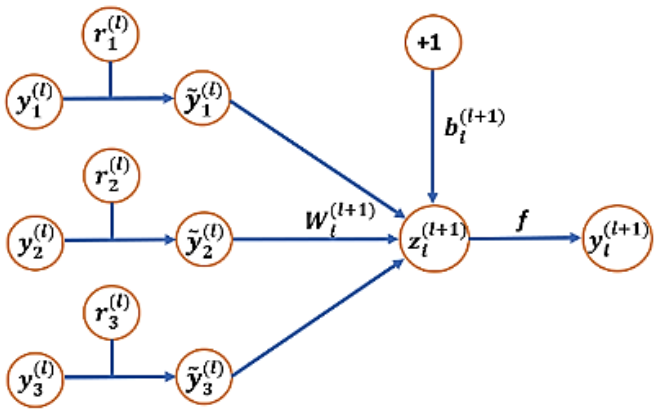

Fig. 5. 11. The dropout network

The dropout layer improves the accuracy of forecasting by preventing the neural network from overfitting. The dropout network is shown in Fig. 5.11 and can represent as follows:

$$r_j^{(l)} \sim Bernoulli(p) \tag{5.14}$$

$$\tilde{y}^{(l)} = r^{(l)} * y^{(l)} \tag{5.15}$$

$$z_i^{(l+1)} = W_i^{(l+1)} \tilde{y}^{(l)} + b_i^{(l+1)} \tag{5.16}$$

$$y_i^{(l+1)} = \sigma\left(z_i^{(l+1)}\right) \tag{5.17}$$

Where * presents element-wise product.

A vector of independent Bernoulli random variables for the specific layer $l, r^{(l)}$ each of which has probability being 1. $y^{(l)}$ and $\tilde{y}^{(l)}$ denote outputs and thinned outputs for the specific layer l. $\tilde{y}^{(l)}$is obtained by randomly sampled $r^{(l)}$ multiplied elementwise with $y^{(l)}$. Then generated $\tilde{y}^{(l)}$ are fed to the layer as input. The same process is repeated at each layer.

5.5 Case Study

The developed STLF model is verified by comparing with DWT_Bi-LSTM_LSTM, SWT_LSTM, SWT_Bi-LSTM model through MATLAB deep learning toolbox and wavelet toolbox using a case study. In this case study, two different cases are considered: 1) Case 1 – load without space heater and 2) Case 2 – load with space heater. For both cases, in order to select the best basis wavelet functions, the mean absolute percentage error (MAPE) of reconstructed signal and actual signal are compared among Haar (haar), Fejer-Korovkin filters (fk), Coiflets (coif), Symlets (sym), Daubechies (db), and Discrete approximation of Meyer (dmey) wavelets as shown in Table 5.2. It is found that Haar wavelet has comparatively less percentage of reconstruction error among other wavelets for both cases. Hence Haar wavelet is

used for SWT and ISWT. The Pearson correlation coefficient (PCC) was used in [5] to determine the number of wavelets and recommended three decomposition steps of SWT.

$$MAPE = \frac{1}{n} \times \sum_{i=1}^{n} \left| \frac{(L_a - L_f)}{L_f} \right| \times 100 \quad (5.18)$$

Table 5. 2: MAPE of reconstructed signal and actual signal for different basis wavelet function

	Wavelet	MAPE(%)
Case 1	Haar	4.5113e-14
	Fejer-Korovkin filters	1.3556e-14
	Coiflets	2.6704e-10
	Symlets	1.5876e-10
	Daubechies	9.4170e-11
	Discrete approximation of Meyer	0.0012
Case 2	Haar	5.2138e-14
	Fejer-Korovkin filters	2.0130e-14
	Coiflets	4.9429e-10
	Symlets	3.3480e-10
	Daubechies	1.8231e-10
	Discrete approximation of Meyer	0.0021

Table 5. 3: Training option to train data in the deep learning toolbox

Option	Parameter
Max Epochs	150
Gradient Threshold	1
Initial Learn Rate	0.010
Mini Batch Size	30
Learn Rate Drop Period	75
Learn Rate Drop Factor	0.316

For both cases, during the deep learning training process, one Bi-LSTM layer with 120 hidden units and one LSTM layer with 120 hidden units are designed for this model. Each layer has dropout layer with 0.3 probability. Adam optimizer is used for this case study. Table 5.3 shows the used training option for both cases study to train data in the deep learning toolbox.

Three statistical featured including average, median and L1 norm are determined as tabulated in Table 5.4 for evaluating the forecasting accuracy.

Table 5. 4: Statistical features

Features	Equation
Average	$\mu_x = \frac{1}{n}\sum_{i=1}^{n} x_i$
Median	$med = \frac{1}{2}(x_{\left\lvert\frac{n+1}{2}\right\rvert} + x_{\left\lvert\frac{n}{2}\right\rvert+1})$
L1 Norm	$\|L\|_1 = \sum_{i=1}^{n}\lvert x_i\rvert$

Where, x_i is the ith sampled measurement point, i = 1, 2, …, n for n observations.

Three different comparison: 1) Comparison 1 – among SWT_Bi_LSTM_LSTM with dropout layer for a set of lagged power load data vectors (i.e. proposed model) and other developed STLF model Comparison 2 – between proposed model and SWT_Bi_LSTM_LSTM with dropout layer for instantaneous power load data; and 3) Comparison 3 – between proposed model and SWT_Bi_LSTM_LSTM without dropout layer for a set of lagged power load data vectors are studied.

$$Percentage\ of\ accuracy = \left(1 - \left|\frac{Test - \text{Forcast}}{\text{Forecast}}\right|\right) \times 100 \tag{5.19}$$

5.5.1 Comparison 1

Table 5. 5: Structure of other STLF model

Model	Structure
DWT_Bi-LSTM_LSTM	DWT (Haar wavelet, three decomposition steps) decomposition for original data Bi-LSTM (120 hidden units) Dropout (0.3 probability) LSTM (120 hidden units) Dropout (0.3 probability) Fully connected layer Regression layer IDWT
SWT_LSTM	SWT (Haar wavelet, three decomposition steps) decomposition for original data LSTM (120 hidden units) Dropout (0.3 probability) Fully connected layer Regression layer ISWT
SWT_Bi-LSTM	SWT (Haar wavelet, three decomposition steps) decomposition for original data Bi-LSTM (120 hidden units) Dropout (0.3 probability) Fully connected layer Regression layer ISWT

In Comparison 1, the proposed model is compared with other developed STLF models DWT_Bi-LSTM_LSTM, SWT_LSTM, SWT_Bi-LSTM to evaluate the accuracy of proposed model. The structure of the three developed STLM models are listed in Table 5.5. The same neural network properties are used to train the data for all models.

Table 5. 6: Comparison among proposed model and other developed STLF model for Case 1

Model	Average power (KW)	Percentage of accuracy for average power (%)	Median	Percentage of accuracy for median (%)	L1 norm	Percentage of accuracy for L1 norm (%)
Test	0.7988		0.6450		19.1712	
Proposed model	0.7791	97.5338	0.7150	89.1473	18.6998	97.5411
DWT_Bi-LSTM_LSTM	0.7149	89.4967	0.7382	85.5504	17.1567	89.4921
SWT_LSTM	1.2426	44.4417	1.2607	95.4574	29.8233	44.4370
SWT_Bi-LSTM	0.9205	84.7646	0.9211	42.8062	22.0923	84.7631

The comparison of the proposed model vs. other STLF models are shown in Table 5.6 and 5.7 for Case 1 and Case 2, respectively. Table 5.6 show that the proposed forecast model is comparatively much more accurate than the other developed models in Case 1. For example, the predicted daily average power consumption accuracy for the proposed model, DWT_Bi-LSTM_LSTM, SWT_LSTM and SWT_Bi-LSTM are 97.5338%, 89.4967%, 44.4417% and 84.7646%; respectively. For Case 2 as shown in Table 5.7, the proposed model forecast is also more accurate compared to the other STLF models but with a much higher error than Case 1. Case 2 has less prediction accuracy because Case 2 – 24 hourly daily load profile varies rapidly

than Case 1 as shown in Fig. 5.1 and 5.2.

Table 5. 7: Comparison among proposed model and other developed STLF model for Case 2

Model	Average power (KW)	Percentage of accuracy for average power (%)	Median	Percentage of accuracy for median (%)	L1 norm	Percentage of accuracy for L1 norm (%)
Test	3.5190		2.4825		84.4554	
Proposed model	3.6878	95.2032	2.7958	87.3797	88.5070	95.2027
DWT_Bi-LSTM_LSTM	3.7352	93.8562	3.7355	49.5267	89.6450	93.8552
SWT_LSTM	3.7165	94.3876	3.712	50.4733	89.1951	94.3879
SWT_Bi-LSTM	4.3726	75.7431	4.3741	23.8026	104.9413	75.7435

5.5.2 Comparison 2

In Comparison 2, SWT_Bi_LSTM_LSTM with dropout layer for a set of lagged power load data vectors (i.e. proposed model) and SWT_Bi_LSTM_LSTM with dropout layer for instantaneous power load data are considered. Table 5.8 shows the forecasting result of Comparison 2. The SWT_Bi_LSTM_LSTM with dropout layer for instantaneous power load data model creates significantly higher error compared to proposed model for both cases. For example, for Case 1: the accuracy of daily average power, median and L1 norm with respect to proposed model are 97.5338%, 85.5504% and 97.5411% respectively; and for the other model, the values are 80.6084%, 52.093% and 80.6089% respectively. Therefore, it is concluded from Comparison 2 that considering a set of lagged power load data vectors improves forecasting

accuracy.

Table 5. 8: Comparison between proposed model and SWT_Bi_LSTM_LSTM with dropout layer for instantaneous power load data for both cases

	Model	Average power (KW)	Percentage of accuracy for average power (%)	Median	Percentage of accuracy for median (%)	L1 norm	Percentage of accuracy for L1 norm (%)
Case 1	Test	0.7988		0.6450		19.1712	
	Proposed model	0.7791	97.5338	0.7382	85.5504	18.6998	97.5411
	SWT_Bi-LSTM_LSTM for instantaneous power load data	0.9537	80.6084	0.9540	52.093	22.8887	80.6089
Case 2	Test	3.5190		2.4825		84.4554	
	Proposed model	3.6878	95.2032	2.7958	87.3797	88.5070	95.2027
	SWT_Bi-LSTM_LSTM for instantaneous power load data	4.4892	72.4297	4.4909	80.9023	107.7406	72.4290

5.5.3 Comparison 3

Table 5. 9: Comparison between proposed model and SWT_Bi_LSTM_LSTM without dropout layer for a set of lagged power load data vectors for both cases

	Model	Average power (KW)	Percentage of accuracy for average power (%)	Median	Percentage of accuracy for median (%)	L1 norm	Percentage of accuracy for L1 norm (%)
Case 1	Test	0.7988		0.6450		19.1712	
	Proposed model	0.7791	97.5338	0.7150	89.1473	18.6998	97.5411
	SWT_Bi-LSTM_LSTM without dropout layer	0.6692	83.7757	0.6423	99.5796	16.0613	83.7783
Case 2	Test	3.5190		2.4825		84.4554	
	Proposed model	3.6878	95.2032	2.7958	87.3797	88.5070	95.2027
	SWT_Bi-LSTM_LSTM without dropout layer	4.1392	82.3857	4.1162	34.1913	99.3401	82.3757

In Comparison 3, a comparison between the proposed model and SWT_Bi_LSTM_LSTM without dropout layer for a set of lagged power load data vectors are studied. Comparison 3 is conducted in order to evaluate whether adding a dropout layer after each Bi-LSTM and LSTM layer leads to better prediction accuracy. A comparison between proposed model and SWT_Bi-

LSTM_LSTM without dropout layer is shown in Table 5.9. It is found that the proposed model has higher forecasting accuracy for both cases because adding a dropout layer after the Bi-LSTM and LSTM neural network boost the prediction accuracy.

5.6 Conclusion

The nature of variable weather conditions and random human behaviour cause randomness in the power consumption profile at the individual household level and create a serious difficulty to improve the short-term power load accuracy. A robust short-term power load forecasting has been developed by using wavelet transform and deep learning method in this paper. The developed model consists of SWT and a Bi-LSTM and LSTM neural network with dropout layers.

In order to evaluate the accuracy of the proposed model, three comparisons for each of two cases are studied by using the real power load dataset of a house in St. John's, Newfoundland and Labrador, Canada. From Comparison 1, it is found that the proposed model has higher forecasting accuracy compared to the other developed STLF model. From Comparison 2, it is found that considering a set of lagged power load data vectors introduced significantly better forecasting accuracy than the original data input, as this increases the dimensions of the training data. Comparison 3 has been conducted to evaluate the effectiveness of adding dropout layers after the Bi-LSTM and LSTM neural network and it shows that the dropout layer improves the accuracy of the proposed model.

References:

[1] M. Q. Raza and A. Khosravi, "A review on artificial intelligence based load demand forecasting techniques for smart grid and buildings," *Renewable and Sustainable Energy Reviews, vol. 50, pp. 1352–1372, 2015.*

[2] F. Mcloughlin, A. Duffy, and M. Conlon, "Evaluation of time series techniques to characterise domestic electricity demand," *Energy, vol. 50, pp. 120–130, 2013.*

[3] M. Aydinalp-Koksal and V. I. Ugursal, "Comparison of neural network, conditional demand analysis, and engineering approaches for modeling end-use energy consumption in the residential sector," *Applied Energy, vol. 85, no. 4, pp. 271–296, 2008.*

[4] M. Imani and H. Ghassemian, "Residential load forecasting using wavelet and collaborative representation transforms," *Applied Energy, vol. 253, p. 113505, 2019.*

[5] K. Yan, W. Li, Z. Ji, M. Qi, and Y. Du, "A Hybrid LSTM Neural Network for Energy Consumption Forecasting of Individual Households," *IEEE Access, vol. 7, pp. 157633–157642, 2019.*

[6] M. Aydinalp, V. I. Ugursal, and A. S. Fung, "Modeling of the space and domestic hot-water heating energy-consumption in the residential sector using neural networks," *Applied Energy, vol. 79, no. 2, pp. 159–178, 2004.*

[7] Ringwood JV, Bofell D, Murray FT, "Forecasting electricity demand on short, medium and long time scales using neural networks," *Journal of Intelligent and Robotic Syst 2001;31:129–47.*

[8] Z. W. Geem and W. E. Roper, "Energy demand estimation of South Korea using artificial neural network," *Energy Policy, vol. 37, no. 10, pp. 4049–4054, 2009.*

[9] A. Baliyan, K. Gaurav, and S. K. Mishra, "A Review of Short-Term Load Forecasting using Artificial Neural Network Models," *Procedia Computer Science, vol. 48, pp. 121–125, 2015.*

[10] A. Ghanbari, S. Abbasian-Naghneh, and E. Hadavandi, "An intelligent load forecasting expert system by integration of ant colony optimization, genetic algorithms and fuzzy logic," *2011 IEEE Symposium on Computational Intelligence and Data Mining (CIDM), 2011.*

[11] S. Bouktif, A. Fiaz, A. Ouni, and M. Serhani, "Optimal Deep Learning LSTM Model for Electric Load Forecasting using Feature Selection and Genetic Algorithm: Comparison with Machine Learning Approaches †," *Energies, vol. 11, no. 7, p. 1636, 2018.*

[12] N. Amjady and F. Keynia, "Short-term load forecasting of power systems by combination of wavelet transform and neuro-evolutionary algorithm," *Energy, vol. 34, no. 1, pp. 46–57, 2009.*

[13] J. Zheng, C. Xu, Z. Zhang, and X. Li, "Electric load forecasting in smart grids using Long-Short-Term-Memory based Recurrent Neural Network," *2017 51st Annual Conference on Information Sciences and Systems (CISS), 2017.*

[14] A. K. Fard and M.-R. Akbari-Zadeh, "A hybrid method based on wavelet, ANN and ARIMA model for short-term load forecasting," *Journal of Experimental & Theoretical Artificial Intelligence, vol. 26, no. 2, pp. 167–182, 2013.*

[15] J. Kim, J. Moon, E. Hwang, and P. Kang, "Recurrent inception convolution neural network for multi short-term load forecasting," *Energy and Buildings, vol. 194, pp. 328–341, 2019.*

[16] Y. Liu, L. Guan, C. Hou, H. Han, Z. Liu, Y. Sun, and M. Zheng, "Wind Power Short-Term Prediction Based on LSTM and Discrete Wavelet Transform," *Applied Sciences, vol. 9, no. 6, p. 1108, 2019.*

[17] H. Su, E. Zio, J. Zhang, M. Xu, X. Li, and Z. Zhang, "A hybrid hourly natural gas demand forecasting method based on the integration of wavelet transform and enhanced Deep-RNN model," *Energy, vol. 178, pp. 585–597, 2019.*

[18] C. Keerthisinghe, G. Verbic, and A. C. Chapman, "A Fast Technique for Smart Home Management: ADP With Temporal Difference Learning," *IEEE Transactions on Smart Grid, vol. 9, no. 4, pp. 3291–3303, 2018.*

[19] Y. Wang, D. Gan, M. Sun, N. Zhang, Z. Lu, and C. Kang, "Probabilistic individual load forecasting using pinball loss guided LSTM," *Applied Energy, vol. 235, pp. 10–20, 2019.*

[20] B. Yildiz, J. I. Bilbao, J. Dore, and A. B. Sproul, "Short-term forecasting of individual household electricity loads with investigating impact of data resolution and forecast horizon," *Renewable Energy and Environmental Sustainability, vol. 3, p. 3, 2018.*

[21] W. Kong, Z. Y. Dong, D. J. Hill, F. Luo, and Y. Xu, "Short-Term Residential Load Forecasting Based on Resident Behaviour Learning," *IEEE Transactions on Power Systems, vol. 33, no. 1, pp. 1087–1088, 2018.*

[22] M. Imani and H. Ghassemian, "Electrical Load Forecasting Using Customers Clustering and Smart Meters in Internet of Things," *2018 9th International Symposium on Telecommunications (IST), 2018.*

[23] P. Guo, J. C. Lam, and V. O. Li, "Drivers of domestic electricity users' price responsiveness: A novel machine learning approach," *Applied Energy, vol. 235, pp. 900–913, 2019.*

[24] W. Kong, Z. Y. Dong, Y. Jia, D. J. Hill, Y. Xu, and Y. Zhang, "Short-Term Residential Load Forecasting Based on LSTM Recurrent Neural Network," *IEEE Transactions on Smart Grid, vol. 10, no. 1, pp. 841–851, 2019.*

[25] "Energy Efficiency Trends in Canada 1990 to 2013," *Natural Resources Canada*, 31-Jan-2019. [Online]. Available: https://www.nrcan.gc.ca/energy/publications/19030. [Accessed: 15-Apr-2020].

[26] F. Wang, Y. Yu, Z. Zhang, J. Li, Z. Zhen, and K. Li, "Wavelet Decomposition and Convolutional LSTM Networks Based Improved Deep Learning Model for Solar Irradiance Forecasting," *Applied Sciences, vol. 8, no. 8, p. 1286, Jan. 2018.*

[27] Srivastava, N., G. Hinton, A. Krizhevsky, I. Sutskever, R. Salakhutdinov, "Dropout: A Simple Way to Prevent Neural Networks from Overfitting," *Journal of Machine Learning Research. Vol. 15, pp. 1929-1958, 2014.*

[28] Yarin, Ghahramani, and Zoubin, "A Theoretically Grounded Application of Dropout in Recurrent Neural Networks," *arXiv.org*, 05-Oct-2016. [Online]. Available: https://arxiv.org/abs/1512.05287. [Accessed: 15-Apr-2020].

[29] A. Graves and J. Schmidhuber, "Framewise phoneme classification with bidirectional LSTM and other neural network architectures," *Neural Networks*, 19-Aug-2005. [Online]. Available: https://www.sciencedirect.com/science/article/pii/S0893608005001206. [Accessed: 15-Apr-2020].

[30] A. Graves, N. Jaitly, and A.-R. Mohamed, “Hybrid speech recognition with Deep Bidirectional LSTM,” *2013 IEEE Workshop on Automatic Speech Recognition and Understanding*, 2013.

[31] S. Wang, X. Wang, S. Wang, and D. Wang, “Bi-directional long short-term memory method based on attention mechanism and rolling update for short-term load forecasting,” *International Journal of Electrical Power & Energy Systems,* vol. 109, pp. 470–479, 2019.

[32] J. Kim and N. Moon, “BiLSTM model based on multivariate time series data in multiple field for forecasting trading area,” *Journal of Ambient Intelligence and Humanized Computing*, 2019.

[33] K. B. Sahay, S. Sahu, and P. Singh, “Short-term load forecasting of Toronto Canada by using different ANN algorithms,” *2016 IEEE 6th International Conference on Power Systems (ICPS),* 2016.

Chapter 6

Conclusion

6.1 Summary

The ultimate goal of this thesis is to determine a transfer function-based load model for commercial and industrial loads from the composite load model; and to devise an STLF method for an electrically heated house load by employing deep learning and wavelet transform techniques. The developed transfer function-based load model is verified to be effective for small motor composition load, or commercial load; and large motor composition load, or industrial load. A robust STLF model is proposed in this thesis. The main content of Chapters 3, 4 and 5 are summarized as follows:

In Chapter 3, the 3rd order transfer function-based load model has been derived mathematically from a composite load model consisting of an induction motor and a ZIP load. The composition of load is 25 HP induction motor and 120kW static load; the typical 25 HP induction motors parameters and experimentally calculated static load parameters are used in this model. This developed model has been verified by comparing with the original composite load model for commercial load. This comparison provides a complete understanding of both load models dynamic responses. Next, three simplified load models are applied to the full transfer function-based load model developed in this chapter. From the simulation results, it is found that the reduced models have less accuracy compared to full transfer function-based load model and without frequency dependency can cause significant error. This simulation results

confirmed that the reduced model with the 1st order voltage and 1st order frequency terms has the smallest errors among the reduced models due to its consideration of both voltage and frequency dependency.

Several conclusions are drawn in this chapter as follows: 1) the reason of better performance of 3rd order transfer-function is explained theoretically; 2) the linearization process during derivation causes a loss of dynamic characteristics of the transfer function-based load model but it follows the trend of the dynamic system response very well; 3) after simplifying the full model, the reduced model has larger error compared to the full model; and 4) among three reduced models, the one with 1st order voltage and 1st order frequency terms shows the smallest errors due to its consideration of both voltage and frequency dependency.

In Chapter 4, the 3rd order transfer function-based load model has been derived directly from the composite load model for industrial load. In high motor composition load i.e. 1500HP induction motor and 120kW static load, induction motors are dominant in the load composition. Next, the dynamic responses of the developed model have been verified by comparing with the original composite load model for various disturbances. The comparison showed that the dynamic responses of the developed model are less transient and more linear, due to the linearization process during the derivation of the transfer function-based load model. This was experimentally confirmed by comparing the results obtained from the transfer function-based load model with the results from the original composite load model. However, it has been determined that the tendency of the dynamic responses of both models agree under various disturbances, except for frequency disturbances.

In Chapter 5, STLF model for electrically heated house is proposed based on the SWT and RNN techniques. The actual power load data is classified according to seasonal power usage

behaviour and each load classification follows the below procedure to forecast the electrically heated house:

1) Generate a set of lagged power load data vectors from the historical power load data
2) Decomposes the vectors into sub-components by SWT
3) Extracts features from the sub-components by using a Bi-LSTM neural network layer with dropout layer
4) Predict the power load from each extracted feature by using an LSTM layer with dropout layer
5) Reconstruct actual power load forecast signal by combining predicted sub-components by ISWT.

The accuracy of the developed model is verified by using the real power load dataset of a house in St. John's, Newfoundland and Labrador, Canada. Three comparisons for each of two cases are studied. The conclusions of the three comparisons are drawn as follows:

1) Comparison 1- the proposed model is more accurate compared to the other developed STLF model because the Bi-LSTM layer has the ability to learn the complicated features of the actual data and dropout layer stops overfitting of the neural networks.

2) Comparison 2- a set of lagged power load data vectors generate higher prediction accuracy compared to the original data input. The inclusion of lagged vectors representing the recent past improves the accuracy of the prediction, because the behaviour of house loads is known to follow daily and weekly patterns. The implication is that general insights about time-varying loads can be leveraged using the neural network model to improve forecasting ability.

3) Comparison 3- adding dropout layers after the Bi-LSTM and LSTM neural network improves the forecasting accuracy of the developed model because dropout layer prevents the overfitting of neural networks.

6.2 Future Work

Presently, the integration of smart grid technologies including renewable distributed generators and electric vehicles causes uncertainty and difficulty for dynamic load modeling. Future work on the dynamic load model could be to incorporate the transfer function-based load model of distributed generators and electric vehicles. The transfer function-based load model proposed in this work was derived from a composite load model consisting of induction motor and static loads. The future investigation would involve the development of dynamic load models, and analysis of the dynamic response of a system containing smart grid technologies.

The proposed STLF method has been applied, and the accuracy of the model analysed considering the electrically heated house load. Other load classes could be modeled and analyzed, such as industrial and commercial loads. Different load classes are distinguished by several factors. Among these are motor composition (the proportion contributed by AC motors to the load bus), and time-varying and weather-dependent compositions. Future work would be to examine the performance of the proposed STLF method on different load classes. To do this it would be necessary to identify the composition of the load classes, to determine their variability with respect to weather and other factors.

List of Publication

[1] Hlaumay Marma and Xiaodong Liang, “Comparative Study of Composite Load Model and Transfer Function Based Load Model”, IEEE Industry Applications Society (IAS) Annual Meeting, 2019.

[2] Hlaumay Marma and Xiaodong Liang, “Composite Load Model and Transfer Function Based Load Model for High Motor Composition Load”, IEEE Canada Electrical Power and Energy Conference, 2019.

[3] Hlaumay Marma, M. Tariq Iqbal and Christopher Thomas Seary, “Short-term Power Load Forecast of an Electrically Heated House in St. John’s, Newfoundland, Canada”, European Journal of Electrical Engineering & Computer Science (EJECE), 2020.

APPENDIX A Derivation of Transfer Function-Based Model

A.1 Induction Motor

The induction motors can be represented by the following differential equations [11]:

$$v_{ds} = R_s i_{ds} - \omega_s \Psi_{qs} + \frac{d\Psi_{ds}}{dt} \quad \text{(A.1-1)}$$

$$v_{qs} = R_s i_{qs} + \omega_s \Psi_{ds} + \frac{d\Psi_{qs}}{dt} \quad \text{(A.1-2)}$$

$$v_{dr} = R_r i_{dr} - (\omega_s - \omega_r)\Psi_{qr} + \frac{d\Psi_{dr}}{dt} \quad \text{(A.1-3)}$$

$$v_{qr} = R_r i_{qr} + (\omega_s - \omega_r)\Psi_{dr} + \frac{d\Psi_{qr}}{dt} \quad \text{(A.1-4)}$$

$$T_e = 1.5P(\Psi_{ds} i_{qs} - \Psi_{qs} i_{ds}) \quad \text{(A.1-5)}$$

$$\Psi_{ds} = L_s i_{ds} + L_m i_{dr} \quad \text{(A.1-6)}$$

$$\Psi_{qs} = L_s i_{qs} + L_m i_{qr} \quad \text{(A.1-7)}$$

$$\Psi_{dr} = L_m i_{ds} + L_r i_{dr} \quad \text{(A.1-8)}$$

$$\Psi_{qr} = L_m i_{qs} + L_r i_{qr} \quad \text{(A.1-9)}$$

$$\frac{d\omega_r}{dt} = \frac{p}{2H}(T_e - T_m) \quad \text{(A.1-10)}$$

$$L_s = l_s + L_m \quad \text{(A.1-11)}$$

$$L_r = l_r + L_m \quad \text{(A.1-12)}$$

$$J = \frac{2H}{p} \quad \text{(A.1-13)}$$

The stator transient of induction motor is negligible, i.e.,

$$\frac{d\Psi_{ds}}{dt} = 0 \text{ and } \frac{d\Psi_{qs}}{dt} = 0 \quad \text{(A.1-14)}$$

The rotor of induction motor is shorted:

$v_{dr} = 0$ and $v_{qr} = 0$ (A.1-15)

Substitute Equations (A.1-6)-(A.1-9), (A.1-14)-(A.1-15) in Equations (A.1-1) to (A.1-5):

$$v_{ds} = R_s i_{ds} - \omega_s(L_s i_{qs} + L_m i_{qr}) \quad \text{(A.1-16)}$$

$$v_{qs} = R_s i_{qs} + \omega_s(L_s i_{ds} + L_m i_{dr}) \quad \text{(A.1-17)}$$

$$0 = R_r i_{dr} - (\omega_s - \omega_r)(L_m i_{qs} + L_r i_{qr}) + L_m \frac{di_{ds}}{dt} + L_r \frac{di_{dr}}{dt} \quad \text{(A.1-18)}$$

$$0 = R_r i_{qr} + (\omega_s - \omega_r)(L_m i_{ds} + L_r i_{dr}) + L_m \frac{di_{qs}}{dt} + L_r \frac{di_{qr}}{dt} \quad \text{(A.1-19)}$$

$$T_e = 1.5P(i_{dr} i_{qs} - i_{qr} i_{ds}) \quad \text{(A.1-20)}$$

Substitute Equations (A.1-20) in Equation (A.1-10):

$$\frac{d\omega_r}{dt} = \frac{p}{2H}(1.5P(i_{dr} i_{qs} - i_{qr} i_{ds}) - T_m) \quad \text{(A.1-21)}$$

Linearize (A.1-16)-(A.1-19) and (A.1-21):

$$\Delta v_{ds} = R_s \Delta i_{ds} - \omega_{s0} L_s \Delta i_{qs} - \omega_{s0} L_m \Delta i_{qr} - \left(L_s i_{qs0} + L_m i_{qr0}\right)\Delta\omega_s \quad \text{(A.1-22)}$$

$$\Delta v_{qs} = R_s \Delta i_{qs} + \omega_{s0} L_s \Delta i_{ds} + \omega_{s0} L_m \Delta i_{dr} + (L_s i_{ds0} + L_m i_{dr0})\Delta\omega_s \quad \text{(A.1-23)}$$

$$0 = (R_r + L_r S)\Delta i_{dr} + (\omega_{r0} - \omega_{s0}) L_m \Delta i_{qs} + (\omega_{r0} - \omega_{s0}) L_r \Delta i_{qr} + L_m S \Delta i_{ds} + \left(L_m i_{qs0} + L_r i_{qr0}\right)\Delta\omega_r - \left(L_m i_{qs0} + L_r i_{qr0}\right)\Delta\omega_s \quad \text{(A.1-24)}$$

$$0 = (R_r + L_r S)\Delta i_{qr} + L_m S \Delta i_{qs} - (\omega_{r0} - \omega_{s0}) L_m \Delta i_{ds} - (\omega_{r0} - \omega_{s0}) L_r \Delta i_{dr} - (L_m i_{ds0} + L_r i_{dr0})\Delta\omega_r + (L_m i_{ds0} + L_r i_{dr0})\Delta\omega_s \quad \text{(A.1-25)}$$

$$S\Delta\omega_r = \frac{3p^2 L_m}{4H}(i_{dr0}\Delta i_{qs} - i_{qr0}\Delta i_{ds} + i_{qs0}\Delta i_{dr} - i_{ds0}\Delta i_{qr}) \quad \text{(A.1-26)}$$

Δi_{qr} can be determined from Equation (A.1-22):

$$\Delta i_{qr} = \frac{1}{\omega_{s0} L_m}[R_s \Delta i_{ds} - \omega_{s0} L_s \Delta i_{qs} - \left(L_s i_{qs0} + L_m i_{qr0}\right)\Delta\omega_s - \Delta v_{ds}] \quad \text{(A.1-27)}$$

Δi_{dr} can be determined from Equation (A.1-23):

$$\Delta i_{dr} = \frac{1}{\omega_{s0} L_m}[\Delta v_{qs} - R_s \Delta i_{qs} - \omega_{s0} L_s \Delta i_{ds} - (L_s i_{ds0} + L_m i_{dr0})\Delta\omega_s] \quad \text{(A.1-28)}$$

Substitute Equations (A.1-27) and (A.1-28) in Equation (A.1-24):

$$0 = (R_r + L_r S)\Delta v_{qs} - (\omega_{r0} - \omega_{s0}) L_r \Delta v_{ds} + [\omega_{s0}(\omega_{r0} - \omega_{s0})(L_m^2 - L_r L_s) - R_r R_s - SL_r R_s]\Delta i_{qs} - [R_r(L_s i_{ds0} + L_m i_{dr0}) + (\omega_{r0} - \omega_{s0}) L_r\big(L_s i_{qs0} + L_m i_{qr0}\big) + \omega_{s0} L_m \big(L_m i_{qs0} + L_r i_{qr0}\big) + SL_r(L_s i_{ds0} + L_m i_{dr0})\,]\Delta\omega_s + [L_r R_s(\omega_{r0} - \omega_{s0}) - \omega_{s0} L_s R_r + S\omega_{s0}(L_m^2 - L_r L_s)]\Delta i_{ds} + \omega_{s0} L_m\big(L_m i_{qs0} + L_r i_{qr0}\big)\Delta\omega_r \quad \text{(A.1-29)}$$

$$0 = x_{11}\Delta v_{qs} + x_{12}\Delta v_{ds} + x_{13}\Delta i_{qs} + x_{14}\Delta\omega_s + x_{15}\Delta i_{ds} + x_{16}\Delta\omega_r \quad \text{(A.1-30)}$$

Where,

$$x_{11} = (R_r + L_r S) = x_{112} + x_{111} S$$

$$x_{12} = -(\omega_{r0} - \omega_{s0}) L_r$$

$$x_{13} = \omega_{s0}(\omega_{r0} - \omega_{s0})(L_m^2 - L_r L_s) - R_r R_s - SL_r R_s = x_{132} + x_{131} S$$

$$x_{14} = -[R_r(L_s i_{ds0} + L_m i_{dr0}) + (\omega_{r0} - \omega_{s0}) L_r\big(L_s i_{qs0} + L_m i_{qr0}\big) + \omega_{s0} L_m \big(L_m i_{qs0} + L_r i_{qr0}\big) + SL_r(L_s i_{ds0} + L_m i_{dr0})\,] = x_{142} + x_{141} S$$

$$x_{15} = L_r R_s(\omega_{r0} - \omega_{s0}) - \omega_{s0} L_s R_r + S\omega_{s0}(L_m^2 - L_r L_s) = x_{152} + x_{151} S$$

$$x_{16} = \omega_{s0} L_m\big(L_m i_{qs0} + L_r i_{qr0}\big)$$

$$x_{111} = L_r$$

$$x_{112} = R_r$$

$$x_{131} = -L_r R_s$$

$$x_{132} = \omega_{s0}(\omega_{r0} - \omega_{s0})(L_m^2 - L_r L_s) - R_r R_s$$

$$x_{141} = -L_r(L_s i_{ds0} + L_m i_{dr0})$$

$$x_{142} = -[R_r(L_s i_{ds0} + L_m i_{dr0}) + (\omega_{r0} - \omega_{s0})L_r\left(L_s i_{qs0} + L_m i_{qr0}\right) + \omega_{s0}L_m\left(L_m i_{qs0} + L_r i_{qr0}\right)]$$

$$x_{151} = \omega_{s0}(L_m^2 - L_r L_s)$$

$$x_{152} = L_r R_s(\omega_{r0} - \omega_{s0}) - \omega_{s0}L_s R_r$$

Substitute Equations (A.1-27) and (A.1-28) in Equation (A.1-25):

$$0 = -(\omega_{r0} - \omega_{s0})L_r \Delta v_{qs} - (R_r + L_r S)\Delta v_{ds} + [L_r R_s(\omega_{r0} - \omega_{s0}) - \omega_{s0}L_s R_r + S\omega_{s0}(L_m^2 - L_r L_s)]\Delta i_{qs} + [(\omega_{r0} - \omega_{s0})L_r(L_s i_{ds0} + L_m i_{dr0}) + \omega_{s0}L_m\left(L_m i_{ds0} + L_r i_{dr0}\right) - R_r\left(L_s i_{qs0} + L_m i_{qr0}\right) - SL_r\left(L_s i_{qs0} + L_m i_{qr0}\right)]\Delta\omega_s + [R_r R_s - \omega_{s0}(\omega_{r0} - \omega_{s0})(L_m^2 - L_r L_s) + SL_r R_s]\Delta i_{ds} - \omega_{s0}L_m(L_m i_{ds0} + L_r i_{dr0})\Delta\omega_r \quad \text{(A.1-31)}$$

$$0 = x_{21}\Delta v_{qs} + x_{22}\Delta v_{ds} + x_{23}\Delta i_{qs} + x_{24}\Delta\omega_s + x_{25}\Delta i_{ds} + x_{26}\Delta\omega_r \quad \text{(A.1-32)}$$

Where,

$$x_{21} = -(\omega_{r0} - \omega_{s0})L_r$$

$$x_{22} = -(R_r + L_r S) = x_{222} + x_{221}S$$

$$x_{23} = L_r R_s(\omega_{r0} - \omega_{s0}) - \omega_{s0}L_s R_r + S\omega_{s0}(L_m^2 - L_r L_s) = x_{232} + x_{231}S$$

$$x_{24} = [(\omega_{r0} - \omega_{s0})L_r(L_s i_{ds0} + L_m i_{dr0}) + \omega_{s0}L_m\left(L_m i_{ds0} + L_r i_{dr0}\right) - R_r\left(L_s i_{qs0} + L_m i_{qr0}\right) - SL_r\left(L_s i_{qs0} + L_m i_{qr0}\right)] = x_{242} + x_{241}S$$

$$x_{25} = R_r R_s - \omega_{s0}(\omega_{r0} - \omega_{s0})(L_m^2 - L_r L_s) + SL_r R_s = x_{252} + x_{251}S$$

$$x_{26} = -\omega_{s0}L_m(L_m i_{ds0} + L_r i_{dr0})$$

$$x_{221} = -L_r$$

$$x_{222} = -R_r$$

$$x_{231} = \omega_{s0}(L_m^2 - L_r L_s)$$

$$x_{232} = L_r R_s(\omega_{r0} - \omega_{s0}) - \omega_{s0} L_s R_r$$

$$x_{241} = -L_r\left(L_s i_{qs0} + L_m i_{qr0}\right)$$

$$x_{242} = (\omega_{r0} - \omega_{s0}) L_r (L_s i_{ds0} + L_m i_{dr0}) + \omega_{s0} L_m \left(L_m i_{ds0} + L_r i_{dr0}\right) - R_r\left(L_s i_{qs0} + L_m i_{qr0}\right)$$

$$x_{251} = L_r R_s$$

$$x_{252} = R_r R_s - \omega_{s0}(\omega_{r0} - \omega_{s0})(L_m^2 - L_r L_s)$$

Substitute Equations (A.1-27) and (A.1-28) in Equation (A.1-26):

$$0 = i_{qs0}\Delta v_{qs} + i_{ds0}\Delta v_{ds} + (\omega_{s0} L_m\, i_{dr0} + \omega_{s0} L_s i_{ds0} - R_s i_{qs0})\,\Delta i_{qs} + [i_{ds0}\left(L_s i_{qs0} + L_m i_{qr0}\right) - i_{qs0}(L_s i_{ds0} + L_m i_{dr0})]\Delta\omega_s - (\omega_{s0} L_m\, i_{qr0} + \omega_{s0} L_s i_{qs0} + R_s i_{ds0})\Delta i_{ds} - \left(\frac{4H}{3p^2 L_m}\right) S\Delta\omega_r \quad \text{(A.1-33)}$$

$$0 = x_{31}\Delta v_{qs} + x_{32}\Delta v_{ds} + x_{33}\Delta i_{qs} + x_{34}\Delta\omega_s + x_{35}\Delta i_{ds} + x_{36}\Delta\omega_r \quad \text{(A.1-34)}$$

Where,

$$x_{31} = i_{qs0}$$

$$x_{32} = i_{ds0}$$

$$x_{33} = (\omega_{s0} L_m\, i_{dr0} + \omega_{s0} L_s i_{ds0} - R_s i_{qs0})$$

$$x_{34} = [i_{ds0}\left(L_s i_{qs0} + L_m i_{qr0}\right) - i_{qs0}(L_s i_{ds0} + L_m i_{dr0})]$$

$$x_{35} = -(\omega_{s0} L_m\, i_{qr0} + \omega_{s0} L_s i_{qs0} + R_s i_{ds0})$$

$$x_{36} = -\left(\frac{4H}{3p^2 L_m}\right) S = x_{361} S$$

$$x_{361} = -\left(\frac{4H}{3p^2 L_m}\right)$$

Δi_{ds} can be determined from Equation (A.1-34):

$$\Delta i_{ds} = -\left(\frac{1}{x_{35}}\right)[x_{31}\Delta v_{qs} + x_{32}\Delta v_{ds} + x_{33}\Delta i_{qs} + x_{34}\Delta\omega_s + x_{36}\Delta\omega_r \quad \text{(A.1-35)}$$

The power source voltage in dq reference frame can be expressed by

$$v_{dg} = 0 \tag{A.1-36}$$

$$v_{qg} = \sqrt{2}E \tag{A.1-37}$$

Since the source voltage is directly applied to the motor stator in this configuration, therefore:

$$v_{ds} = v_{dg} = 0 \tag{A.1-38}$$

$$v_{qs} = v_{qg} = \sqrt{2}E \tag{A.1-39}$$

Linearize (A.1-38) and (A.1-39):

$$\Delta v_{ds} = 0 \tag{A.1-40}$$

$$\Delta v_{qs} = \sqrt{2}\Delta E \tag{A.1-41}$$

Substitute Equations (A.1-40) in Equations (A.1-30), (A.1-32):

$$0 = x_{11}\Delta v_{qs} + x_{13}\Delta i_{qs} + x_{14}\Delta\omega_s + x_{15}\Delta i_{ds} + x_{16}\Delta\omega_r \tag{A.1-42}$$

$$0 = x_{21}\Delta v_{qs} + x_{23}\Delta i_{qs} + x_{24}\Delta\omega_s + x_{25}\Delta i_{ds} + x_{26}\Delta\omega_r \tag{A.1-43}$$

Substitute Equations (A.1-40) in Equation (A.1-34):

$$\Delta i_{ds} = -\left(\frac{1}{x_{35}}\right)[x_{31}\Delta v_{qs} + x_{33}\Delta i_{qs} + x_{34}\Delta\omega_s + x_{36}\Delta\omega_r \tag{A.1-44}$$

$$\Delta i_{ds} = x_{41}\Delta v_{qs} + x_{42}\Delta i_{qs} + x_{43}\Delta\omega_s + x_{44}S\Delta\omega_r \tag{A.1-45}$$

Where,

$$x_{41} = -\left(\frac{1}{x_{35}}\right)x_{31}$$

$$x_{42} = -\left(\frac{1}{x_{35}}\right)x_{33}$$

$$x_{43} = -\left(\frac{1}{x_{35}}\right)x_{34}$$

$$x_{44} = -\left(\frac{1}{x_{35}}\right) x_{361}$$

Substitute Equations (A.1-35) in Equations (A.1-42):

$$0 = (y_{11}S + y_{12})\Delta v_{qs} + (y_{21}S + y_{22})\Delta i_{qs} + (y_{31}S + y_{32})\Delta\omega_s + (y_{41}S^2 + y_{42}S + y_{43})\Delta\omega_r \quad \text{(A.1-46)}$$

Where,

$$y_{11} = x_{35}x_{111} - x_{151}x_{31}$$

$$y_{12} = x_{35}x_{112} - x_{152}x_{31}$$

$$y_{21} = x_{35}x_{131} - x_{151}x_{33}$$

$$y_{22} = x_{35}x_{132} - x_{152}x_{33}$$

$$y_{31} = x_{35}x_{141} - x_{151}x_{34}$$

$$y_{32} = x_{35}x_{142} - x_{152}x_{34}$$

$$y_{41} = -x_{361}x_{151}$$

$$y_{42} = -x_{361}x_{152}$$

$$y_{43} = x_{35}x_{16}$$

Substitute Equations (A.1-35) in Equations (A.1-43):

$$0 = (y_{51}S + y_{52})\Delta v_{qs} + (y_{61}S + y_{62})\Delta i_{qs} + (y_{71}S + y_{72})\Delta\omega_s + (y_{81}S^2 + y_{82}S + y_{83})\Delta\omega_r \quad \text{(A.1-47)}$$

Where,

$$y_{51} = -x_{251}x_{31}$$

$$y_{52} = x_{35}x_{21} - x_{252}x_{31}$$

$$y_{61} = x_{35}x_{231} - x_{251}x_{33}$$

$$y_{62} = x_{35}x_{232} - x_{252}x_{33}$$

$$y_{71} = x_{35}x_{241} - x_{251}x_{34}$$

$$y_{72} = x_{35}x_{242} - x_{252}x_{34}$$

$$y_{81} = -x_{361}x_{251}$$

$$y_{82} = -x_{361}x_{252}$$

$$y_{83} = x_{35}x_{26}$$

Δi_{qs} and $\Delta\omega_r$ can be determined from Equations (A.1-46) and (A.1-47):

$$\Delta i_{qs} = \frac{(z_{11}S^3+z_{12}S^2+z_{13}S+z_{14})}{(O_1S^3+O_2S^2+O_3S+O_4)}\Delta v_{qs} + \frac{(z_{21}S^3+z_{22}S^2+z_{23}S+z_{24})}{(O_1S^3+O_2S^2+O_3S+O_4)}\Delta\omega_s \quad \text{(A.1-46)}$$

$$\Delta\omega_r = \frac{(z_{31}S^2+z_{32}S+z_{33})}{(O_1S^3+O_2S^2+O_3S+O_4)}\Delta v_{qs} + \frac{(z_{41}S^2+z_{42}S+z_{43})}{(O_1S^3+O_2S^2+O_3S+O_4)}\Delta\omega_s \quad \text{(A.1-47)}$$

Where,

$$O_1 = y_{21}y_{81} - y_{61}y_{41}$$

$$O_2 = y_{21}y_{82} + y_{22}y_{81} - y_{61}y_{42} - y_{62}y_{41}$$

$$O_3 = y_{21}y_{83} + y_{22}y_{82} - y_{61}y_{43} - y_{62}y_{42}$$

$$O_4 = y_{22}y_{83} - y_{62}y_{43}$$

$$z_{11} = y_{51}y_{41} - y_{11}y_{81}$$

$$z_{12} = y_{51}y_{42} + y_{52}y_{41} - y_{11}y_{82} - y_{12}y_{81}$$

$$z_{13} = y_{51}y_{43} + y_{52}y_{42} - y_{11}y_{83} - y_{12}y_{82}$$

$$z_{14} = y_{52}y_{43} - y_{12}y_{83}$$

$$z_{21} = y_{71}y_{41} - y_{31}y_{81}$$

$$z_{22} = y_{71}y_{42} + y_{72}y_{41} - y_{31}y_{82} - y_{32}y_{81}$$

$$z_{23} = y_{71}y_{43} + y_{72}y_{42} - y_{31}y_{83} - y_{32}y_{82}$$

$$z_{24} = y_{72}y_{43} - y_{32}y_{83}$$

$$z_{31} = y_{11}y_{61} - y_{51}y_{21}$$

$$z_{32} = y_{11}y_{62} + y_{12}y_{61} - y_{51}y_{22} - y_{52}y_{21}$$

$$z_{33} = y_{12}y_{62} - y_{52}y_{22}$$

$$z_{41} = y_{31}y_{61} - y_{71}y_{21}$$

$$z_{42} = y_{31}y_{62} + y_{32}y_{61} - y_{71}y_{22} - y_{72}y_{21}$$

$$z_{43} = y_{32}y_{62} - y_{72}y_{22}$$

Substitute Equation (A.1-47) in Equation (A.1-45):

$$\Delta i_{ds} = \frac{(z_{51}S^3+z_{52}S^2+z_{53}S+z_{54})}{(O_1S^3+O_2S^2+O_3S+O_4)}\Delta v_{qs} + \frac{(z_{61}S^3+z_{62}S^2+z_{63}S+z_{64})}{(O_1S^3+O_2S^2+O_3S+O_4)}\Delta\omega_s \quad \text{(A.1-48)}$$

Where,

$$z_{51} = x_{41}O_{11} + x_{42}z_{11} + x_{44}z_{31}$$

$$z_{52} = x_{41}O_{12} + x_{42}z_{12} + x_{44}z_{32}$$

$$z_{53} = x_{41}O_{13} + x_{42}z_{13} + x_{44}z_{33}$$

$$z_{54} = x_{41}O_{14} + x_{42}z_{14}$$

$$z_{61} = x_{43}O_{11} + x_{42}z_{21} + x_{44}z_{41}$$

$$z_{62} = x_{43}O_{12} + x_{42}z_{22} + x_{44}z_{42}$$

$$z_{63} = x_{43}O_{13} + x_{42}z_{23} + x_{44}z_{43}$$

$$z_{64} = x_{43}O_{14} + x_{42}z_{24}$$

Substitute Equation (A.1-41) and $\Delta\omega_s = 2\pi\Delta f$ in Equations (A.1-46) and (A.1-47):

$$\Delta i_{qs} = \frac{(a_{11}S^3+a_{12}S^2+a_{13}S+a_{14})}{(O_1S^3+O_2S^2+O_3S+O_4)}\Delta E + \frac{(a_{21}S^3+a_{22}S^2+a_{23}S+a_{24})}{(O_1S^3+O_2S^2+O_3S+O_4)}\Delta f \quad \text{(A.1-49)}$$

$$\Delta i_{ds} = \frac{(a_{51}S^3+a_{52}S^2+a_{53}S+a_{54})}{(O_1S^3+O_2S^2+O_3S+O_4)}\Delta E + \frac{(a_{61}S^3+a_{62}S^2+a_{63}S+a_{64})}{(O_1S^3+O_2S^2+O_3S+O_4)}\Delta f \quad \text{(A.1-50)}$$

Where,

$a_{11} = \sqrt{2}z_{11}$	$a_{21} = 2\pi z_{21}$	$a_{51} = \sqrt{2}z_{51}$	$a_{61} = 2\pi z_{61}$
$a_{12} = \sqrt{2}z_{12}$	$a_{22} = 2\pi z_{22}$	$a_{52} = \sqrt{2}z_{52}$	$a_{62} = 2\pi z_{62}$
$a_{13} = \sqrt{2}z_{13}$	$a_{23} = 2\pi z_{23}$	$a_{53} = \sqrt{2}z_{53}$	$a_{63} = 2\pi z_{63}$
$a_{14} = \sqrt{2}z_{14}$	$a_{24} = 2\pi z_{24}$	$a_{54} = \sqrt{2}z_{54}$	$a_{64} = 2\pi z_{64}$

The real power P and the reactive power Q of the induction motor can be formulated by

$$P_{IM} = \frac{3}{2}(v_{ds}i_{ds} + v_{qs}i_{qs}) \quad \text{(A.1-51)}$$

$$Q_{IM} = \frac{3}{2}(v_{qs}i_{ds} - v_{ds}i_{qs}) \quad \text{(A.1-52)}$$

Substitute Equation (A.1-40) and (A.1-41) in Equations (A.1-51) and (A.1-52):

$$P_{IM} = \frac{3}{2}(\sqrt{2}Ei_{qs}) \quad \text{(A.1-53)}$$

$$Q_{IM} = \frac{3}{2}(\sqrt{2}Ei_{ds}) \quad \text{(A.1-54)}$$

For the total real power, the Taylor expansion for Equation (A.1-53) can be written as follows:

$$P_{IM} = P_{IM0} + a_E\Delta E + a_{iqs}\Delta i_{qs} + a_{Eiqs}\Delta E\Delta i_{qs} \quad \text{(A.1-55)}$$

Where,

$$a_E = \frac{3}{2}(\sqrt{2}i_{qs0})$$

$$a_{iqs} = \frac{3}{2}(\sqrt{2}E_0)$$

$$a_{Eiqs} = \frac{3}{\sqrt{2}}$$

For the total reactive power, the Taylor expansion for Equation (A.1-54) can be written as follows:

$$Q_{IM} = Q_{IM0} + b_E\Delta E + b_{ids}\Delta i_{ds} + a_{Eids}\Delta E\Delta i_{ds} \quad \text{(A.1-56)}$$

Where,

$$b_E = \frac{3}{2}(\sqrt{2} i_{ds0})$$

$$b_{ids} = \frac{3}{2}(\sqrt{2} E_0)$$

$$b_{Eids} = \frac{3}{\sqrt{2}}$$

Substitute Equation (A.1-49) and (A.1-50) in Equations (A.1-55) and (A.1-56):

$$P_{IM} = P_{IM0} + GP_{EIM}\Delta E + GP_{fIM}\Delta f + GP_{E2IM}\Delta E^2 + GP_{EfIM}\Delta E\Delta f \quad \text{(A.1-57)}$$

$$Q_{IM} = Q_{IM0} + GQ_{EIM}\Delta E + GQ_{fIM}\Delta f + GQ_{E2IM}\Delta E^2 + GQ_{EfIM}\Delta E\Delta f \quad \text{(A.1-58)}$$

Where, the coefficients are expressed by

$$GP_{EIM} = \frac{F_{11}S^3 + F_{12}S^2 + F_{13}S + F_{14}}{N_1S^3 + N_2S^2 + N_3S + N_4}$$

$$GP_{fIM} = \frac{F_{21}S^3 + F_{22}S^2 + F_{23}S + F_{24}}{N_1S^3 + N_2S^2 + N_3S + N_4}$$

$$GP_{E2IM} = \frac{F_{31}S^3 + F_{32}S^2 + F_{33}S + F_{34}}{N_1S^3 + N_2S^2 + N_3S + N_4}$$

$$GP_{EfIM} = \frac{F_{41}S^3 + F_{42}S^2 + F_{43}S + F_{44}}{N_1S^3 + N_2S^2 + N_3S + N_4}$$

$$GQ_{EIM} = \frac{F_{51}S^3 + F_{52}S^2 + F_{53}S + F_{54}}{N_1S^3 + N_2S^2 + N_3S + N_4}$$

$$GQ_{fIM} = \frac{F_{61}S^3 + F_{62}S^2 + F_{63}S + F_{64}}{N_1S^3 + N_2S^2 + N_3S + N_4}$$

$$GQ_{E2IM} = \frac{F_{71}S^3 + F_{72}S^2 + F_{73}S + F_{74}}{N_1S^3 + N_2S^2 + N_3S + N_4}$$

$$GQ_{EfIM} = \frac{F_{81}S^3 + F_{82}S^2 + F_{83}S + F_{84}}{N_1S^3 + N_2S^2 + N_3S + N_4}$$

Where,

$$F_{11} = a_E N_1 + a_{iqs} a_{11}$$

$$F_{12} = a_E N_2 + a_{iqs} a_{12}$$

$$F_{13} = a_E N_3 + a_{iqs} a_{13}$$

$$F_{14} = a_E N_4 + a_{iqs} a_{14}$$

$$F_{21} = a_{iqs} a_{21}$$

$$F_{22} = a_{iqs} a_{22}$$

$$F_{23} = a_{iqs} a_{23}$$

$$F_{24} = a_{iqs} a_{24}$$

$$F_{31} = a_{Eiqs} a_{11}$$

$$F_{32} = a_{Eiqs} a_{12}$$

$$F_{33} = a_{Eiqs} a_{13}$$

$$F_{34} = a_{Eiqs} a_{14}$$

$$F_{41} = a_{Eiqs} a_{21}$$

$$F_{42} = a_{Eiqs} a_{22}$$

$$F_{43} = a_{Eiqs} a_{23}$$

$$F_{44} = a_{Eiqs} a_{24}$$

$$F_{51} = b_E N_1 + b_{ids} a_{31}$$

$$F_{52} = b_E N_2 + b_{ids} a_{32}$$

$$F_{53} = b_E N_3 + b_{ids} a_{33}$$

$$F_{54} = b_E N_4 + b_{ids} a_{34}$$

$$F_{61} = b_{ids} a_{41}$$

$$F_{62} = b_{ids} a_{42}$$

$F_{63} = b_{ids}a_{43}$

$F_{64} = b_{ids}a_{44}$

$F_{71} = b_{Eids}a_{31}$

$F_{72} = b_{Eids}a_{32}$

$F_{73} = b_{Eids}a_{33}$

$F_{74} = b_{Eids}a_{34}$

$F_{81} = b_{Eids}a_{41}$

$F_{82} = b_{Eids}a_{42}$

$F_{83} = b_{Eids}a_{43}$

$F_{84} = b_{Eids}a_{44}$

A.2 ZIP Model

A ZIP model can be represented by the following polynomial equations [3]:

$$P_{ZIP} = P_{ZIP0}\left(a_p\left(\frac{v}{v_0}\right)^2 + b_p\left(\frac{v}{v_0}\right) + c_p\right)(1 + k_{pf}\Delta f) \quad \text{(A.2-1)}$$

$$Q_{ZIP} = Q_{ZIP0}\left(a_q\left(\frac{v}{v_0}\right)^2 + b_q\left(\frac{v}{v_0}\right) + c_q\right)(1 + k_{qf}\Delta f) \quad \text{(A.2-2)}$$

$$a_p + b_p + c_p = 1 \quad \text{(A.2-3)}$$

$$a_q + b_q + c_q = 1 \quad \text{(A.2-4)}$$

The ZIP load model can be written in the similar format of real and reactive power of induction motor. Equations (A.2-1) and (A.2-2) can be rewritten as follows:

$$P_{ZIP} = P_{ZIP0} + GP_{EZIP}\Delta E + GP_{fZIP}\Delta f + GP_{E2ZIP}\Delta E^2 + GP_{EfZIP}\Delta E\Delta f + GP_{E2fZIP}\Delta E^2\Delta f \quad \text{(A.2-5)}$$

$$Q_{ZIP} = Q_{ZIP0} + GQ_{EZIP}\Delta E + GQ_{fZIP}\Delta f + GQ_{E2ZIP}\Delta E^2 + GQ_{EfZIP}\Delta E\Delta f + GQ_{E2fZIP}\Delta E^2\Delta f \quad \text{(A.2-6)}$$

Where, the coefficients are expressed by

$$GP_{EZIP} = \frac{P_{ZIP0}(b_p+2a_p)}{E_0}$$

$$GP_{fZIP} = P_{ZIP0}k_{pf}$$

$$GP_{E2ZIP} = \frac{P_{ZIP0}a_p}{{E_0}^2}$$

$$GP_{EfZIP} = \frac{P_{ZIP0}(b_p+2a_p)k_{pf}}{E_0}$$

$$GP_{E2fZIP} = \frac{P_{ZIP0}a_pk_{pf}}{{E_0}^2}$$

$$GQ_{EZIP} = \frac{Q_{ZIP0}(b_q+2a_q)}{E_0}$$

$$GQ_{fZIP} = Q_{ZIP0}k_{qf}$$

$$GQ_{E2ZIP} = \frac{Q_{ZIP0}a_q}{{E_0}^2}$$

$$GQ_{EfZIP} = \frac{Q_{ZIP0}(b_q+2a_q)k_{qf}}{E_0}$$

$$Gq_{E2fZIP} = \frac{Q_{ZIP0}a_qk_{qf}}{{E_0}^2}$$

The $\Delta E^2\Delta f$ term in the ZIP load model represented by (A.2-5) and (A.2-6), is ignored as the influence of the high order terms are much smaller.

A.3 Overall System

The total power of composite load model is the summation of induction motor and ZIP model power consumption. Therefore, the transfer function-based load model transformed from the composite load model is formulated as follow:

$$P = P_{IM} + P_{ZIP} \quad \text{(A.3-1)}$$

$$Q = Q_{IM} + Q_{ZIP} \quad \text{(A.3-2)}$$

The final form of the load model is

$$P = P_0 + GP_1\Delta E + GP_2\Delta f + GP_3\Delta E^2 + GP_4\Delta E\Delta f \quad \text{(A.3-3)}$$

$$Q = Q_0 + GQ_1\Delta E + GQ_2\Delta f + GQ_3\Delta E^2 + GQ_4\Delta E\Delta f \quad \text{(A.3-4)}$$

Where,

The initial real power P0 and reactive power Q0 are

$$P_0 = P_{IM0} + P_{ZIP0}$$

$$Q_0 = Q_{IM0} + Q_{ZIP0}$$

Where, the coefficients are expressed by

$$GP_1 = \frac{P_{11}S^3+P_{12}S^2+P_{13}S+P_{14}}{N_1S^3+N_2S^2+N_3S+N_4}$$

$$GP_2 = \frac{P_{21}S^3+P_{22}S^2+P_{23}S+P_{24}}{N_1S^3+N_2S^2+N_3S+N_4}$$

$$GP_3 = \frac{P_{31}S^3+P_{32}S^2+P_{33}S+P_{34}}{N_1S^3+N_2S^2+N_3S+N_4}$$

$$GP_4 = \frac{P_{41}S^3+P_{42}S^2+P_{43}S+P_{44}}{N_1S^3+N_2S^2+N_3S+N_4}$$

$$GQ_1 = \frac{Q_{11}S^3+Q_{12}S^2+Q_{13}S+Q_{14}}{N_1S^3+N_2S^2+N_3S+N_4}$$

$$GQ_2 = \frac{Q_{21}S^3+Q_{22}S^2+Q_{23}S+Q_{24}}{N_1S^3+N_2S^2+N_3S+N_4}$$

$$GQ_3 = \frac{Q_{31}S^3+Q_{32}S^2+Q_{33}S+Q_{34}}{N_1S^3+N_2S^2+N_3S+N_4}$$

$$GQ_4 = \frac{Q_{41}S^3+Q_{42}S^2+Q_{43}S+Q_{44}}{N_1S^3+N_2S^2+N_3S+N_4}$$

$$P_{11} = F_{11} + GP_{EZIP}N_1$$

$$P_{12} = F_{12} + GP_{EZIP}N_2$$

$$P_{13} = F_{13} + GP_{EZIP}N_3$$

$$P_{14} = F_{14} + GP_{EZIP}N_4$$

$$P_{21} = F_{21} + GP_{fZIP}N_1$$

$$P_{22} = F_{22} + GP_{fZIP}N_2$$

$$P_{23} = F_{23} + GP_{fZIP}N_3$$

$$P_{24} = F_{24} + GP_{fZIP}N_4$$

$$P_{31} = F_{31} + GP_{E2ZIP}N_1$$

$$P_{32} = F_{32} + GP_{E2ZIP}N_2$$

$$P_{33} = F_{33} + GP_{E2ZIP}N_3$$

$$P_{34} = F_{34} + GP_{E2ZIP}N_4$$

$$P_{41} = F_{41} + GP_{EfZIP}N_1$$

$$P_{42} = F_{42} + GP_{EfZIP}N_2$$

$$P_{43} = F_{43} + GP_{EfZIP}N_3$$

$$P_{44} = F_{44} + GP_{EfZIP}N_4$$

$$Q_{11} = F_{51} + GQ_{EZIP}N_1$$

$$Q_{12} = F_{52} + GQ_{EZIP}N_2$$

$$Q_{13} = F_{53} + GQ_{EZIP}N_3$$

$$Q_{14} = F_{54} + GQ_{EZIP}N_4$$

$$Q_{21} = F_{61} + GQ_{fZIP}N_1$$

$$Q_{22} = F_{62} + GQ_{fZIP}N_2$$

$$Q_{23} = F_{63} + GQ_{fZIP}N_3$$

$$Q_{24} = F_{64} + GQ_{fZIP}N_4$$

$$Q_{31} = F_{71} + GQ_{E2ZIP}N_1$$

$$Q_{32} = F_{72} + GQ_{E2ZIP}N_2$$

$$Q_{33} = F_{73} + GQ_{E2ZIP}N_3$$

$$Q_{34} = F_{74} + GQ_{E2ZIP}N_4$$

$$Q_{41} = F_{81} + GQ_{EfZIP}N_1$$

$$Q_{42} = F_{82} + GQ_{EfZIP}N_2$$

$$Q_{43} = F_{83} + GQ_{EfZIP}N_3$$

$$Q_{44} = F_{84} + GQ_{EfZIP}N_4$$

APPENDIX B Initial Value of Transfer Function-Based Load Model

For Initialization of Transfer function-based Load Model, below Parameters Are Given:

Using the induction motor equations, initial value of induction motor can be calculated.

$$v_{ds0} = R_s i_{ds0} - \omega_{s0}(L_s i_{qs0} + L_m i_{qr0}) \quad \text{(B.1-1)}$$

$$v_{qs0} = R_s i_{qs0} + \omega_{s0}(L_s i_{ds0} + L_m i_{dr0}) \quad \text{(B.1-2)}$$

$$0 = R_r i_{dr0} - (\omega_{s0} - \omega_{r0})(L_m i_{qs0} + L_r i_{qr0}) \quad \text{(B.1-3)}$$

$$0 = R_r i_{qr0} + (\omega_{s0} - \omega_{r0})(L_m i_{ds0} + L_r i_{dr0}) \quad \text{(B.1-4)}$$

$$v_{ds0} = 0 \quad \text{(B.1-5)}$$

$$v_{qs0} = \sqrt{2}E_0 \quad \text{(B.1-6)}$$

Δi_{dr} can be determined from Equation (B.1-3):

$$i_{dr0} = \frac{1}{R_r}[(\omega_{s0} - \omega_{r0})(L_m i_{qs0} + L_r i_{qr0})] \quad \text{(B.1-7)}$$

$$i_{dr0} = u_{11} i_{qs0} + u_{12} i_{qr0} \quad \text{(B.1-8)}$$

Where,

$$u_{11} = \frac{L_m}{R_r}(\omega_{s0} - \omega_{r0})$$

$$u_{12} = \frac{L_r}{R_r}(\omega_{s0} - \omega_{r0})$$

Δi_{qr} can be determined from Equation (B.1-3):

$$i_{qr0} = -\frac{1}{R_r}[(\omega_{s0} - \omega_{r0})(L_m i_{ds0} + L_r i_{dr0})] \quad \text{(B.1-9)}$$

$$i_{qr0} = u_{21} i_{ds0} + u_{22} i_{dr0} \quad \text{(B.1-10)}$$

Where,

$$u_{21} = -\frac{L_m}{R_r}(\omega_{s0} - \omega_{r0})$$

$$u_{22} = -\frac{L_r}{R_r}(\omega_{s0} - \omega_{r0})$$

Substitute Equation (B.1-8) in Equation (B.1-10):

$$i_{qr0} = \frac{1}{(1-u_{12}u_{22})}[u_{21}i_{ds0} + u_{22}u_{11}i_{qs0}] \quad \text{(B.1-11)}$$

$$i_{qr0} = u_{31}i_{ds0} + u_{32}i_{qs0} \quad \text{(B.1-12)}$$

Where,

$$u_{31} = \frac{1}{(1-u_{12}u_{22})}u_{21}$$

$$u_{32} = \frac{1}{(1-u_{12}u_{22})}u_{22}u_{11}$$

Substitute Equations (B.1-5) and (B.1-12) in Equation (B.1-1):

$$i_{ds0} = u_4 i_{qs0} \quad \text{(B.1-13)}$$

Where,

$$u_4 = \frac{(\omega_{s0}L_s + \omega_{s0}L_m u_{32})}{(R_s - \omega_{s0}L_m u_{31})}$$

Substitute Equation (B.1-13) in Equation (B.1-12):

$$i_{qr0} = u_5 i_{qs0} \quad \text{(B.1-14)}$$

Where,

$$u_5 = (u_{31}u_4 + u_{32})$$

Substitute Equation (B.1-13) in Equation (B.1-14):

$$i_{dr0} = u_6 i_{qs0} \quad \text{(B.1-15)}$$

Where,

$$u_6 = (u_{11} + u_5)$$

Substitute Equations (B.1-6), (B.1-13) and (B.1-15) in Equation (B.1-2):

$$i_{qs0} = u_7 E_0 \tag{B.1-16}$$

$$u_7 = \frac{\sqrt{2}}{(R_s + \omega_{s0} L_s u_4 + \omega_{s0} L_m u_6)}$$

Substitute Equation (B.1-16) in Equations (B.1-13), (B.1-14) and (B.1-15); we can calculate i_{qr0}, i_{dr0} and i_{ds0}.